



Documento di sintesi del piano di comunicazione e disseminazione - III anno

M. Valenti, G. Adinolfi, R. Ciavarella, S. Fabozzi,
G. Ferruzzi, V. Palladino, A. Ricca

DOCUMENTO DI SINTESI DEL PIANO DI COMUNICAZIONE E DISSEMINAZIONE - III ANNO
M. Valenti (ENEA), G. Adinolfi (ENEA), R. Ciavarella (ENEA), S. Fabozzi (ENEA),
G. Ferruzzi (ENEA), V. Palladino (ENEA), A. Ricca (ENEA).

Dicembre 2021

Report Ricerca di Sistema Elettrico

Accordo di Programma Ministero della Transizione Ecologica - ENEA

Piano Triennale di Realizzazione 2019-2021 - III annualità

Obiettivo: Sistema Elettrico

Progetto: *2.7 Modelli e strumenti per incrementare l'efficienza energetica nel ciclo di produzione, trasporto, distribuzione dell'elettricità*

Work package: *Analisi delle problematiche di gestione per l'integrazione nelle attuali reti in AC di nuove reti in DC in MT/BT (Media Tensione/Bassa Tensione)*

Linea di attività LA1.18: *Comunicazione e disseminazione 3*

Responsabile del Progetto: Maria Valenti, ENEA

Indice

SOMMARIO.....	4
1 CICLO DI SEMINARI	4
2 PRESENTAZIONE DEL PROGETTO 2.7 AL FESTIVAL DELLO SVILUPPO SOSTENIBILE 2021	5
3 PRESENTAZIONE DEL PROGETTO 2.7 ALLA PITCH MARATHON DELLA EU CHAPTER CONFERENCE DEL GCSP “GRAND CHALLENGES SCHOLARS PROGRAM”	6
4 SPECIAL SESSION - CONFERENZA EEEIC2021	8
5 EVENTO CONCLUSIVO DEL PROGETTO	9
6 ARTICOLI DI DISSEMINAZIONE SCIENTIFICA.....	9
6.1 A PLANNING TOOL FOR RELIABILITY ASSESSMENT OF OVERHEAD DISTRIBUTION LINES IN HYBRID AC/DC GRIDS	11
6.2 METHODOLOGIES FOR POWER SYSTEM RELIABILITY EVALUATION: AN OVERVIEW	27
6.3 FREQUENCY DYNAMICS OF POWER SYSTEMS WITH TEMPORALLY DISTRIBUTED DISTURBANCES, SUSTAINABLE ENERGY, GRIDS AND NETWORKS.....	33
6.4 ENERGY FROM THE WAVES: INTEGRATION OF A HESS TO A WAVE ENERGY CONVERTER IN A DC BUS ELECTRICAL ARCHITECTURE TO ENHANCE GRID POWER QUALITY	44
6.5 ADAPTIVE PROTECTION SCHEME FOR AC MICROGRIDS: SIMULATIONS FOR GRID-CONNECTED/ISLANDED MODE	60

Sommario

Le attività di disseminazione condotte nell'ambito della LA1.18 sono state orientate sia alla finalizzazione delle azioni preparatorie della LA1.11, già descritte nell'ambito del report RdS/PTR(2020)/008, sia nella redazione e sottomissione di ulteriori 5 articoli scientifici a rivista e/o conferenza internazionale, e nella presentazione dei risultati del progetto a due eventi di tipo divulgativo sul tema delle reti intelligenti. Di seguito, si riporta una sintesi di tali attività:

- Presentazione del progetto da parte di ENEA e dei co-beneficiari in 4 webinar del ciclo di seminari organizzati nell'ambito delle attività della LA1.11.
- Presentazione dei risultati del progetto 2.7 alla sessione "Mini-grid models and optimization methods for sustainability, energy services and zero-emission mobility" della pitch marathon organizzata nell'ambito della EU Chapter Conference del GCSP "Grand Challenges Scholars Program" promossa dalla NAE National Academy of Engineering.
- Presentazione dei risultati del progetto 2.7 – in modalità webinar - ad evento di divulgazione sull'affidabilità delle reti ibride AC/DC organizzato dall'ente sardo per la ricerca e lo sviluppo tecnologico "Sardegna Ricerche" nell'ambito del Festival dello Sviluppo Sostenibile 2021.
- Partecipazione alla special session "Reliability and energy efficiency issues in DC and hybrid AC/DC microgrids", nell'ambito della conferenza internazionale EEEIC 2021 - International Conference on Environment and Electrical Engineering (special session organizzata nell'ambito delle attività della LA1.11).
- Sottomissione da parte di ENEA e dei co-beneficiari di 12 articoli scientifici a conferenza e rivista internazionale (di cui 7 lavori preparati nel SAL 2020 e 5 nel corso del SAL 2021).
- Evento finale di disseminazione organizzato dal Politecnico di Milano (dicembre 2021).

1 Ciclo di Seminari

Nel corso del 2021, sono stati erogati i quattro webinar del ciclo di seminari, le cui attività preparatorie sono state condotte nell'ambito della LA1.11 (SAL 2020) e descritte nel Report RdS/PTR(2020)/008. Nel presente report si riportano i risultati in termini di partecipazione per ciascun Webinar.

- **Le problematiche di affidabilità nelle reti ibride di distribuzione – Giovanna Adinolfi (ENEA).**
Data: 21/04/2021.
Iscritti al webinar: 182 utenti.
Picco di spettatori simultanei in diretta web: 75 utenti.
Numero di visualizzazione del video disponibile online: 332 visualizzazioni.
- **Scenari energetici ed evoluzione delle reti elettriche di distribuzione – Salvatore Favuzza e Gaetano Zizzo (Università degli Studi di Palermo).**
Data: 04/06/2021.
Iscritti al webinar: 65 utenti.
Picco di spettatori simultanei in diretta web: 28 utenti.
Numero di visualizzazione del video disponibile online: 216 visualizzazioni.
- **Logiche di gestione energetica di una rete ibrida proprietaria per l'alimentazione di sistemi di mobilità – Giovanni Lutzemberger (Università degli Studi di Pisa).**
Data: 25/06/2021.

Iscritti al webinar: 88 utenti.

Picco di spettatori simultanei in diretta web: 26 utenti.

Numero di visualizzazione del video disponibile online: 257 visualizzazioni.

- **I vantaggi delle reti in corrente continua nella transizione energetica verso tecnologie sostenibili – Morris Brenna** (Politecnico di Milano).

Data: 27/09/2021.

Iscritti al webinar: 110 utenti.

Picco di spettatori simultanei in diretta web: 49 utenti.

Numero di visualizzazione del video disponibile online: 236 visualizzazioni.

Data la natura divulgativa dell'evento, che ha visto anche la partecipazione di stakeholder non provenienti dal settore scientifico, le presentazioni predisposte da ENEA e dai co-beneficiari hanno incluso in una prima parte una panoramica generale della tematica affrontata e in una seconda parte la descrizione degli obiettivi e dei risultati ottenuti con il progetto 2.7 di Ricerca di Sistema. Benché la scelta dello slot temporale pomeridiano sia risultato premiante in termini di numero di iscrizioni e partecipazione (seminario del 21/04/2021), tutti i seminari hanno suscitato interesse, come dimostrato dal continuo aumento delle visualizzazioni dei video resi disponibili on line sul canale YouTube di ENEA.

2 Presentazione del Progetto 2.7 al Festival dello Sviluppo Sostenibile 2021

ENEA ha presentato i risultati del progetto 2.7 nell'ambito della sessione formativa "Affidabilità delle reti ibride AC/DC" organizzata dall'ente sardo per la ricerca e lo sviluppo tecnologico "Sardegna Ricerche" nelle more della disseminazione del Progetto "Power Integration Grids".

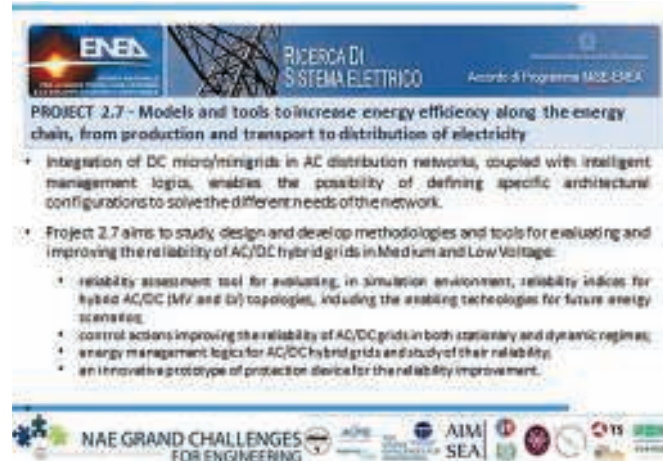
La presentazione, dal titolo "Reti DC e reti AC: problematiche di affidabilità nelle reti di distribuzione", è stata predisposta ed erogata dalla ricercatrice Giovanna Adinolfi (ENEA) in modalità Webinar (data evento: 29/09/2021).



Come nel caso del ciclo di seminari organizzato da ENEA, la natura divulgativa dell'evento inserito tra le attività del Festival dello Sviluppo Sostenibile 2021, ha richiesto la predisposizione di un contributo inclusivo sia di una sezione introduttiva della tematica che di una sezione più tecnica relativa alle specificità del progetto 2.7. Il seminario reso anche disponibile online a valle della presentazione è stato visualizzato da 61 utenti.

3 Presentazione del Progetto 2.7 alla Pitch Marathon della EU Chapter Conference del GCSP “Grand Challenges Scholars Program”

ENEA ha presentato i risultati del progetto 2.7 nel corso della Pitch Marathon organizzata durante la EU Chapter Conference del GCSP “Grand Challenges Scholars Program” e promossa dalla NAE National Academy of Engineering. In particolare, il progetto è stato presentato nel corso della sessione intitolata “Mini-grid models and optimization methods for sustainability (22/03/2021), di cui si riporta di seguito locandina. La presentazione è stata tenuta dalla ricercatrice ENEA Simona De Iulii.



The slide features the ENEA logo and the text 'RICERCA DI SISTEMA ELETTRICO' and 'Accordo di Programma MIT-ENEA'. The main title is 'PROJECT 2.7 - Models and tools to increase energy efficiency along the energy chain, from production and transport to distribution of electricity'. The content includes two main bullet points: one about DC microgrids and intelligent management logic, and another about studying and developing methodologies for AC/DC hybrid grids. A list of specific goals follows, including reliability assessment tools, control actions, energy management logic, and a prototype protection device. The bottom of the slide displays logos for 'NAE GRAND CHALLENGES FOR ENGINEERING', 'AIM SEA', and other partners.

La Pitch Marathon, durata 12 ore, durante le quali sono state presentati modelli, algoritmi e tecnologie del settore delle reti su scala minigrid, ha riscontrato un enorme interesse, con la presenza di 582 partecipanti su Zoom, 6311 visualizzazioni su LinkedIn, 154 Dipartimenti di Ricerca coinvolti provenienti da 49 Paesi rappresentati dai diversi continenti.



22nd of March 2021

PITCH MARATHON
BETWEEN 8.00 A.M. TO 8.00 P.M. (CET)

GRAND CHALLENGES SCHOLARS PROGRAM
(EU CHAPTER CONFERENCE)

MINI-GRID MODELS AND OPTIMIZATION METHODS FOR SUSTAINABILITY, ENERGY SERVICES, AND ZERO-EMISSION MOBILITY

Special Remarks by
GCSP, AIMSEA, ASME E4C, Field Study for Mini Grid Optimization

Link zoom at:

technicalsolidarity.org
tecnologiesolidali.org

info: andrea.micangeli@uniroma1.it



4 Special Session - conferenza EEEIC2021

Nel corso del SAL 2020, è stata organizzata, come già descritto nel Report RdS/PTR(2020)/008, una special session sul tema delle problematiche di affidabilità nelle reti elettriche DC e ibride AC/DC, all'interno della conferenza internazionale EEEIC 2021 - International Conference on Environment and Electrical Engineering. Nel corso della Session, tenutasi il 10/09/2021 e presieduta, in qualità di chair, da Maria Valenti, ricercatrice ENEA, sono stati presentati 7 lavori, come da pagina del programma riportata di seguito. In aggiunta ai lavori specifici sul progetto 2.7, al termine della sessione, in fase di conclusioni, è stato illustrato brevemente il progetto Ricerca di Sistema.



- N4-TS3 218** **A NOVEL TOOL FOR HYBRID AC/DC GRIDS OPTIMIZATION AND RELIABILITY ASSESSMENT**
Mauro Atrigna (ENEA), Giovanna Adinolfi (ENEA - Italian National Agency for New Technologies, Energy and Sustainable Economic Development-), Roberto Ciavarella (ENEA), Giorgio Graditi (ENEA Portici)*, Angelo Merola (ENEA), Antonio Ricca (ENEA), Maria Valenti (ENEA)
- N4-TS3 221** **A RELIABILITY PREDICTION MODEL FOR POWER TRANSFORMERS**
Giovanna Adinolfi (ENEA - Italian National Agency for New Technologies, Energy and Sustainable Economic Development-)*, Mauro Atrigna (ENEA), Roberto Ciavarella (ENEA), Giorgio Graditi (ENEA Portici), Angelo Merola (ENEA), Maria Valenti (ENEA), Antonio Ricca (ENEA)
- N4-TS3 223** **POWERLAB: A FLEXIBLE EXPERIMENTAL ARCHITECTURE FOR SMART MICROGRID TESTING**
giulica sforza (ENEA - Italian National Agency for New Technologies, Energy and Sustainable Economic Development), Giovanna Adinolfi (ENEA - Italian National Agency for New Technologies, Energy and Sustainable Economic Development-), Mauro Atrigna (ENEA), Amedeo Buonanno (ENEA, Department of Energy Technologies and Renewable Energy Sources), Roberto Ciavarella (ENEA), Angelo Merola (ENEA), Francesco Pascarella (ENEA), Antonio Ricca (ENEA), Maria Valenti (ENEA), Giorgio Graditi (ENEA Portici)*
- N4-TS3 228** **EFFECTS OF HEAT WAVES ON THE FAILURE OF POWER DISTRIBUTION GRID: A FAULT PREDICTION SYSTEM BASED ON MACHINE LEARNING**
Mauro Atrigna (ENEA), Amedeo Buonanno (ENEA, Department of Energy Technologies and Renewable Energy Sources), Raffaele Carlì (Politecnico di Bari), Graziana Cavone (Politecnico di Bari), Paolo Scarabaggio (Politecnico di Bari)*, Maria Valenti (ENEA), Giorgio Graditi (ENEA Portici), Mariagrazia Diotoli (Politecnico di Bari)
- N4-TS3 235** **DEVELOPMENT OF AN ENERGY MANAGEMENT SYSTEM FOR AC/DC HYBRID NETWORKS: FROM ABSTRACT FUNCTIONAL REQUIREMENTS TO THE FLEXIBLE TOOL**
Davide Fioriti (DESTEC)*, edit Giovanni Lutzemberger (University of Pisa - DESTEC), Davide Poli (University of Pisa - DESTEC)
- N4-TS3 258** **A SIMULATION ANALYSIS FOR ASSESSING THE RELIABILITY OF AC/DC HYBRID MICROGRIDS – PART I: UNDERGROUND STATION AND CAR PARKING**
Gaetano Zizzo (Università di Palermo)*, Mariano G Ippolito (DEIM - Università di Palermo), Salvatore Favuzza (University of Palermo), Fabio Massaro (University of Palermo), Rossano Musca (University of Palermo), Antonio Bori (UniPa), Vincenzo Porgi (University of Palermo), Salar Moradi (Università di Palermo)
- N4-TS3 259** **A SIMULATION ANALYSIS FOR ASSESSING THE RELIABILITY OF AC/DC HYBRID MICROGRIDS – PART II: PORT AREA AND RESIDENTIAL AREA**
Gaetano Zizzo (Università di Palermo)*, Vincenzo Porgi (University of Palermo), Antonio Bori (UniPa), Salvatore Favuzza (University of Palermo), Fabio Massaro (University of Palermo), Mariano G Ippolito (DEIM - Università di Palermo), Rossano Musca (University of Palermo), Salar Moradi (Università di Palermo)

5 Evento conclusivo del progetto

L'evento conclusivo del progetto è stato organizzato dal Politecnico di Milano in modalità ibrida (in presenza presso il Politecnico e con possibilità di partecipazione da remoto) in data 14/12/2021. L'evento è stato promosso sulla pagina del quotidiano Libertà di Piacenza in data 11/12/2021.

All'evento ha partecipato un elevato numero di studenti stranieri e, pertanto, le presentazioni sono state tenute in lingua inglese.

6 Articoli di disseminazione scientifica

Durante il triennio di progetto, ENEA e i co-beneficiari hanno sottomesso 13 articoli a rivista e/o conferenza internazionale (di cui 7 preparati nel corso del SAL 2020). Di seguito, si riporta elenco dei 13 articoli e si allegano i 5 pubblicati nel corso del SAL 2021 (per gli articoli redatti nel SAL 2020 si veda Report RdS/PTR(2020)/008); un ultimo lavoro è ancora in fase di review.

ENEA

- 1) Adinolfi, G.; Ciavarella, R.; Graditi, G.; Ricca A.; Valenti, M. (2021). "A Planning Tool for Reliability Assessment of Overhead Distribution Lines in Hybrid AC/DC Grids" *Sustainability* 13, no. 11: 6099. <https://doi.org/10.3390/su13116099>.
- 2) Ricca A., Adinolfi G., Caliano M., Graditi G., Valenti M., (2021). Methodologies for power system reliability evaluation: An overview 2021 AEIT International Annual Conference, AEIT 2021, DOI: 10.23919/AEIT53387.2021.9626959.
- 3) Atrigna M.; Adinolfi, G.; Ciavarella R.; Graditi, G.; Merola R.; Ricca, A.; Valenti, M. (2021). A novel Tool for Hybrid AC/DC Grids Optimization and Reliability Assessment, 2021 IEEE International Conference on Environment and Electrical Engineering and 2021 IEEE Industrial and Commercial Power Systems Europe (EEEIC / I&CPS Europe), pp. 1-6, DOI: 10.1109/EEEIC/ICPSEurope51590.2021.9584648.
- 4) Adinolfi G.; Ciavarella R.; Ricca A.; Merola A.; Valenti M.; Graditi, G. (2021). A reliability prediction model for power transformers, 2021 IEEE International Conference on Environment and Electrical Engineering and 2021 IEEE Industrial and Commercial Power Systems Europe (EEEIC / I&CPS Europe), pp. 1-4, DOI: 10.1109/EEEIC/ICPSEurope51590.2021.9584596.
- 5) Sforza, G.; Adinolfi, G.; Atrigna, M.; Buonanno, A.; Ciavarella, R.; Merola, A.; Pascarella, F.; Ricca, A.; Valenti, M.; Graditi, G. (2021). PowerLab: a flexible experimental architecture for smart microgrid testing, 2021 IEEE International Conference on Environment and Electrical Engineering and 2021 IEEE Industrial and Commercial Power Systems Europe (EEEIC / I&CPS Europe), pp. 1-6, DOI: 10.1109/EEEIC/ICPSEurope51590.2021.9584644.

Università di Palermo (UNIPA)

- 6) Mariano, G.; Ippolito, R.; Musca, S.; Zizzo, G. (2021). Frequency dynamics of power systems with temporally distributed disturbances, *Sustainable Energy, Grids and Networks*, Volume 28, 100536, ISSN 2352-4677, <https://doi.org/10.1016/j.segan.2021.100536>.
- 7) Bonì, A.; Favuzza, S.; Ippolito, M.G.; Massaro, F.; Modari, S.; Musca, R.; Porgi, V.; Zizzo, G. (2021). A Simulation Analysis for Assessing the Reliability of AC/DC Hybrid Microgrids – Part I: Underground Station and Car Parking, 2021 IEEE International Conference on Environment and Electrical Engineering and 2021 IEEE Industrial and Commercial Power Systems Europe (EEEIC / I&CPS Europe), pp. 1-6, DOI: 10.1109/EEEIC/ICPSEurope51590.2021.9584826.
- 8) Bonì, A.; Favuzza, S.; Ippolito, M.G.; Massaro, F.; Modari, S.; Musca, R.; Porgi, V.; Zizzo, G. (2021). A Simulation Analysis for Assessing the Reliability of AC/DC Hybrid Microgrids – Part II: Port Area and Residential Area, 2021 IEEE International Conference on Environment and

Electrical Engineering and 2021 IEEE Industrial and Commercial Power Systems Europe (EEEIC / I&CPS Europe), pp. 1-6, DOI: 10.1109/EEEIC/ICPSEurope51590.2021.9584607.

Università di Pisa (UNIFI)

- 9) Fioriti D.; Lutzemberger G. and Poli D., Ricca A., (2022)"Enhanced reliability in AC/DC hybrid networks by predictive Energy Management System", submitted to 2022 IEEE International Conference on Environment and Electrical Engineering and 2022 IEEE Industrial and Commercial Power Systems Europe (EEEIC/I&CPS Europe)- Under Review.
- 10) Fioriti D.; Lutzemberger G. and Poli D. (2021). Development of an Energy Management System for AC/DC hybrid networks: from abstract functional requirements to the flexible tool, *2021 IEEE International Conference on Environment and Electrical Engineering and 2021 IEEE Industrial and Commercial Power Systems Europe (EEEIC / I&CPS Europe)*, pp. 1-6, DOI: 10.1109/EEEIC/ICPSEurope51590.2021.9584645.

Università di Milano (POLIMI)

- 11) Barelli, L.; Cardelli, E.; Pelosi, D.; Ciupageanu, D.A.; Ottaviano, P.A.; Longo, M.; Zaninelli, D. (2022). Energy from the Waves: Integration of a HESS to a Wave Energy Converter in a DC Bus Electrical Architecture to Enhance Grid Power Quality. *Energies* 2022, 15, 10. <https://doi.org/10.3390/en15010010>.
- 12) Longo, M.; Brenna M. and Khan M.A.H. (2021). Adaptive Protection Scheme for AC Microgrids: Simulations for Grid-Connected/Islanded Mode," *2021 6th International Conference on Smart and Sustainable Technologies (SpliTech)*, 2021, pp. 01-06, DOI: 10.23919/SpliTech52315.2021.9566458.
- 13) Navoni I.; Longo M. and Brenna M. (2021). Bidirectional Solid-State Circuit Breakers for DC Microgrid Applications," *2021 IEEE International Conference on Environment and Electrical Engineering and 2021 IEEE Industrial and Commercial Power Systems Europe (EEEIC / I&CPS Europe)*, 2021, pp. 1-6, DOI: 10.1109/EEEIC/ICPSEurope51590.2021.9584802.

6.1 A Planning Tool for Reliability Assessment of Overhead Distribution Lines in Hybrid AC/DC Grids



Article

A Planning Tool for Reliability Assessment of Overhead Distribution Lines in Hybrid AC/DC Grids

Giovanna Adinolfi *, Roberto Ciavarella, Giorgio Graditi, Antonio Ricca and Maria Valenti

Department of Energy Technologies and Renewable Sources, ENEA, 00196 Rome, Italy; roberto.ciavarella@enea.it (R.C.); giorgio.graditi@enea.it (G.G.); antonio.ricca@enea.it (A.R.); maria.valenti@enea.it (M.V.)

* Correspondence: giovanna.adinolfi@enea.it

Abstract: Integration of DC grids into AC networks will realize hybrid AC/DC grids, a new energetic paradigm which will become widespread in the future due to the increasing availability of DC-based generators, loads and storage systems. Furthermore, the huge connection of intermittent renewable sources to distribution grids could cause security and congestion issues affecting line behaviour and reliability performance. This paper aims to propose a planning tool for congestion forecasting and reliability assessment of overhead distribution lines. The tool inputs consist of a single line diagram of a real or synthetic grid and a set of 24-h forecasting time series concerning climatic conditions and grid resource operative profiles. The developed approach aims to avoid congestions criticalities, taking advantage of optimal active power dispatching among “congestion-nearby resources”. A case study is analysed to validate the implemented control strategy considering a modified IEEE 14-Bus System with introduction of renewables. The tool also implements reliability prediction formulas to calculate an overhead line reliability function in congested and congestions-avoided conditions. A quantitative evaluation underlines the reliability performance achievable after the congestion strategy action.

Keywords: congestion logics; failure rate; forecasting; hybrid AC/DC grids; medium voltage distribution grid; reliability assessment; renewables; temperature rise; overhead lines



Citation: Adinolfi, G.; Ciavarella, R.; Graditi, G.; Ricca, A.; Valenti, M. A Planning Tool for Reliability Assessment of Overhead Distribution Lines in Hybrid AC/DC Grids. *Sustainability* **2021**, *13*, 6090. <https://doi.org/10.3390/su13116090>

Academic Editor: Detlef Schulte

Received: 27 April 2021
Accepted: 24 May 2021
Published: 28 May 2021

Publisher's Note: MDPI stays neutral with regard to jurisdictional claims in published maps and institutional affiliations.



Copyright: © 2021 by the authors. Licensee MDPI, Basel, Switzerland. This article is an open access article distributed under the terms and conditions of the Creative Commons Attribution (CC BY) license (<https://creativecommons.org/licenses/by/4.0/>).

1. Introduction

Energy transition is creating a massive renewable introduction in the main AC grid with security and stability possible consequences for the grid itself, and for users and prosumers [1,2]. Electrical systems originally designed to function according to a unidirectional functioning model (unidirectional power flows from large generators to end users), have started to operate according to a bidirectional model, accommodating electricity production from multiple, distributed and intermittent generation sources.

In this context, a modernization process of the electrical networks is necessary to enable advanced monitoring and smart management logics for grid operation to improve efficiency and preserve security and adequacy.

Nowadays, availability of DC-based storage systems, and also generation (photovoltaic and fuel cells) systems and loads, are boosting a novel energy paradigm consisting of DC grids connected to AC grids, i.e., hybrid AC/DC grids.

In particular, the integration of DC microgrids into the AC distribution networks makes it possible to promote DC energy communities (renewables + storage + DC loads) reducing energy losses, increasing grid stability and contributing to congestion solutions.

Congestion problems are more evident where renewables installations are concentrated, and in the presence of low meshed and limited capacity grids. Usually, such criticalities are solved with Renewable Energy Sources (RES) curtailment or shutdown. It is evident that energy transition cannot be implemented with these constraining actions.

Renewable sources have to be integrated and managed, congestion events must be forecast, and grid reliability must be calculated and monitored with the aim of implementing solutions that can preserve power systems safety and adequacy.

In the literature, managing congestion issues has been addressed by preventive or corrective methods. Preventive congestion management methods consider the transmission rights and the available transfer capability. The latter approach focuses on customer information to optimally satisfy consumption profiles in order to mitigate the congestion that causes drawbacks for customers [3]. In particular, the demand-response method is a preventive methodology based on available transfer capability, in which customers participate in some programs devoted to selectively modify consumption curves on the basis of location and time determined by independent operators [1].

Congestion management methods can be also classified in technical and nontechnical (or market) methods. Market methods are characterized by a noncost-free approach, in which network and generation dispatching security factors, congestion pricing and market-based criteria are considered. Such an approach focuses on the actions aimed to correct congestion, set congestion price or system rescheduling by the reduction of trading contracts, transmission plans, the modulation of generation output, load shedding and the implementation of interruptible load rights. Market-based congestion management methods are considered indirect control methods, since they involve the distributed capacity market, shadow price and the flexible market. Dynamic congestion occurs if the power system suffers from large disturbances that cannot be countered by the power of energy traded in the power market [2]; the dynamic congestion management market involves several participants with different market attributes. When a dynamic congestion occurs, resources involved in the dynamic congestion management market are considered by acting operations aimed at minimizing the total dynamic congestion cost of the system [4].

Technical methods neglect economic impact, and only pay attention to the outages along the network [1]. This approach proposes algorithms to improve power capability, decrease system losses and enhance system stability by controlling power flow. Such a congestion management strategy is considered a direct control method and involves distribution network reconfiguration, removal of loads, reduction of distributed energy output, and the control of active and reactive power. Typical examples of direct control methods are load shedding, optimal location of Distributed Generation (DG), generator rescheduling, Optimal Power Flow (OPF), Flexible Alternating Current Transformer System (FACTS) devices and Demand Response (DR) programs [5]. Network reconfiguration was also considered as an effective solution: the literature reported that the optimal network layout could be achieved through a genetic algorithm [6].

In detail, the FACTS devices [7] assure a quick response, allowing an effective modulation of current and system parameters, thus assuring an improvement of system transmission capacity and a reduction of network loss, and, as a consequence, the system stability is achieved.

The power flow management method was analysed by Dolan et al. [8] who proposed two different approaches. The first was modelled as a Constraint Satisfaction Problem (CSP), while the second was based on an Optimal Power Flow (OPF) approach. The two approaches to power flows managing can significantly increase the output of DG units in a thermally constrained network, alleviating line congestion by reducing distributed power output.

Among the direct methods, the management of distributed energy sources arouses great interest in the smart grid-based network scenario. To counter energy congestion due to RES utilization, the increasing of energy reserve in a power system was highlighted as a viable solution [9]. A strategy focused on the control of storage, electric vehicles (EVs), as well as flexible loads connected at the distributed level, increases the availability of active resources that, in turn, enable power system reliability. Congestion management for AC transmission and distribution power systems, and hybrid network reliability have been investigated in several papers in the literature [3,10–13].

Furthermore, reliability aspects of power systems have been considered in the literature with respect to different methodologies, models and by different performance indices [14–16].

In fact, reliability represents a topic of great interest, especially in the latest energetic contexts characterized by huge renewable generation sources injecting energy into the grid. Renewable production reaches high levels at specific hours of the day, causing critical line overloading. Such congestion events cause temperature rise, which can strongly affect the power line's reliability. On the basis of these premises, it is evident that reliability evaluation is an essential study for design, operation and maintenance of power lines in which behaviour can be affected by various stresses [17] such as thermal, electrical, mechanical and environmental effects. It is, therefore, necessary to develop appropriate models able to represent the behaviour of the components or systems of interest in the presence of the aforementioned stresses. Such models can be obtained by analytical and simulation-based statistical methods [18,19].

Analytical methods are based on the representation of a system by means of a mathematical model. In other words, the evaluation of reliability indices is carried out by solving mathematical equations. It is evident that these mathematical equations can be characterized by medium and high complexity degrees with difficult solutions. In these cases, simplified models are used whose solutions can be calculated by approximate analytical techniques. Possible solutions can be obtained also by statistical methods; time-sequential simulations [18,19] are especially used in power systems contexts. These techniques allow the estimation of reliability indices directly by simulating the system under investigation and its components in chronological time.

Fault Tree Analysis [20–22], Failure Mode and Effect Analysis [23], Monte Carlo [19] and Markov chains [24] represent applied methodologies to power systems reliability assessment.

However, a lack of data and research exists on the relationship between congestion management and reliability in hybrid networks. In this paper, we focus attention on this particular aspect to understand the impact of congestion events on overhead reliability performances.

The novel contribution of the proposed methodology consists of the development of a planning tool able to forecast hybrid grid critical operating conditions in order to avoid them, as well as to improve power system line reliability. The proposed control analyses, at 24 h ahead planning stage, the line's reliability and possible grid congestion events. Then, it evaluates the optimal active power dispatching solutions to prevent critical events and improve reliability by involving, as a first step, the resources nearest to the congested area, and then the farthest ones. The proposed tool represents a promising approach to evaluate possible ancillary services (i.e., congestion control logic) on a 24-h ahead horizon-time, also preserving the reliability of the hybrid AC/DC power system components. Thus, it could represent a useful instrument for Virtual Power Plants (VPPs) agents and aggregators during preliminary planning phases and during operating conditions. This paper is organized as follows. Section 2 explains the overhead line electro-thermal model and the reliability prediction model for overhead line characterization. Section 3 presents the proposed tool and a scheme of the congestion algorithm. Section 4 is dedicated to the modified IEEE 14-Bus system as a possible synthetic grid to the developed strategy validation, and achieved results are reported.

2. Overhead Line Electro-Thermal and Reliability Assessment Models

2.1. Grid Lines: Model and Thermal Behavior Study

In the case of industrial or hospital loads, energy distribution takes place through MV lines. Limited lengths characterize such lines to assure low voltage drops. This aspect allows the study of lumped-parameter circuits to model MV line behavior by a series impedance and a shunt admittance (Figure 1), thus neglecting propagative effects.

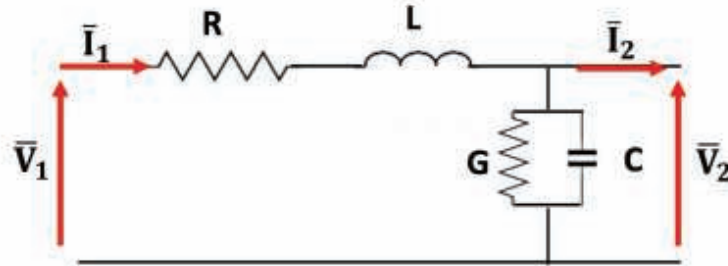


Figure 1. Power line lumped-parameter model.

The reported model can be further simplified for MV short lines as in Figure 2.

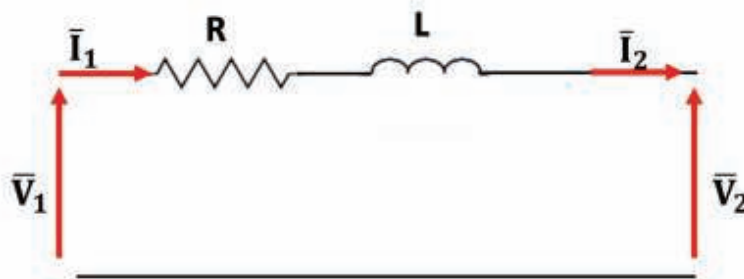


Figure 2. Short line equivalent circuit model.

The considered overhead MV lines have to be characterized considering their thermal behaviour. Actual operating conditions can cause temperature rise events able to impact on overhead line performance. Environmental factors, such as high temperature and low wind velocity, can further worsen line temperature rise due to overloading events. A planning tool for congestion events forecasting and reliability assessment cannot disregard adequate modelling of the cable's thermal behavior. In the literature, numerical simulations or approximated methodologies have been proposed to address this task [25]. In the following, an applied approximated model is described.

In detail, in every infinitesimal time interval dt , the current flowing in a cable produces a temperature variation due to the energy conservation law (Equation (1)).

$$\dot{Q}_{in} + \dot{Q}_{gen} = \Delta\dot{Q}_{stor} + \dot{Q}_{out} \quad (1)$$

where:

\dot{Q}_{in} is the heat flow rate due to the solar radiation on an overhead cable;

\dot{Q}_{gen} is the heat generation rate in a cable due to the line conductor, dielectric, armour and sheath losses;

\dot{Q}_{out} is the dissipated heat flow rate;

$\Delta\dot{Q}_{stor}$ is the heat accumulation rate in the cable.

As a first approximation, \dot{Q}_{gen} is considered as the heat generation rate due to the Joule effect losses in the cable conductor, represented by the formula in Equation (2).

$$d\dot{Q}_{gen} = P_p dt \rightarrow \dot{Q}_{gen} = P_p \quad (2)$$

The produced heat spreads out through the insulating layer according to heat conductive laws, and the \dot{Q}_{stor} and \dot{Q}_{out} terms can be calculated applying Equations (3) and (4) respectively.

$$\dot{Q}_{stor} = m \cdot c_p \cdot \frac{d(\Delta\theta)}{dt} \tag{3}$$

$$\dot{Q}_{out} = U \cdot A \cdot \Delta\theta \tag{4}$$

where:

- m is the cable mass [kg];
- c_p is the cable heat capacity [J/(kg °C)];
- $\Delta\theta$ is the cable temperature rise over ambient temperature [°C];
- $d(\Delta\theta)$ is the temperature rise variation in dt [°C];
- U is the heat transfer coefficient [W/m² °C];
- A is the heat transfer surface [m²].

This paper aims to focus on thermal impact due to overloading conditions, thus neglecting the solar irradiation contribution ($\dot{Q}_{in} = 0$). Mathematical steps obtain the temperature rise formula as reported in Equation (5).

$$\Delta\theta = \frac{P_p}{U \cdot A} \left(1 - e^{-t/T} \right) \tag{5}$$

The multiplicand $\frac{P_p}{U \cdot A}$ represents the steady state temperature rise $\Delta\theta_{ss}$ while $\frac{m \cdot c_p}{U \cdot A}$ is the thermal constant T (Equation (6)).

$$T = \frac{m \cdot c_p}{U \cdot A} \tag{6}$$

So, Equation (5) can be written as the following formula:

$$\Delta\theta = \Delta\theta_{ss} \left(1 - e^{-t/T} \right) \tag{7}$$

The temperature rise tends to $\Delta\theta_{ss}$ value and reaches it in four or five thermal constants. It is worth noting that the $\Delta\theta_{ss}$ value depends on the quantitative evaluation of the cable losses.

In detail, these power losses are due to different phenomena occurring in the cable materials. The Joule effect is responsible for a conspicuous dissipated power in the cable conductor material. Equation (8) reports the formula to calculate these Joule losses.

$$P_p = R \cdot I^2 = \rho \cdot \frac{l}{S} \cdot I^2 \tag{8}$$

where:

- R is the conductor material resistance;
- I is the load current;
- ρ is the conductor material electrical resistivity [Ω m];
- l is the cable length;
- S is the cable cross-sectional area [m²].

Other loss phenomena concern line dielectric, armour and sheath materials [7,26]. In addition, the increasing introduction of electronic converters and inverters in the grid determines the presence of harmonic components with cable temperature increase. This study takes account of these aspects considering corrective factors.

The obtained power loss formula and the cable lateral area, reported in Equation (9), can be substituted in the $\Delta\theta_{ss}$ expression, thus providing Equation (10).

$$A = p \cdot l \tag{9}$$

$$\Delta\theta_{ss} = \frac{\rho \cdot I^2}{U \cdot p \cdot S} \tag{10}$$

where p is the cable perimeter [m].

Furthermore, the thermal constant calculation does not represent a straightforward task since a cable consists of different materials, i.e., the central conductor with insulation, sheath and jacket layers. Different thermal behavior and specific heat capacity characterize each material. In addition, the U value definition requires accurate evaluation. An approximate approach allows simplifying the calculation, taking advantage of $\Delta\theta_{ss}$ formula as reported in Equation (11).

$$U = \frac{\rho \cdot I^2}{\Delta\theta_{ss} \cdot p \cdot S} \tag{11}$$

In addition, considering the volumetric mass density γ , the cable mass can be calculated by Equation (12).

$$m = \gamma \cdot S \cdot l \tag{12}$$

Finally, the substitution of Equations (11) and (12) in the thermal constant formula (Equation (6)) provides the following expression.

$$T = \frac{c_p \cdot \gamma}{\rho} \Delta\theta_{ss} \left(\frac{S}{I}\right)^2 \tag{13}$$

A similar approach can be applied to the cable temperature decrease in the case of load current reduction.

Furthermore, the thermal behaviour of a cable under varying load conditions depends on the flowing current I_c , its duration and on the current value in the preceding interval. The load current produces a temperature rise that can be evaluated by Equation (14).

$$\Delta\theta_c = \Delta\theta_z \left(\frac{I_c}{I_z}\right)^2 \tag{14}$$

where:

I_z is the cable rated current;

$\Delta\theta_z$ is the temperature rise corresponding to a flowing current equal to I_z .

On the basis of the $\Delta\theta_c$ evaluation, the final temperature rises $\Delta\theta_f$ in the time interval t , in which the load current I_c flows in the cable, can be calculated substituting $\Delta\theta$ and $\Delta\theta_{ss}$ terms for $(\Delta\theta_f - \Delta\theta_i)$ and $(\Delta\theta_c - \Delta\theta_i)$ respectively in Equation (7), thus obtaining Equation (15).

$$\Delta\theta_f = \Delta\theta_c - (\Delta\theta_c - \Delta\theta_i) \cdot e^{-\frac{t}{T}} \tag{15}$$

where $\Delta\theta_i$ represents the initial temperature rise.

In the proposed tool, the overhead line temperature rises have been calculated for each forecasting time step considering ambient temperature and load currents graphs, as below reported.

Inputs for the developed subroutine are cables lengths, sections, steady state temperature resistivity, cable perimeters and U coefficients. Load currents are assumed to be balanced among the power system three-phase lines. In this paper ampacity reduction phenomena are neglected to mainly focus attention on overhead line behavior in case of heavy load conditions. Recently, and in coming years, they could represent frequent functioning conditions in the case of not updated energy transmission and distribution systems. In these conditions, the possibility to forecast and avoid congestion events means avoidance of cable damage and customer outage with increased performance in terms of reliability indices.

2.2. Overhead Lines Reliability Assessment

In this section, the focus is on reliability assessment concerning the considered overhead lines. In detail, reliability $R(t)$ is defined as the probability that a product, system or service will perform its intended function adequately for a specified period of time, or it will operate in a defined environment without failure.

Reliability is, therefore, a function of time characterized by a monotonically decreasing graph; it decreases over time in the absence of external interventions.

The concept of reliability is implicitly associated with failure events. Data concerning malfunction, breakdown events and maintenance and repair actions allow assessment of the degree of reliability of nonrepairable and repairable units.

In detail, overhead line $R(t)$ evaluation can be carried out by different models, methodology and standards. In this paper, the Military Handbook 217 [27] is applied considering the approximated overhead lines model (Figure 2). This reliability prediction model is one of the most applied manuals for estimating component reliability. Written for the first time in 1961 [18] for military and aerospace purposes, it has been updated several times over the years, up to the most recent version “Military Handbook, Reliability Prediction of Electronic Equipment”, MIL-HDBK-217, Revision F, Notice 2 [27].

The application of the MIL-HDBK-217 model allows system reliability assessment starting from a single component failure rates calculation. This failure rate is obtained considering a base failure rate λ_b multiplied by π_i factors representative of the different stresses (thermal, environment, electrical, etc) on component reliability. System failure rate is evaluated adequately analysing components subsystems, their series/shunt configurations and calculating the relative reliability indices.

$$\lambda = \lambda_b \cdot \sum_{i,Stresses} \pi_i \tag{16}$$

The reported lines lumped-parameters model permits short line failure rate evaluation considering the series configuration represented by the cable series impedance:

$$\bar{Z} = R + jX \tag{17}$$

According to MIL-HDBK-217F, and to the lumped-parameter models, the resistor and inductor failure rates can be calculated by the following formulas, respectively.

$$\lambda = \lambda_b \cdot \pi_T \cdot \pi_P \cdot \pi_S \cdot \pi_Q \cdot \pi_E \frac{Failures}{10^6 \text{ hours}} \tag{18}$$

$$\lambda = \lambda_b \cdot \pi_T \cdot \pi_Q \cdot \pi_E \frac{Failures}{10^6 \text{ hours}} \tag{19}$$

where:

- π_T is the thermal stress factor;
- π_E is the environment factor;
- π_Q is the quality factor;
- π_P is the power factor;
- π_S is the power stress factor.

The MIL-HDBK-217F provides tables and formulas for the identification and calculation of these factors in specific operating conditions and applications.

The thermal stress factor π_T is a function of the component temperature. In the considered application, this temperature value is calculated taking into account the ambient temperature and line power losses.

Furthermore, the cable longitudinal impedance represents a series connection through which failure rate can be obtained summing the resistive and inductor failure rates.

$$\lambda_{line} = \lambda_R + \lambda_L \tag{20}$$

On the base of the overall system failure rate, the reliability function $R(t)$ can be estimated. In this paper, memory of previous failure events, ageing and further impacting factors are omitted in order to solely evaluate the incidence of congestion events on each line reliability performance. Thus, overhead lines $R(t)$ function is evaluated according to the exponential model as reported in Equation (21).

$$R(t)_{line} = e^{-\lambda_{line}t} \quad (21)$$

where t is the mission time.

3. Hybrid Grids Planning Tool

3.1. Planning Tool Overview

The proposed tool is a planning software tool whose inputs consist of the single line diagram of the grid under investigation and 24-h ahead forecasting time series concerning not only ambient temperature and wind velocity profiles but also RES generations, storage and loads system graphs.

It is based on a Python script interacting with a grid model developed in DlgSILENT Powerfactory environment. Starting from the input data, per each forecasting time step, DlgSILENT Powerfactory executes the Load Flow (LF) calculation. This analysis is used to evaluate grid operating conditions and detect eventual line congestion events. Then LF results are sent to the Python script for evaluating line reliability and, if necessary, congestion avoidance control (Figure 3) is applied.

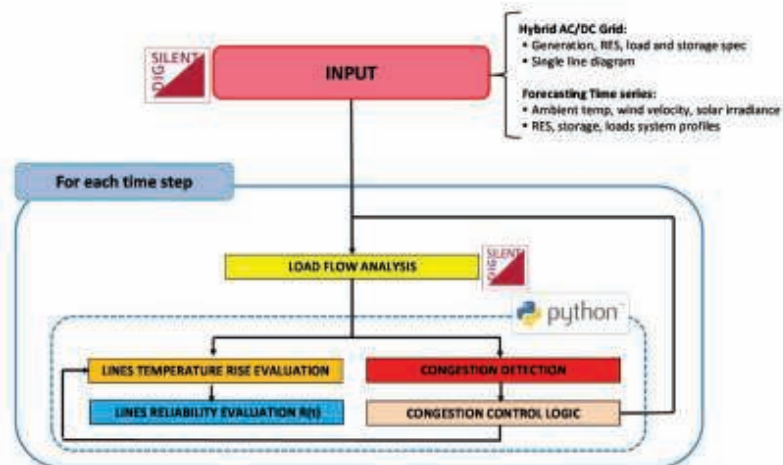


Figure 3. Planning tool schematic representation.

3.2. Congestion Detection Control

In detail, congestion control is synthetically reported in Figure 4. It consists of different functions:

- Congestion Detection;
- Active Power Flexibility Evaluation;
- Sensitivities Analysis;
- Active Power Redispatching;
- Line Reliability $R(t)$ Evaluation

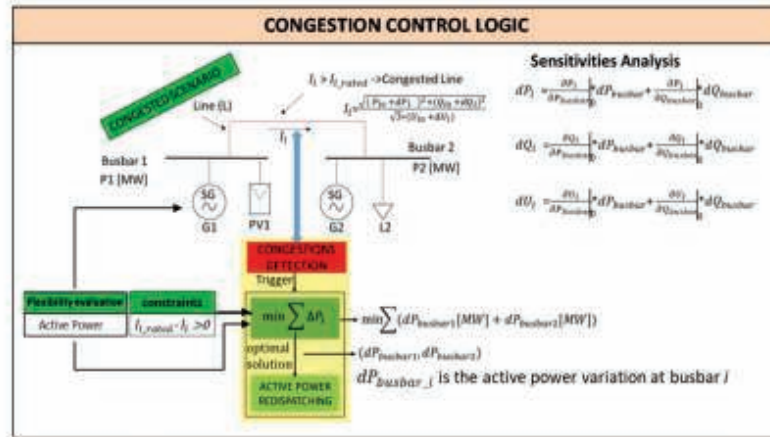


Figure 4. Grid Congestion Management and Lines Reliability Evaluation—main functionalities.

The Congestion Detection function is in charge of continuous grid monitoring; in particular, it measures the current for each line and compares it with line rated current. When the measured current value is greater than the reference value, the active power flexibility evaluation function and the Sensitivities Analysis are triggered.

The Active Power Flexibility function evaluates the active power flexibility made available from each asset in the grid. With this aim, an internal table is created including, for each resource, information (e.g., maximum/minimum active/reactive power per each asset, busbar connected with the asset, etc.) needed to calculate the optimal solution (minimum active power variation at each busbar) and to solve the detected congestion problems. The implemented optimization function [5,7,26] is:

$$f = \min \left(\sum_{i=1}^{N_{busbar}} \left(\Delta P_{busbar_i}^+ + \Delta P_{busbar_i}^- \right) \right) \quad (22)$$

where:

$\Delta P_{busbar_i}^+$ is the positive active power variation at busbar i ;

$\Delta P_{busbar_i}^-$ is the negative active power variation at busbar i ;

N_{busbar} is the total number of busbars.

The optimization problem constraint is:

$$I_j - \frac{\sqrt{\left(P_j^0 + \frac{\partial P_j}{\partial P_i} \cdot \Delta P_{busbar_i} + \frac{\partial P_j}{\partial Q_i} \cdot \Delta Q_{busbar_i} \right)^2 + \left(Q_j^0 + \frac{\partial Q_j}{\partial P_i} \cdot \Delta P_{busbar_i} + \frac{\partial Q_j}{\partial Q_i} \cdot \Delta Q_{busbar_i} \right)^2}}{\sqrt{3} \cdot \left(U_j^0 + U_{Nom_j} \cdot \left(\frac{\partial V_j}{\partial P_i} \cdot \Delta P_{busbar_i} + \frac{\partial V_j}{\partial Q_i} \cdot \Delta Q_{busbar_i} \right) \right)} \geq 0 \quad \forall i, j \quad (23)$$

where:

I_j is the rating current value of line j ;

P_j^0 is the active power initial condition that flows through line j ;

Q_j^0 is the reactive power initial condition that flows through line j ;

P_j is the active power that flows through line j ;

Q_j is the reactive power that flows through line j ;

$\frac{\partial P_j}{\partial P_i}$ is the effect on active power of the injection of ΔP at busbar i for line j ;

$\frac{\partial P_j}{\partial Q_i}$ is the effect on active power of the injection of ΔQ at busbar i for line j ;

$\frac{\partial Q_j}{\partial P_i}$ is the effect on reactive power of the injection of ΔP at busbar i for line j ;

$\frac{\partial Q_j}{\partial Q_i}$ is the effect on reactive power of the injection of ΔQ at busbar i for line j ;

U_j^0 is the voltage initial condition for line j ;
 U_{Nom_j} is the nominal voltage for line j ;
 $u_j = \frac{U_j}{U_{N_j}}$ where U_j is the voltage of the line j .

The formula represents the difference between the line rating current and the line current based on the active and reactive power variation of the resources. All derivatives in Equation (23) are calculated with the Load Flow sensitivities function provided by DigSILENT Powerfactory environment.

Once the optimal solution in terms of minimal active power variation at each Busbar is calculated, the active power redispatching function is activated. This function performs the following steps:

- a list is defined for each grid busbar with the connected assets;
- a priority list is defined for the active power redispatching based on the optimal solution;
- the reliability assessment is carried for each grid line after the control action.

The developed control strategy is able to localize the instability event and to solve the detected issues involving more suitable local resources (optimal solution).

The effectiveness of the proposed methodology is verified investigating the modified IEEE 14-Bus System above reported.

4. Case Study and Results

To test the proposed logic performance, a hybrid synthetic grid model was carried out modifying the IEEE 14 Bus System. Then, the developed tool was applied to this synthetic grid to evaluate how the control logics perform when power grid congestion problems occur due to a high RES generation presence.

In detail, the IEEE 14 Bus System is an AC grid representing a Midwest United States power system simplified model constituted by fourteen AC buses, five generators, sixteen lines and eleven loads. The related graph is reported in Figure 5. It was studied by the single line diagram provided by DigSILENT Powerfactory software. In detail, this power system is characterized by the reference machine G1 and the synchronous machine G2 which inject active power and regulate connected buses voltage levels. The other three generators are synchronous compensators absorbing and injecting reactive power from/into the AC grid. Five transformers adjust bus voltage levels. Eleven loads are distributed in the grid absorbing active and reactive power by the power system lines.

The synthetic grid was modified to obtain a hybrid AC/DC grid including DC renewables generators, loads and storage systems. In detail, the hybrid IEEE 14-Bus System results already characterized by fourteen AC buses but further DC busbars are added. MV Busbar_DC₁ and Busbar_DC₂ are connected to AC BUS_0013 and BUS_0014, respectively, as reported in Figure 6. Two additional bidirectional DC/AC converters interface the original buses with the new DC ones, allowing DC RES (such as PhotoVoltaic (PV) generators) and DC loads connection. Overhead lines, whose model is described above, characterize the hybrid IEEE 14-Bus system.

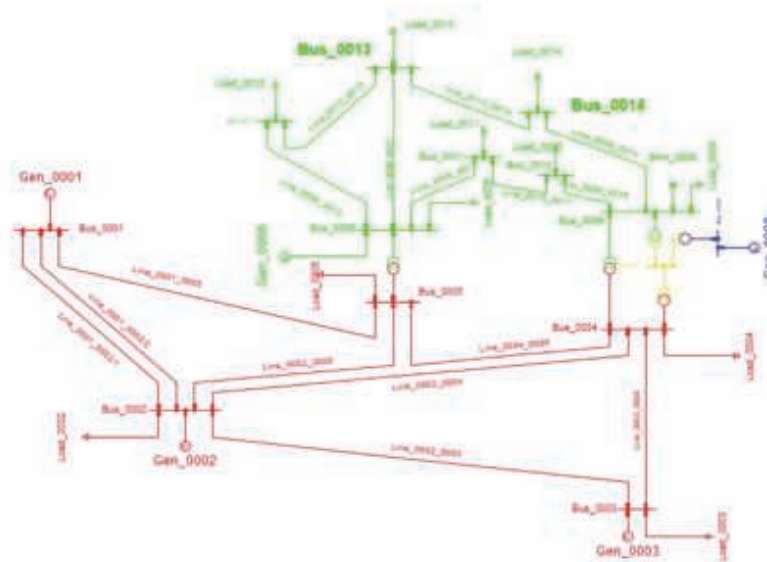


Figure 5. IEEE 14 Bus System.

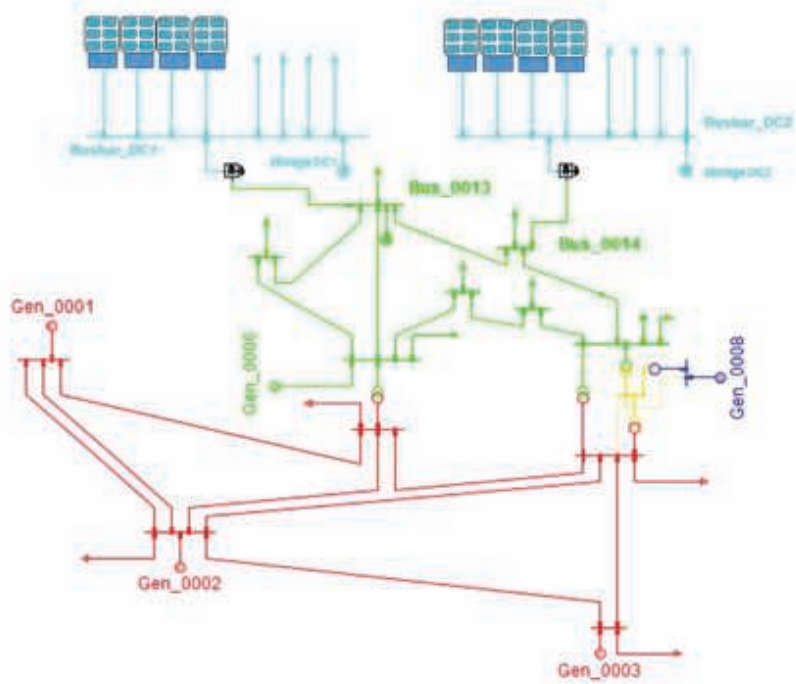


Figure 6. Hybrid IEEE 14-Bus System.

After the DigSILENT Powerfactory grid model was constructed, the operating conditions were customized by integrating the time series of loads and generation resources (24-h ahead values) into the model. Then, a preliminary LF analysis was carried out for estimating the line loading levels and their reliability.

Figure 7 shows the maximum line loading obtained per each time step. At time steps 53, 54 and 55 the maximum loading is equal to 98.78%, 110.33% and 98.82% respectively. These percentages results are higher than the loading level threshold set for the control activation. In particular, the AC Line_0006_0013 and the AC Line_0009_0014 lines result in congested conditions.

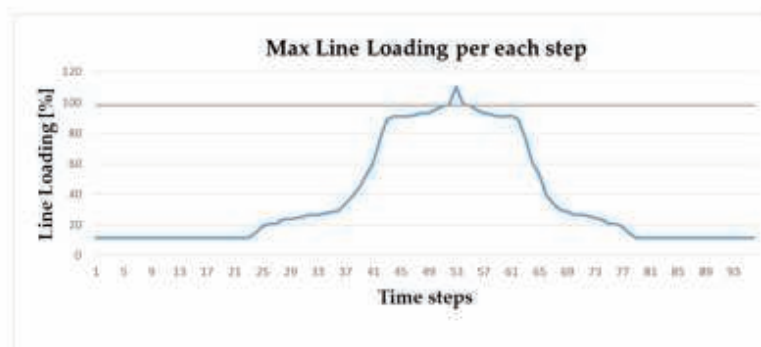


Figure 7. Max line loading per each time step: congested scenario.

The control calculates the optimal solution for each congested time step in order to solve the detected problems and improve the congested line's reliability as shown in the following figures. In detail, Figure 8 shows the maximum line loading per each time step before and after the control action.

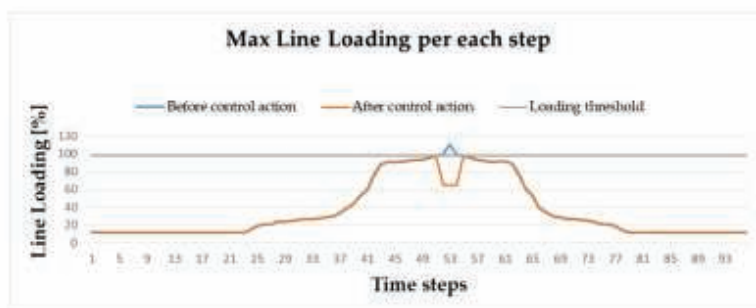


Figure 8. Max Line Loading per each time step before and after control action.

The implemented control action permits forecasting to avoid lines congestion problems. In fact, optimum dispatching among grid resources allows active power management, preventing overloading conditions. Furthermore, the control action determines a positive reliability variation for congested lines and other grid lines. Insignificant reliability worsening occurs only for a few lines. Therefore, the proposed control strategy globally improves line reliability performance as shown in Figure 9.

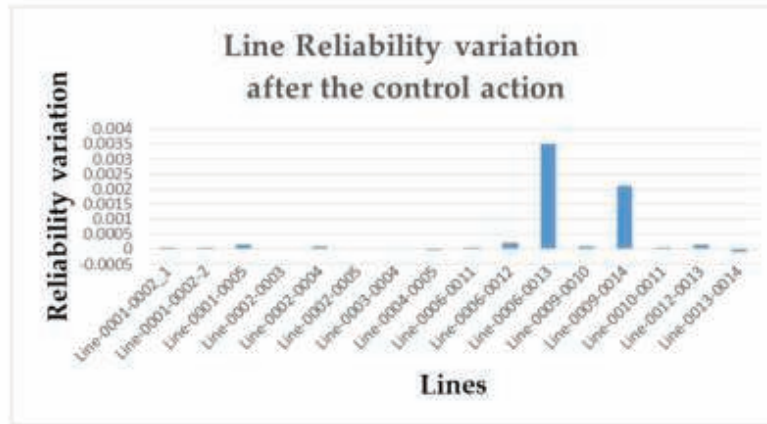


Figure 9. Line reliability variation after the control action.

In addition, Figure 10 shows a comparative analysis among line temperature rise before and after control action. Temperature rises tend to decrease for each grid line, especially in the case of congested lines where temperature decrease is approximately 10 °C.

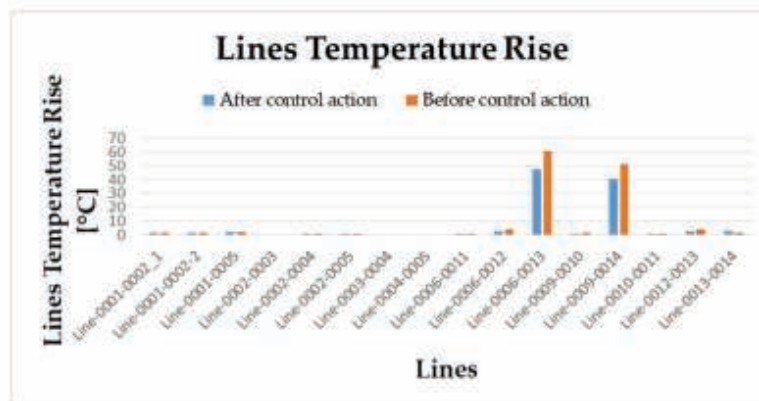


Figure 10. Line temperature rise comparison.

Finally, the proposed control is able to localize the instability event and solve it by optimum involvement of local available resources. In the analyzed case study, the congestion issue is due to high RES introduction in the main AC grid. Since RES are connected to DC buses, the congestion control avoids a line overloading event due to renewables generation involving storage systems connected to DC buses, as shown in Figure 11.

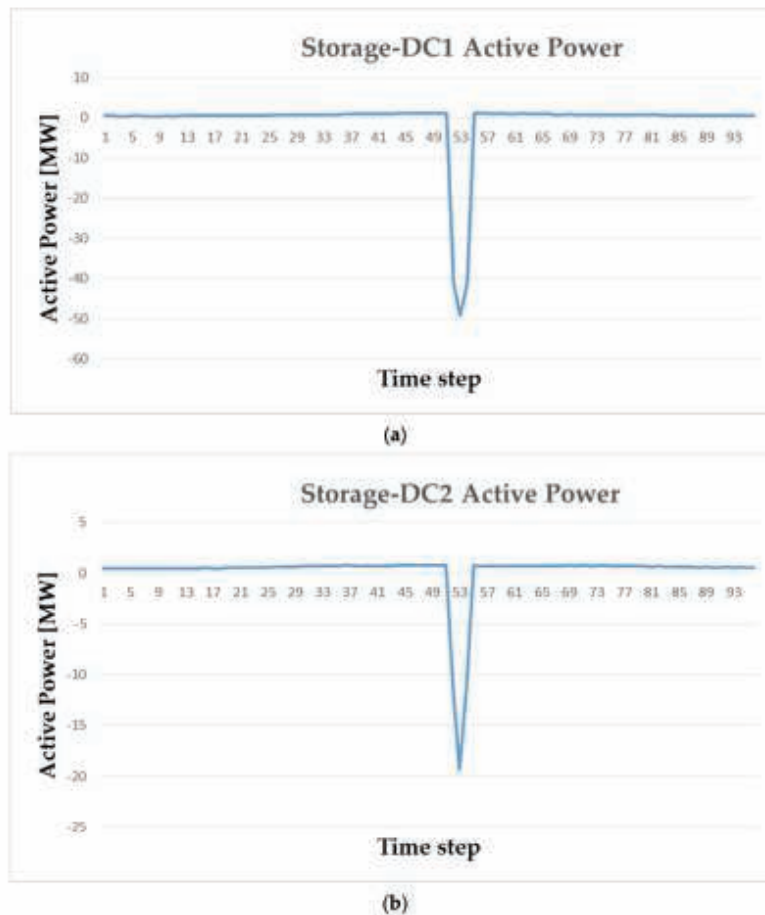


Figure 11. Storage systems operating conditions: (a) Storage-DC1; (b) Storage-DC2.

5. Discussion

The developed planning tool to forecast and avoid congestion events implements a strategy also able to improve overhead line reliability. It is characterized by the novel concept of solving the issues by prioritizing grid resources closely placed to the cause of the critical events. As shown in the considered case study, congestion issues caused by renewables are solved involving a local storage resource. This approach permits minimization of the critical event's impact on the hybrid power system lines, assuring reliability performance improvement.

Without loss of generality, the proposed strategy can be applied to different power grid architectures and future configurations [28–30], including different RES generators, storage technologies, load systems and various operative profiles.

6. Conclusions

In this paper, a planning tool for congestion events forecasting and reliability assessment in the case of overhead lines is developed with particular attention to a novel energy paradigm represented by hybrid grids. Line electro-thermal models and reliability

prediction formulas are implemented to correctly carry out real and synthetic grid load flow analysis.

A congestion strategy is proposed. It represents a novel control logic since a “closed-congestion” approach is activated to optimally dispatch active power among grid resources near the congested overhead line, with a limited impact on the hybrid AC/DC grid.

The methodology validation is carried out considering a modified IEEE 14-Bus system to permit RES introduction and DC bus connection to the main AC grid. The obtained hybrid grid permits analysis of a high RES penetration scenario. Results demonstrate the proposed strategy effort in avoidance of congestion events, also determining line reliability improvement for the congested lines and the whole hybrid grid. The tool could represent promising software to support VPPs agents and aggregators to forecast criticalities and reliability performance in order to provide ancillary services.

Author Contributions: Conceptualization: G.A. and R.C.; methodology: G.A. and R.C.; model implementation: G.A. and R.C.; data curation: G.A., R.C., G.G., A.R. and M.V.; writing, review and editing: G.A., R.C., G.G., A.R. and M.V. All authors have read and agreed to the published version of the manuscript.

Funding: This research was funded by the Research Fund for the Italian Electrical System under the Contract Agreement “Accordo di Programma 2019–2021—PTR_19_21_ENEA_PRG_10” between ENEA and the Ministry of Economic Development.

Institutional Review Board Statement: Not applicable.

Informed Consent Statement: Not applicable.

Data Availability Statement: Not applicable.

Conflicts of Interest: The authors declare no conflict of interest.

References

- Dehnavi, E.; Abdi, H. Determining Optimal Buses for Implementing Demand Response as an Effective Congestion Management Method. *IEEE Trans. Power Syst.* **2016**, *32*, 1. [\[CrossRef\]](#)
- Yuan, C.; Hu, C.; Li, T. Review of Congestion Management Methods for Power Systems. *IOP Conf. Ser. Earth Environ. Sci.* **2019**, *233*, 032025. [\[CrossRef\]](#)
- Pillay, A.; Prabhakar Karthikeyan, S.; Kothari, D.P. Congestion management in power systems—A review. *Int. J. Electr. Power Energy Syst.* **2015**, *70*, 83–90. [\[CrossRef\]](#)
- Jin, M.; Song, Y.H.; Qiang, L.; Shengwei, M. Dynamic Congestion Management in Open Electricity Markets. *Autom. Electr. Power Syst.* **2004**, *10*, 23–28.
- Ciavarella, R.; Di Somma, M.; Graditi, G.; Valenti, M. Congestion Management in distribution grid networks through active power control of flexible distributed energy resources. In Proceedings of the 2019 IEEE Milan PowerTech, Milan, Italy, 23–27 June 2019; pp. 1–6.
- Shariatkhah, M.H.; Haghifam, M.R. Using feeder reconfiguration for congestion management of smart distribution network with high DG penetration. In Proceedings of the CIRED 2012 Workshop: Integration of Renewables into the Distribution Grid, Lisbon, Portugal, 29–30 May 2012; pp. 1–4.
- Graditi, G.; Ciavarella, R.; Di Somma, M.; Valenti, M. A control strategy for participation of DSO flexible resources in TSO ancillary services provision. In Proceedings of the ICCEP 2019: 7th International Conference on Clean Electrical Power: Renewable Energy Resources Impact, Otranto, Italy, 2–4 July 2019; pp. 586–592.
- Dolan, M.J.; Davidson, E.M.; Kockar, I.; Ault, G.W.; McArthur, S.D.J. Reducing Distributed Generator Curtailment Through Active Power Flow Management. *IEEE Trans. Smart Grid* **2014**, *5*, 149–157. [\[CrossRef\]](#)
- Hirth, L.; Ueckerdt, F.; Edenhofer, O. Integration costs revisited—An economic framework for wind and solar variability. *Renew. Energy* **2015**, *74*, 925–939. [\[CrossRef\]](#)
- Ni, L.; WEN, F.; LIU, W.; MENG, J.; LIN, G.; DANG, S. Congestion management with demand response considering uncertainties of distributed generation outputs and market prices. *J. Mod. Power Syst. Clean Energy* **2017**, *5*, 66–78. [\[CrossRef\]](#)
- Hazra, J.; Das, K.; Seetharam, D.P. Smart grid congestion management through demand response. In Proceedings of the 2012 IEEE Third International Conference on Smart Grid Communications (SmartGridComm), Tainan, Taiwan, 5–8 November 2012; pp. 109–114.
- Sagwal, R.; Kumar, A. Congestion Management Solution for Hybrid System Considering Voltage Stability Margin. *Procedia Technol.* **2016**, *25*, 726–734. [\[CrossRef\]](#)

13. Asija, D.; Choudekar, P. Congestion management using multi-objective hybrid DE-PSO optimization with solar-ess based distributed generation in deregulated power Market. *Renew. Energy Focus* **2021**, *36*, 32–42. [[CrossRef](#)]
14. Billinton, R.; Allen, R.N. *Reliability Assessment of Large Electric Power Systems*; Kluwer Academic Publishers: Norwell, MA, USA, 1988.
15. Adinolfi, G.; Ciavarella, R.; Merola, A. *Analisi e Valutazione Preliminare Delle Problematiche di Affidabilità Delle reti di Distribuzione Ibride AC/DC; Deliverable RdS/PTR2019/159, PROJECT 2.7 Contract Agreement "Accordo di Programma 2019–2021—PTR_19_21_ENEA_PRG_10"*; ENEA and the Ministry of Economic Development: Roma, Italy, 2019.
16. Adinolfi, G.; Atrigna, M.; Ricca, A.; Valenti, M. *Studio Degli Standard e Analisi dei Modelli di Riferimento per la Stima Dell'affidabilità di Componenti e Apparat Delle reti Ibride AC/DC; Deliverable RdS/PTR2019/160, PROJECT 2.7 Contract Agreement "Accordo di Programma 2019–2021—PTR_19_21_ENEA_PRG_10"*; ENEA and the Ministry of Economic Development: Roma, Italy, 2019.
17. Passarelli, G. *Modelli Affidabilistico-Diagnostici per i Componenti Delle reti Elettriche*; Alma Mater Studiorum—Università di Bologna: Bologna, Italy, 2008.
18. Allan, R.N.; Billinton, R.; Breipohl, A.M.; Grigg, C.H. Bibliography on the application of probability methods in power system reliability evaluation. *IEEE Trans. Power Syst.* **1999**, *14*, 51–57. [[CrossRef](#)]
19. Allan, R.N.; Bhuiyan, M.R. Effects of failure and repair process distribution on composite system adequacy indices in sequential Monte Carlo simulation. In Proceedings of the Joint International IEEE Power Conference, Power Tech, Los Alamitos, CA, USA, 5–8 September 1993; pp. 622–628.
20. Haasl, D.F.; Roberts, N.H.; Vesely, W.E.; Goldberg, F.F. *Fault Tree Handbook*; Office of Nuclear Regulatory Research: Washington, DC, USA, 1981.
21. Dugan, J.B.; Bavuso, S.J.; Boyd, M.A. Dynamic fault-tree models for fault-tolerant computer systems. *IEEE Trans. Reliab.* **1992**, *41*, 363–377. [[CrossRef](#)]
22. Rao, K.D.; Rao, V.V.S.S.; Verma, A.K.; Srividya, A. *Dynamic Fault Tree Analysis: Simulation Approach BT—Simulation Methods for Reliability and Availability of Complex Systems*; Faulin, J., Juan, A.A., Martorell, S., Ramirez-Márquez, J.-E., Eds.; Springer: London, UK, 2010; pp. 41–64. ISBN 978-1-84882-213-9.
23. Stamatis, D.H. *Failure Mode and Effect Analysis: FMEA from Theory to Execution*; ASQ Quality Press: Milwaukee, WI, USA, 2003.
24. Ibe, O. Continuous-Time Markov Chains. In *Markov Processes for Stochastic Modeling*, 2nd ed.; Elsevier: Oxford, UK, 2013; pp. 85–102.
25. Enescu, D.; Colella, P.; Russo, A. Thermal Assessment of Power Cables and Impacts on Cable Current Rating: An Overview. *Energies* **2020**, *13*, 5319. [[CrossRef](#)]
26. Graditi, G.; Di Somma, M.; Ciavarella, R.; Valenti, M.; Cigolotti, V.; Kadam, S.; Brunner, H.; Sosnina, M.; Khavari, A.; Calin, M.; et al. "Project Handbook (DoW)" *Deliverable D1.5 INTERPLAN Project*; European Commission: Brussels, Belgium, 2018.
27. Defense Standardization Program Office (DSPO). *Reliability Prediction of Electronic Equipment (Military Handbook)*; Department of Defense: Washington, DC, USA, 1991; p. 205.
28. Graditi, G.; Adinolfi, G. Temperature influence on photovoltaic power optimizer components reliability. In Proceedings of the International Symposium on Power Electronics Power Electronics, Electrical Drives, Automation and Motion, Sorrento, Italy, 19 June–22 July 2012; pp. 1113–1118.
29. Scognamiglio, A.; Adinolfi, G.; Graditi, G.; Saretta, E. Photovoltaics in Net Zero Energy Buildings and Clusters: Enabling the Smart City Operation. *Energy Procedia* **2014**, *61*, 1171–1174. [[CrossRef](#)]
30. Catelani, M.; Ciani, L.; Graditi, G.; Adinolfi, G. Measurement and Comparison of Reliability Performance of Photovoltaic Power Optimizers for Energy Production. *Metro. Meas. Syst.* **2015**, *22*, 139–152. [[CrossRef](#)]

6.2 Methodologies for power system reliability evaluation: An overview

Methodologies for power system reliability evaluation: an overview

Antonio Ricca
 Department of Energy Technologies
 and Renewable Sources - ENEA
 Portici (NA), Italy
 antonio.ricca@enea.it

Giovanna Adinolfi
 Department of Energy Technologies
 and Renewable Sources - ENEA
 Portici (NA), Italy
 giovanna.adinolfi@enea.it

Martina Caliano
 Department of Energy Technologies
 and Renewable Sources - ENEA
 Portici (NA), Italy
 martina.caliano@enea.it

Giorgio Graditi
 Department of Energy Technologies
 and Renewable Sources - ENEA
 Portici (NA), Italy
 giorgio.graditi@enea.it

Maria Valenti
 Department of Energy Technologies
 and Renewable Sources - ENEA
 Portici (NA), Italy
 maria.valenti@enea.it

Abstract— The need to increase electrification together with larger shares of variable power generation sources makes the electrical power system reliability an even more important topic. However, reliability assessment is a complex task due to the dependence on experimental data and insufficient statistical general information. The presence of new technologies and renewable energy integration into the power systems worsen this issue. Different reliability prediction models, methods and related metrics are described in this paper to provide a reference summary for the power system context.

Keywords— failure rate, FTA, Markov, Monte Carlo, reliability

I. INTRODUCTION

Reliability evaluation of power systems is a complicate analysis due to the intrinsic complexity of an electrical grid, containing many components and subsystems, and to the relevant number of stresses impacting on each component.

Reliability of a device or a system is the probability that it will perform effectively for a specified period of time under stated use conditions. In particular, the reliability is a monotone decreasing function of time, represented as $R(t)$, which becomes 0 at an infinite time. In fact, the probability that a system will satisfactorily work after an infinite time is null without external actions. Therefore, from a mathematical point of view, the domain of $R(t)$ is the interval $[0, 1]$, and the initial value of the function is not necessarily equal to 1. The concept of reliability is strictly related to the failure: information about malfunctioning, failure, maintenance and fixing procedures allows evaluating, along the time, the reliability degree of repairable and non-repairable units.

In an electrical system, usually constituted by several components, the failure event represents the malfunctioning (transitory or permanent) of at least one of its components. More in the detail, the reliability is defined as the ability of an electrical system to continuously provide the desired electrical power to final users within defined standards.

Electrical systems reliability can be evaluated by [1]:

- Adequacy, as the system ability to satisfy the energy demand by respecting safety and quality requirements;
- Safety, as the system ability to face the changes of the operating state of the system within operating limits.

Since the premises, it is clear that reliability analysis and failure rate evaluation become a crucial study for the design, operation and the maintenance of the electrical systems, as well as for the new infrastructures.

The failure is the interruption of the ability of a device to fulfil the required function. The time-to failure is the useful lifetime for a component (or a system); in other words, it is the time between the commissioning and the recording of the first malfunctioning. By considering a complex system, or a stock of a wide quantity of devices, $n_p(t)$ represents the number of failures recorded for the referenced samples at time t , and $n_p(t + \delta t)$ the number of failures recorded at time $t + \delta t$. The failure rate $h(t)$ is defined as reported in (1). Of course, the failure rate unit is the inverse of a time [h^{-1}].

$$h(t) = \lim_{\delta t \rightarrow 0} \frac{n_p(t+\delta t) - n_p(t)}{n_p(t) \cdot \delta t} \quad (1)$$

A typical representation of the failure rate is the Bathtub curve (Fig. 1), in which 3 sectors can be identified.

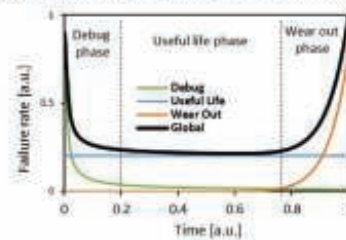


Fig. 1. Bathtub curve

The first part of the curve represents the early failure zone characterized by the Debug phase, in which failures rates are relatively high due to fabrication defects, design errors, or troubles related to inappropriate usage of the device/system. However, the probability of early failures decreases along the time. In fact, it is reasonable that such problems should be detected, debugged and fixed in the product developing and innovation phases. Therefore, the “infant mortality” curve is characterized by a quick decreasing in the time.

The central part of the Bathtub curve is characterized by the Normal Life (or Useful Life) phase. A device “surviving” to the debug phase is likely free of fabrication defects and has been correctly installed: thus, the device can be started for the

regular working. In this phase, random failures can occur, and the conditional failure probability is constant along the whole phase, thus the failure rate appears constant. Such failures can be due to unappropriated device employment, worse maintenance, or accidents. The failure risk in this phase can be reduced by both improving operation check and scheduling adequate maintenance methodologies.

The final part of the Bathtub curve represents the Wear-Out phase, in which failures can occur for device aging. In this phase, the failure probability increases along the time, due to wearing out of the devices or to embrittlement of components. The failure rate can be reduced by replacing the aged components (or more sensitive to wear-out phenomena), and by adopting an appropriate maintenance philosophy.

Of course, the extension of each sector of the Bathtub curve strictly depends on device or component characteristics. From a mathematical point of view, the time dependence of the failure rate can be represented by (2). In the reported expression, β characterizes the failure rate curve in the three sectors. In particular, if $\beta < 1$ the failure rate decreases along the time, thus describing the debug phase. In the case $\beta = 1$, the failure rate becomes constant (h_0 , also indicated as λ_0). Finally, if $\beta > 1$, the failure rate increases along the time, thus describing the wear-out phase.

$$h(t) = h_0 \cdot t^{\beta-1} \quad (2)$$

An extension for the hazard curve, related to the maintenance operations (both occasional or scheduled), is the sawtooth bathtub curve. Such variation accounts to periodic maintenance operations on components for which wearing-out phenomena are more relevant. Whereas the periodic maintenance is not applied, reliability will quickly degrade and the probability of a failure occurring increases accordingly. If a perfect maintenance is carried out on the components, the failure rate is reduced to the same level each time: a similar condition is represented in the Bathtub curve as the typical sawtooth trend (Fig. 2).

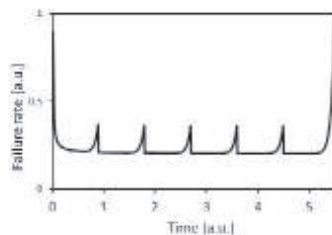


Fig. 2. Sawtooth bathtub curve

However, the ideal maintenance never exists, and the component reliability will usually be a bit worse than the last time maintenance was performed. Moreover, after each maintenance, a short and transitory increasing of failure rate similar to the debug phase is observed, due to errors in maintenance or assembling procedures.

A. Metrics and reliability indexes

The evaluation of metrics and reliability indexes is generally based on three key factors: interruption frequency, interruption duration, severity/entity of the interruption. The first two factors are relevant to the user and utility points of

view, while latter factor relies to the number of affected users, or to the load priority [2].

Reliability metrics are tools to quantitatively evaluate the reliability of an electrical grid, or a portion of it. The option of which metric is to be used depends upon the system to which it applies and the application domain. In a general point of view, metrics application allows to evaluate the reliability indexes for an electrical system. MTTF (Mean Time To Failure) and MTBF (Mean Time Between Failure) are two of the more widely used indexes.

MTTF represents the mean time between the system commissioning and the failure. Obviously, it is a statistical value, to be intended as an average value upon a long period and a wide number of units. MTBF is the average time between two consecutive failures; such concept implicates that a failed component should be fixed and re-commissioned. It is the widest used index for the reliability estimation. The MTTR (Mean Time To Repair) index is introduced beside the MTBF index: it is the mean time needed to fix a failure in a device or in a system.

From a mathematical point of view, the correlation between these 3 indexes is reported in (3).

$$MTBF = MTTF + MTTR \quad (3)$$

II. PREDICTIVE METHODS FOR ELECTRICAL COMPONENTS RELIABILITY EVALUATION

The operation along the time of the single units constituting an electrical system can be affected by several factors, as thermal, electrical, and mechanical stresses. Therefore, appropriate lifetime models are needed to represent components and systems behavior under the reliability aspect. The lifetime model is based on theoretical studies and experimental tests in which stocks of a specific component are considered, and an analysis on its functionality after one or more simultaneous stresses was carried out. Dedicated accelerated tests can be set to achieve failure rate and repair rate (if available) for many devices. In addition, the application of statistical approaches allows identifying expressions that well represents the experimental data, thus allowing the identification of a phenomenological life model for the component under investigation. Arrhenius-based model [3] is a typical example of phenomenological model; it is applied in several contexts, and contemplates the effects of thermal stresses on the reliability. The consequences of electrical stresses can be evaluated through the Inverse Power Model (IPM) [3]: such model enables studying the effects of electrical fields on insulations life. To evaluate the effect of two or more simultaneous stresses, several models can be applied: the synergic effect of several stresses cannot be evaluated as the sum of the effects of each stress, but it is usually the most severe effect. In the sectors for which there is an advanced knowledge of phenomena and chemical-physical processes affecting the behavior of some devices, theoretical studies based on physical models and chemical-physical mensuration are available [3] for the definition of reliability model. Whereas the maturity level is not advanced, usually probabilistic reliability models are applied. In the detail, such models are based on the supposition that the failure event can be represented as a random variable, and can be modelled through probability theories, based on parameters achieved in experimental tests.

Several Reliability Prediction Models are available for electronic systems and subsystems belonging electrical grids and micro-grids. Such models allow the quantitative estimation of reliability, starting by a base failure rate for each component (achieved through experimental and field data), corrected with π factors related to the different stresses and, in specific cases, with additional factors characterizing the base system. Every reliability prediction model provides formula and tables for the evaluation of π factors related to the components in the specific investigated operating condition [4]. It is worth noting that there is no universally valid model for a specific component or system since each reliability model is determined not only in relation to the specific stresses but also to the application and operation context of reference.

A. Military Handbook 217

The Military Handbook (MIL-217) is one of the most applied models for the reliability prediction of electronic components. It was edited the first time in the 1961 [5] for military and aerospace purposes, and was updated several times along the years, up to the last version "Military Handbook Reliability Prediction of Electronic Equipment" MIL-HDBK-217, Revision F, Notice 2 [6].

The application of MIL-217 allows an analytical evaluation of failure rate and MTBF values for each component, for the devices, and for the overall electrical system. The overall failure rate estimation is based on the roll-up of all failure rates of the involved components.

In the manual, two predictive approaches are proposed: Part Stress Analysis and Part Count Analysis; such approaches differ each other mainly for the level of information required for their application. In particular, the Part Stress Analysis requires a wider amount of information, and it is typically applicable to the detailed design; the Part Count Analysis requires less information, and it is mainly applied in the preliminary design phase. Of course, the latter presents less accurate results with respect to the former one, and typically provides significantly higher failure rate values.

The Part Count Analysis (PCA) is usually employed in the early stage of the design process, or in the proposal and bidding compilation phase. At this stage, design evaluation and specifications, allocations, etc. can be estimated through preliminary data on reliability prediction. Naturally, in this design stage, not all the operating parameters required for accurate reliability evaluations are available; it is widely accepted that, along the design process, the reliability analysis moves to the Part Stress Analysis as the devices under design are more accurately outlined. Such approach allows an uncertainty minimization for the failure rate evaluation, thus converging to more realistic reliability values.

Very few information is necessary for the PCA-based reliability evaluation: basically, the failure rate of a device (or a system) is achieved by the sum of the failure rates of all the components of the system. The MIL-217 handbook provides tables for each components category reporting failure rates and (eventually) the Quality Factors for several contexts.

The Part Stress Analysis (PSA) is applied in the detail design phase, and refers to the real operating conditions (temperature, voltage, current, power levels, etc.), by focusing on the effect of such stresses on the device reliability [7], [8]. The MIL-217 handbook categorizes the main electronic components: each category is further divided in several sub-

categories, to provide unique models as close as possible to the component under investigation. Once estimated the failure rates of each part, the failure rate of a complex system is calculated by the combination of parts failure rates according to their series or parallel logical connections.

In a general point of view, the failure rate is determined starting from a base value, corrected by means of several factors accounting the specific stresses (4).

$$\lambda = \lambda_b \cdot \pi_Q \cdot \pi_E \cdot \pi_T \sum_{Other\ Stresses} \pi_i \quad (4)$$

In (4), λ_b represents the base failure rate of the component, referred to normal environment conditions, performing the intended functions, using the default quality level for the component, and operating at the design stress levels.

The π_Q parameter represents the Quality Factor of the component, aiming to correct the failure rate on the basis of the construction quality of the investigated component. In the MIL-217, several π_Q values are provided for a lot of electronic components and are related to specific quality levels.

The π_E parameter represents the Environment Factor: it accounts for the contributions of environmental stresses on the component reliability. Such stresses strictly depend on the application field: for example, different stresses are applied to the component in the case of an installation in an environment characterized by controlled temperature and humidity or in the case the installation environment is characterized by frequent temperature variations, a relatively high humidity, and high mechanical stresses.

The π_T parameter represents the Thermal Factor, reporting the effect of thermal stresses on the component reliability. The operating temperature strongly impacts on reliability for semi-conductors and integrated circuits. The evaluation of thermal stresses accounts for the environmental (in which the device is installed) and the operating temperatures; in addition, the environmental temperature fluctuation should be taken in account.

Beside the reported factors, applied for all the components categories, some specific factors could be considered, such as the Power Rating Factor (π_r), the Electrical Stress Factor (π_s), or the Application Factor (π_a). Finally, other factors peculiar of the investigated device can be considered, such as Learning Factor, Die Complexity Factor, Manufacturing Process Factor, Device Complexity Factor, Programming Cycles Factor, Package Type Factor, etc.

B. RIAC-217 (or 217PLUS™)

The 217 Reliability Prediction Model Handbook [9] was published in the 2006: it reports the models and methodologies (named 217PLUS™) for the predictive analysis of electronic systems and components reliability, by modifying the approach proposed by the earlier MIL-HDBK-2017 [10]. The peculiar of the 217PLUS methodology is the reliability prediction at component level and at system level. As in the MIL-217 approach, the failure rate of a system is achieved by the sum of the contributions of each component; in addition, the 217PLUS method also considers the assembling and manufacturing phases through the Process Grading Factors, categorized in Design, Production, Part Quality, System Management, Operations Repeatability, Induced, Aging. In addition, the 217PLUS method takes in account operation and rest time, and operation cycles for each component: such

approach evaluates the impact of a continuous or intermittent operation on the failure rate of a device. The failure rate of the component is evaluated by an additive-multiplicative approach: the final value is achieved by the sum of the contributions of each failure class, accelerated by means of dedicated functions peculiar for the component category and for the stresses. Among them, operating, environmental, life cycle operating, induced, soldering stresses are considered.

The contribution at system level is based on the correction of the system failure rate (achieved from the contribution of the single components) by system factors (Process Grading Factors) that consider the effects external to the components themselves. An example is reported in (5).

$$\lambda_p = \lambda_{IA} \cdot \left(\begin{array}{c} \pi_D \cdot \pi_{IM} \cdot \pi_E + \pi_D \cdot \pi_G \\ + \pi_M \cdot \pi_{IM} \cdot \pi_E \cdot \pi_G \\ + \pi_S \cdot \pi_G + \pi_I + \pi_N + \pi_W \end{array} \right) \quad (5)$$

In (5), λ_p represents the preliminary failure rate evaluation, while the π parameters represent the Process Grading Factors referred to the process, design, manufacturing, system management, induced, defect detecting, wearing out, and accelerating factors referred to infant mortality, environmental and reliability growing. The Process Grading Factors ($\pi_D, \pi_G, \pi_M, \pi_S, \pi_I, \pi_N, \pi_W$) are calculated (6), in which α_i and β_i are the Weibull equation parameters for each process grading category, while R_i ranges between 0 and 1, is evaluated through an audit on the component, and reports the ranking of the i -th failure cause.

$$\pi_i = \alpha_i \cdot (-\ln R_i)^{\frac{1}{\beta_i}} \quad (6)$$

C. FIDES

The FIDES handbook extends the methodologies of earlier MIL-217 and 217PLUS, by devoting the appropriate relevance to all the operations of the lifecycle of a component or system affecting its reliability [11]. Basically, FIDES approach correlates the electrical system reliability with 3 main contributions: technology, process, and utilization, that are observed along the whole lifecycle of a device, from the production to the maintenance phases. The general reliability model for an electrical system is summarized in (7), in which λ is the failure rate, $\lambda_{physical}$ is the physical contribution, π_{PM} is the factor representing the quality and technical control on device manufacturing, and $\pi_{Process}$ is the factor representing the quality and technical control of design processes.

$$\lambda = \lambda_{physical} \cdot \pi_{PM} \cdot \pi_{Process} \quad (7)$$

The physical contribution accounts for all physical phenomena impacting on the reliability of the system; it is achieved by summing the single contribution of each component of the system (8). Each contribution is achieved by considering the contribution for each physics (λ_0) corrected for the acceleration factor π that depends on the component and the considered physics. The physical phenomena can be thermal, mechanical or chemical (humidity); in particular, the thermal phenomena accounts for the temperature of the device (Th), the thermal cycles affecting the device or the hosting environment (TCy) and the thermal cycling on the welding joints (TCy_S). The $\pi_{induced}$ parameter represents the over-stresses factor. The contribution of each component is normalized on the basis of the working hours in a year (t_{phase}).

$$\lambda_{physical} = \sum_i^{Phases} \left(\frac{t_{phase}}{8760} \right)_i \cdot \left[\begin{array}{c} \lambda_{0Th} \cdot \pi_{Th} + \\ \lambda_{0TCy} \cdot \pi_{TCy} + \\ \lambda_{0TCyS} \cdot \pi_{TCyS} + \\ \lambda_{0Mech} \cdot \pi_{Mech} + \\ \lambda_{0RH} \cdot \pi_{RH} \end{array} \right] \cdot \pi_{induced_i} \quad (8)$$

The over-stresses factor relies to the effects on the failure rate of the integration of the device in a more complex system, as well as of the usage modality. Its evaluation is reported in (9), in which $\pi_{placement}$ represents the impact of the device collocation in the hosting system, $\pi_{application}$ represents the impact of the utilization environment of the system (or product) containing the device, and $\pi_{ruggedising}$ represents the impact of device management philosophy; finally, $C_{sensitivity}$ is the over-stresses sensibility coefficient inherent to the investigated device technology.

$$\pi_{induced} = \left(\begin{array}{c} \pi_{placement} \\ \cdot \pi_{application} \\ \cdot \pi_{ruggedising} \end{array} \right)^{0.511 \cdot \ln(C_{sensitivity})} \quad (9)$$

From a mathematical point of view, the over-stresses factor ranges from 1 (optimal case) to 100 (worst case); of course, the latter case is achievable in the unrealistic condition that all parameters assume extreme values.

The part manufacturing factor (π_{PM}) reports the construction quality of the devices; its evaluation depends on the nature of the device under investigation. The manufacturing factor evaluation is reported in (10).

$$\pi_{PM} = e^{\delta_1(1-Part_Grade)-a_1} \quad (10)$$

The *Part_Grade* parameter (11) is determined by warranty criteria of manufacturer ($QA_{Manufacturer}$), of items quality (QA_{Item}), and of components ($RA_{Component}$), as well as to the confidence of the customer with respect to the manufacturer (c). It can range between 0.5 (optimal case) to 2 (worst case).

$$Part_Grade = \frac{QM_{Manufacture} + QA_{Item} + RA_{Component}}{36} \cdot c \quad (11)$$

The process factor ($\pi_{Process}$) (12) reports the device adequacy in the hosting process and the quality of the operations in which it is subjected. The *Process_Grade* parameter, evaluated through dedicated indicators defined in an audit phase, ranges from 0 (worst case) to 1 (optimal case). Since the parameter δ_2 is assumed to be 2.17, the process factor ranges between 1 ÷ 8.

$$\pi_{Process} = e^{\delta_2(1-Process_Grade)} \quad (12)$$

III. METHODOLOGIES FOR GRID RELIABILITY MODELLING

The definition of the parameters required to the reliability model can be essentially achieved by two approaches: analytical and statistical methods [12]. The analytical methods are based on the system representation through a mathematical model. Of course, if the system is characterized by a medium-high complexity level, the model equations solution becomes complex as well. Therefore, simplified models are often considered, and the solution can be carried out through approximated analytical techniques to reduces difficulties in the calculation phases. A similar approach allows the

evaluation of load points and reliability indexes average values. If in one hand, that values are useful in the design and planning phases, in the other hand a reliability distribution analysis is required to account for its variation in the time.

The statistical methods allow the evaluation of reliability indexes by simulating in the chronological time the real process for the electrical system and components. By this approach, the device/system status at a certain time strictly depends on its state at the previous time. In one hand, the statistical methods enable evaluating the average values of distribution probability whereas analytical methods are not applicable; on the other hand, very long simulative processes can be needed for complex systems.

A. Monte Carlo Simulation method

The Monte Carlo Simulation (MCS) method is a widely used approach for the electrical system reliability evaluation. The effectiveness of this methodology focuses on its flexibility in modelling the systems under investigation regardless the problem typology and size. A repetitive system configuration sampling is carried out, by considering all components and their status. By simulating a wide number of configurations, an accurate evaluation of the failure probability can be achieved. Obviously, the accuracy of achieved metrics and indexes is strictly connected to the number of performed simulations: a higher number of simulations provides a more accurate solution, but higher simulation time should be required. In this sense, the trade-off between accuracy and calculation effort becomes a crucial aspect. Moreover, it is worth noting that the MCS method is widely used since it is based on easy operations and calculations, thus admitting the convergence to a solution also for very complex systems. Its popularity encouraged the study of variants focused on different sampling strategies. Among them, the most interesting approaches are:

- Sampling approach based on status: it is a non-sequential method in which the status of each component is defined on the basis of random variables uniformly distributed, with values in [0; 1] range. If the random variable is greater than the failure probability, the component status is "in service", conversely is "out of service". The overall system status is determined by the combination of the statuses of all the components. As a drawback, such approach does not consider repairing time for the system components.
- Sampling approach based on status transition.
- Sampling approach based on status duration: such approach enables an effective chronological evaluation of the duration of components status.

B. Fault Tree Analysis

The Fault Tree Analysis (FTA) is a useful tool for the modelling of possible failures "path" in an electrical system or device, by estimating the failure events or failure sequences probability. The FTA approach exploits a graphical "Top-Down" representation characterized by the occurring of a single high-level undesired event (Top Event, TE) from which other undesired events for the system are generated in several branches. Therefore, starting from a TE, the Fault Tree proceeds towards the base events passing through the intermediate events. Logical ports (OR, AND, etc.) represent the connections and the relationships between events (if, in an events group, a single event is sufficient to generate the fault,

such events are connected by "OR"; if the concomitance of all the events is necessary to generate the fault, the events are connected by "AND").

The FTA approach results in a quantitative and qualitative evaluation for a specific system [13]. Quantitatively, the fault tree solution contemplates probabilistic parameters for each event below both the failure tree and the logical connections between failure events. In particular, it is possible to define:

- Base events: representing the causes of potential failure paths for the investigated system, base events are all the events that can occur in the normal system/sub-system operating conditions.
- Middle failures: they are the secondary failure events occurring if the system is operating in abnormal conditions. Middle failures can also be "command failure", in which the system operates properly, but at a wrong time / in a wrong space.

The fault tree solution is achieved by "Minimal Cut Set" method, that identifies the minimum paths leading from base events to TE. The Minimal Cut Set method can be applied if:

- Systems and subsystems are characterized by two operating statuses: "In service" and "Out of service".
- Instant transition between statuses.
- Constant failure rate and repair rate.
- Repair tree coincident with failure tree.

If $Q_{A_j}(t)$ is the probability of the failure event A_j at the instant t , the minimal cut set probability Q_{MCS} can be achieved (13).

$$Q_{MCS_i}(t) = \prod_{j=1}^m Q_{A_j}(t) \quad (13)$$

The TE probability is therefore defined (14).

$$Q_{TE}(t) = \sum_{i=1}^n Q_{MCS_i}(t) \quad (14)$$

Finally, the system reliability can be calculated (15).

$$R(t) = 1 - Q_{TE}(t) \quad (15)$$

As aforementioned, the FTA method allows a quantitative and qualitative reliability analysis, however it is not suitable for the study of complex systems characterized by redundancy and priority logics.

C. Failure Mode and Effect Analysis (FMEA)

The Failure Mode and Effect Analysis (FMEA) method is based on the identification, for each component of the system under investigation, of the failure causes and the effects on closer load points and on the system [14]. Once identified the failure modes, the calculation phase contemplates:

- assessing the failure mode recurrence probability, based on historical data of the faulty parts; such probability should be ranked by a number (the lower number, the less probable).
- assigning and classifying the severity rate for each failure mode based on consequences of the fault and the extent of damages for the device.

- defining and to classifying fault detection errors, by assigning the lower number to the more easily detectable errors.

The result of such study is the Risk Probability Number (RPN), calculated as the product of the three indexes, thus resulting in the risk priority for the component.

Beside the tested effectiveness of the FMEA method in several industrial scenarios, it is a simple qualitative approach. For complex systems, the number of possible failure events is very high, thus the method application becomes hard. Grid simplification can be performed [15], thus decomposing the system in a series of equivalent subsystems easy to manage; of course, such approach reduces the method accuracy.

D. Markov Process

The Markov process is a stochastic approach, typically defined in a set of discrete statuses, in which the incoming behavior of a system exclusively depends on the present status, and not on previous ones. Each status is characterized by a set of possible events defining the transitions between the current and next statuses of the process. In a continuous-time Markov chain, the elapsed time for each time is supposed to be exponentially distributed, and the transitions between statuses are defined through a transition rate matrix [16].

The Markov processes can be used for the reliability evaluation of power supply systems. At "component" level, a simple space state representation includes two statuses: On and Off; a such model is defined "state binary model". Complete models of a power supply system should be able to consider degradation, inspection, and maintenance phases, assuring a more accurate representation of real components.

The Markov processes can be used within the Markov Decisional Processes (MDP), to define the optimal decision in the different statuses [17]. The MDP system is employed to model an uncertain dynamic system, in which a sequence of decisions with uncertain outcomes should be taken. Therefore, Markov processes aim to enable the identification of an optimal actions sequence to achieve the highest advantage in a time range. For instance, in a defined space of component statuses for a power system, an optimal maintenance philosophy could be identified to minimize the costs and to assure an adequate reliability requirements level.

IV. CONCLUSIONS

The analysis of reliability is arousing growing interest, due to the penetration of renewable generation in distribution system, and the forecasted hybridization of the electrical grids. The present paper describes the main methods for estimating power systems reliability, related metrics, and application sectors. The electrical systems are characterized by a failure rate which depends on the life phase, being higher in the initial and final phases. The estimation of the failure rate in the normal life phase is possible via several predictive methods, described in MIL-217, 217Plus and FIDES handbooks. The first one introduces the effect of stresses on the failure rate of electrical components. The 217Plus models extend the previous approach by considering reliability both at component and system levels, and by introducing the contribution of the assembling and manufacturing phases. Finally, the FIDES extends the previous methodologies by paying the appropriate relevance to technology, process, and utilization phases; in addition, more accurate evaluation models are elaborated for the different stresses. Aside

prediction models, simulative methods are described for the reliability evaluation. The Monte Carlo Simulation is a flexible model that neglects typology and size of the problems, but takes into account the status of the component, its transition and its duration. The FTA approach pays attention on the possible failure paths in electrical system, by means of logical ports (AND, OR). The FMEA focuses on the failure causes and the effects on closer load points for each component of the system. Finally, in the Markov method, each status is characterized by a set of possible events which define transitions between current and next status.

V. ACKNOWLEDGEMENT

This research was funded by the Research Fund for the Italian Electrical System under the Contract Agreement "Accordo di Programma 2019-2021 - PTR_19_21 ENEA PRG 10" between ENEA and the Ministry of Economic Development.

VI. REFERENCES

- [1] R. Billinton and R. N. Allan, *Reliability Evaluation of Power Systems*, 2nd ed. Boston, MA: Springer US, 1996.
- [2] H. L. Willis, *Power distribution planning reference book*. New York: Marcel Dekker, 2004.
- [3] G. C. Montanari and G. Mazzanti, "Insulation Aging Models," in *Wiley Encyclopedia of Electrical and Electronics Engineering*, Hoboken, NJ, USA: John Wiley & Sons, Inc., 1999.
- [4] G. Adinolfi, R. Ciavarella, G. Graditi, A. Ricca, and M. Valenti, "A Planning Tool for Reliability Assessment of Overhead Distribution Lines in Hybrid AC/DC Grids," *Sustainability*, vol. 13, no. 11, p. 6099, May 2021.
- [5] G. P. Pandian, D. Das, C. Li, E. Zio, and M. Pecht, "A critique of reliability prediction techniques for avionics applications," *Chinese J. Aeronaut.*, vol. 31, no. 1, pp. 10–20, Jan. 2018.
- [6] U. S. A. Department of Defense, *MIL-HDBK-217F - Military Handbook - Reliability prediction of electronic equipment*, F. Washington, D.C., 1990.
- [7] G. Graditi and G. Adinolfi, "Temperature influence on photovoltaic power optimizer components reliability," in *International Symposium on Power Electronics Power Electronics, Electrical Drives, Automation and Motion*, 2012, pp. 1113–1118.
- [8] G. Graditi and G. Adinolfi, "Photovoltaic power optimizers: A comparison in reliability evaluations," 2013.
- [9] W. Denson, P. Lein, and D. Nicholls, "Handbook of 217Plus Reliability Prediction Models - 2015," Quantierion Solutions Incorporated, New York USA, p. 186, 2015.
- [10] D. Nicholls, "What is 217Plus/sap TM and Where Did It Come From?," in *2007 Annual Reliability and Maintainability Symposium*, 2007, no. June 2005, pp. 22–27.
- [11] P. Pougnet, F. Bayle, H. Maanane, and P. R. Dahoo, "Reliability Prediction of Embedded Electronic Systems: the FIDES Guide," *Embed. Mechatron. Syst. Anal. Fail. Predict. Reliab.*, pp. 189–216, Jan. 2019.
- [12] R. N. Allan, R. Billinton, A. M. Breipohl, and C. H. Grigg, "Bibliography on the application of probability methods in power system reliability evaluation," *IEEE Trans. Power Syst.*, vol. 14, no. 1, pp. 51–57, 1999.
- [13] D. F. Haasl, N. H. Roberts, W. E. Vesely, and F. F. Goldberg, "Fault tree handbook," Washington, DC (USA), 1981.
- [14] D. H. Stamatis, *Failure mode and effect analysis: FMEA from theory to execution*. Milwaukee, Wis.: ASQ Quality Press, 2003.
- [15] R. Billinton and W. Li, *Reliability Assessment of Electric Power Systems Using Monte Carlo Methods*. Boston, MA: Springer US, 1994.
- [16] O. C. Ibe, "Continuous-Time Markov Chains," in *Markov Processes for Stochastic Modeling*, O. C. B. T.-M. P. for S. M. (Second E. Ibe, Ed. Oxford: Elsevier, 2013, pp. 85–102.
- [17] Y. Wu, J. Zhang, A. Ravey, D. Chrenko, and A. Mizoui, "Real-time energy management of photovoltaic-assisted electric vehicle charging station by markov decision process," *J. Power Sources*, vol. 476, p. 228504, Nov. 2020.

6.3 Frequency dynamics of power systems with temporally distributed disturbances, Sustainable Energy, Grids and Networks

Sustainable Energy, Grids and Networks 28 (2021) 100536



Contents lists available at ScienceDirect

Sustainable Energy, Grids and Networks

journal homepage: www.elsevier.com/locate/segan



Frequency dynamics of power systems with temporally distributed disturbances

Mariano G. Ippolito, Rossano Musca^{*}, Gaetano Zizzo

Engineering Department, University of Palermo, Italy



ARTICLE INFO

Article history:
Received 25 March 2021
Received in revised form 12 July 2021
Accepted 22 August 2021
Available online 1 September 2021

MSC:
00-01
99-00

Keywords:
Frequency transients
Power imbalances
Primary frequency control
Power system dynamics
System split

ABSTRACT

The frequency dynamics and stability of power systems is essentially affected by nature and characteristics of the disturbances occurring in the system. Conventionally, frequency transients are examined assuming a single disturbance applied at a given time. However, actual incidents in the power systems can be generally composed of a temporal sequence of events, and thus characterized by multiple power imbalances of different magnitudes and time offsets. The consideration of the effects of the temporal distribution of power imbalances is important for two main reasons: the impact on the frequency dynamics of the system in terms of frequency metrics such as minimum instantaneous frequency and maximum absolute rate of change of frequency, and the correct representation of the dynamic behaviour of the system also for complex events such system separation. The work provides an analytical approach for the theoretical study of the frequency dynamics with temporally distributed power imbalances. The analytical approach is then used to examine the impact of multiple disturbances having different magnitudes and time offsets on the typical frequency metrics used to characterize the transient performances of the system. The concepts derived in the work are finally applied to the case of an actual event occurred in the Continental Europe power system, showing the fundamental role of considering temporally distributed power imbalances for a correct and accurate assessment of the dynamics of the system.

© 2021 Elsevier Ltd. All rights reserved.

1. Introduction

The disturbances which cause imbalances in the active power flows are the main factors of frequency transients in power systems. Many incidents have been observed so far as disconnection of concentrated units, like f.i. the outage of big generation power plants. This kind of incidents are usually modelled for simulations and analyses as single power imbalance applied at a given time. In many studies and researches of power systems dynamics, the disturbances are then generally considered to occur instantly and entirely at a given time [1,2]. This approach is useful for understanding the system's behaviour under severe imbalances. However, it leads to a correct consideration and representation of the actual conditions of the frequency dynamics of the system only to some extent: indeed in many actual cases, the power imbalances originated in the system are fractioned over time as temporal sequence of multiple imbalances with different magnitudes. This can be the case of events like cascading disconnections of elements (power plants or substations tripping one after the other, with loss of generation or load in the interconnected system), or also system separations (consecutive

tripping of interconnecting lines, with loss of import or export between the separated synchronous parts) [3–5]. Power systems are currently experiencing an evolution process dominated by the increase of generation share from renewable energy sources and storage systems, and also by the expansion of transmission capacities with an increase of the power flow exchanges within the different parts of the system [6]. In this context, the occurrence of incidents characterized by multiple power imbalances temporally distributed over the frequency transient could therefore potentially become a more frequent and relevant condition for the systems in the next future. Depending on nature and characteristics of the temporal sequence of the power imbalances, the impact on the frequency dynamics of the system can be relevant. The analysis made by ENTSO-E in [7] shows for instance the critical impact of cascading disconnections of dispersed generation following an initial contingency (Fig. 1). The scenarios under examination assumed a temporal sequence of different power imbalances occurring at the specific frequency thresholds. The simulation shows that the considered sequence of events could cause the risk of load shedding activation. In the case of multiple temporally distributed disturbances, the transient response of the system can be also significantly different from the response obtained under the assumption of a single power imbalance of equivalent magnitude concentrated at a given time.

^{*} Correspondence to: University of Palermo, Italy.
E-mail address: rossano.musca@unipa.it (R. Musca).

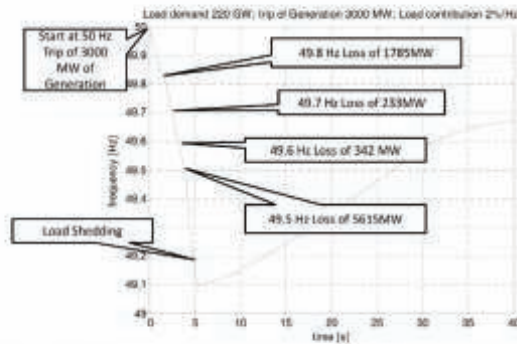


Fig. 1. Simulation of 3 GW generation loss after Italian and German retrofit (MW) for dispersed generation in Continental Europe [7].

The impact of power imbalances on the frequency stability and on the correct modelling and representation of the frequency dynamics is recognized as an important aspect in power system studies and researches [8–10]. The importance of considering the temporal distribution of power imbalances is therefore twofold: for unexpected and uncontrolled power imbalances such as sudden loss of power plants or opening of interconnecting lines, the consideration of the correct temporal sequence allows for a correct representation of the system transient response; for ordered power imbalances such as load shedding or defensive tripping events, the consideration of the correct temporal sequence allows an accurate definition and study of specific control methods such as *f.l.* virtual inertia or fast frequency response in terms of transient performance in the different conditions of the power system.

This work addresses the study of the frequency dynamics of power systems with multiple power imbalances, temporally distributed over the transient. The novelty of the work is indeed the analytical consideration of multiple events and the corresponding impact on the frequency stability, as to the best of the authors knowledge there are no other scientific works considering multiple events likewise. The main contributions can be summarized into the three following aspects:

- an analytical formulation of frequency transient is provided, for a more in-depth understanding of the fundamental aspects related to the occurrence of a temporal sequence of power imbalances, with different magnitudes and time offsets;
- the effects of multiple power imbalances on the frequency dynamics of the system are characterized studying the impact on the typical frequency metrics used to assess the transient performances of the system;
- the relevance of properly considering the temporal sequence of power imbalances for a correct representation of the system behaviour is pointed out by a case study of an actual event occurred in the power system of the Continental Europe synchronous area.

The article is therefore structured in three parts. The first part presents the analytical formulation for the study of the frequency transients with multiple temporally-distributed power imbalances. The theoretical considerations indicate the non-simultaneity of the peak values of the single power imbalances as the fundamental aspect affecting the transient behaviour of the system. The second part of the article discusses the effects of a temporal sequence of different power imbalances on the

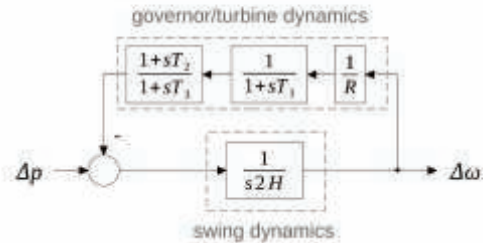


Fig. 2. Block diagram for the basic analytical representation of primary frequency dynamics.

frequency dynamics of the system. To this purpose, the impact on the commonly used frequency metrics is examined, in terms of minimum instantaneous value of the frequency and maximum absolute value of the rate of change of frequency. Finally, the third part applies concepts and observations derived in the previous sections to an actual event, showing the relevance of the temporal distribution of power imbalances for a proper representation of the system dynamics. The considered incident is a sequence of events occurred in the Continental Europe power system in January 2021, which led to the system separation and to consequent large over- and under-frequency transients. Analysis and simulations show that the consideration of a proper temporal sequence of the multiple imbalances due to incidents and defensive actions is fundamental for an accurate representation of the actual transient response, resulting in a correct assessment of the frequency dynamics of the system.

2. Analytical study of multiple power imbalances

2.1. Single temporally-concentrated power imbalance

The simplest and most compact diagram for the representation of frequency containment process in power systems can be outlined as shown in Fig. 2. The box “swing dynamics” represents the aggregated dynamics of the system in the form of the typical swing equation describing the transient behaviour of the synchronous machines. Traditionally, this oscillatory dynamics with the inherent provision of inertia to the system has been competence exclusively of synchronous machines, whose droop coefficient and inertia constant are indicated with *R* and *H*, respectively. The input Δp is the active power mismatch, while the output $\Delta\omega$ of the diagram is the frequency deviation. In recent years, emerging technologies for the specific control of power converters are making non-synchronous generation also able to offer virtual oscillating capabilities [11]. In this case, the swing equation can still be valid to describe the basic principles behind the definition of such converter controls. The box “governor/turbine dynamics” represents instead the dynamics of the governor/turbine typically connected to synchronous machines. This part of the diagram is the main responsible for the frequency containment at the occurrence of a power imbalance in the system. The scheme includes a gain for the droop control on the frequency deviation, a lag and a lead-lag blocks modelling the time constants associated to the turbine response. Depending on the type of the governor/turbine (steam, gas, hydro) the time constants have different physical meanings and values. This basic representation is intended for the description of a common dynamic behaviour of the frequency controllers involved in the frequency containment process, as in general the models of governor/turbines consist of more complex control schemes

of higher order. Even in the case of frequency containment, the traditional role of synchronous machines has started to be progressively covered also by different technologies, such as wind turbines or energy storage systems. Again, the control system composed by a droop control and a relative dynamics modelled with a zero-pole transfer function is still valid to represent the basic dynamics introduced by these technologies different from the conventional synchronous generation. The model reported in the diagram of Fig. 2 is linear, as it does not consider the non-linearities related to the frequency dynamics of power systems. Main sources of non-linearities can be for instance the switching events applied automatically or manually by the protections schemes and defensive plans, the dead-bands included in the droop controllers for the activation of the frequency containment reserve, or also discontinuous control blocks associated to some specific turbine technologies (such as hydro governors or wind turbines). All these non-linearities are here neglected, as they do not invalidate the mathematical analysis about the temporal distributions, but rather they would unnecessarily complicate the analytical discussion. However, the effect of non-linearities related to load or generation disconnection consequent to under- or over-frequency conditions during frequency transients is actually the possible origination of power imbalances occurred at different times. The importance of these switching is therefore here acknowledged, and it will be considered in the analysis, with the application of the concepts of temporal distribution of power imbalances derived in this section to an actual frequency event in the Continental Europe discussed later in the paper.

From the diagram of Fig. 2, it is possible to derive the transfer function between Δp assumed as input and $\Delta\omega$ assumed as output:

$$\frac{\Delta\omega}{\Delta p} = \frac{(RT_3)s + R}{(MRT_3)s^2 + (T_2 + MR)s + 1} = \frac{\frac{1}{M}s + \frac{1}{MT_3}}{s^2 + \frac{T_2 + MR}{MRT_3}s + \frac{1}{MRT_3}} \quad (1)$$

where M is the angular momentum, given by $M = 2H$. In (1), the time constant of the governor T_1 has been neglected for sake of simple analytical examination, with the purpose of relying on known formulas of control theory. Proceeding in this way, the denominator of (1) is in fact in the form of the general expression of the transfer function of a second order system [12]:

$$s^2 + 2\zeta\omega_n s + \omega_n^2 \quad (2)$$

The dynamic behaviour of the system is then characterized by the natural frequency ω_n and the damping ratio ζ , respectively expressed as:

$$\omega_n = \sqrt{\frac{1}{MRT_3}} \quad (3)$$

and

$$\zeta = \frac{T_2 + MR}{2MRT_3\omega_n} = \frac{T_2 + MR}{2} \omega_n \quad (4)$$

If a step function of magnitude ΔP_d is applied as input to the system, then the transfer function of the close-loop system can be written as:

$$\Delta\omega = \frac{\frac{1}{M}s + \frac{1}{MT_3}}{s^2 + 2\zeta\omega_n s + \omega_n^2} \frac{\Delta P_d}{s} \quad (5)$$

The term ΔP_d represents a power imbalance applied instantly in the system: negative values of ΔP_d correspond to power deficit (loss of generation) and they cause under-frequency transients with negative $\Delta\omega$, while positive values of ΔP_d correspond to power surplus (loss of load) and they cause over-frequency transients with positive $\Delta\omega$. Taking the inverse Laplace transform of (5), the time response can be expressed as:

$$\omega(t) = \omega_0 + R\Delta P_d [1 - e^{-\zeta\omega_n t} (\cosh(\omega_d t) + k \sinh(\omega_d t))] \quad (6)$$

where ω_0 is a constant representing the initial value of the frequency before the application of the step, ω_d is the damped natural frequency:

$$\omega_d = \omega_n \sqrt{1 - \zeta^2} \quad (7)$$

and the factor k is given by:

$$k = \frac{\zeta\omega_n - T_3\omega_n^2}{\omega_d} \quad (8)$$

In the typical conditions of power systems, after the occurrence of a power imbalance the system experiences a transient characterized by power-frequency oscillations. This means that the systems are usually in under-damped conditions, with values of the damping ratio less than the unit $\zeta < 1$. In this case, (6) can be rewritten and simplified as:

$$\omega(t) = \omega_0 + R\Delta P_d [1 - e^{-\zeta\omega_n t} (\cos(\omega_d t) + k \sin(\omega_d t))] \quad (9)$$

According to the known transient response of power systems to power imbalances, (9) indicates that the time behaviour of the frequency $\omega(t)$ following the perturbation ΔP_d will be given by the sum of sinusoidal oscillations at frequency ω_d , with an exponential decay defined by the attenuation factor $\zeta\omega_n$. The Laplace transform of (5) is obtained using the symbolic math toolbox of Matlab [13]. A formal derivation of (9) is still provided in Appendix A for a more in-depth insight.

The time derivative of the frequency at the instant of application of the power imbalance ΔP_d is known as rate of change of frequency (RoCoF) and it can be expressed taking the first derivative of (9):

$$\rho(t) = \frac{d\omega(t)}{dt} = R\Delta P_d e^{-\zeta\omega_n t} \left[(k\zeta\omega_n + \omega_d) \sin(\omega_d t) + \frac{1}{MR} \cos(\omega_d t) \right] \quad (10)$$

The maximum absolute value is found right after the occurrence of the perturbation, so it can be expressed evaluating (10) at $t=0$:

$$\rho_{max} = \rho(0) = \frac{\Delta P_d}{M} = \frac{\Delta P_d}{2H} \quad (11)$$

The expression of ρ_{max} corresponds to the well known equation for the per unit calculation of the maximum absolute value of the RoCoF [14]: the value depends directly on the power imbalance ΔP_d and inversely on the system inertia $M = 2H$.

The peak time t_p can be obtained by differentiating the step response $\omega(t)$ expressed by (9) and equating to zero. By proceeding in this way, the peak time t_p is expressed as:

$$t_p = \frac{1}{\omega_d} \arctan \left(\frac{T_3\omega_d}{\zeta T_3\omega_n - 1} \right) \quad (12)$$

The peak value ω_p can be obtained substituting the expression of t_p (12) in (9) and simplifying:

$$\omega_p = \omega(t_p) = \omega_0 + R\Delta P_d \left(1 + e^{-\zeta\omega_n t_p} \sqrt{\frac{T_3 - T_2}{MR}} \right) \quad (13)$$

This value corresponds to the minimum or maximum instantaneous value reached by the frequency after the power imbalance within the very first instants of the frequency containment process.

The final value of the frequency observed at the end of the transient (which corresponds to the steady-state frequency deviation establishing at the end of the frequency containment process stage, before the secondary control starts) is given by:

$$\omega_s = \lim_{t \rightarrow \infty} \omega(t) = \omega_0 + R\Delta P_d \quad (14)$$

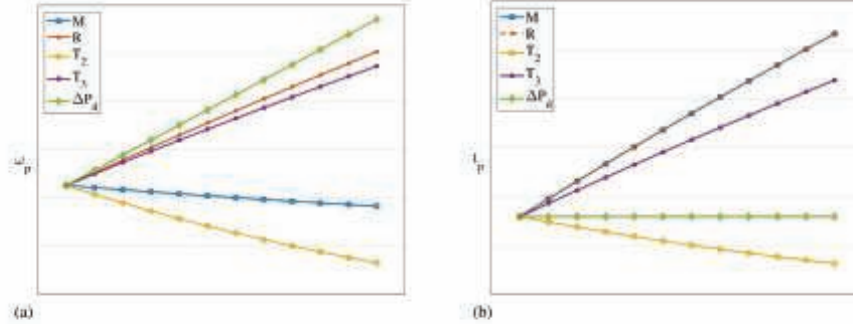


Fig. 3. Peak sensitivities to system parameters increase, from base value to 150%: (a) peak value ω_p ; (b) peak time t_p .

as well known from systems theory, depending essentially on the value of the frequency droop setting R of the turbine.

By observing the formulas derived analytically, the following considerations can be made. From (12), the peak time t_p depends on the given characteristics of the system (angular momentum M , frequency droop R , control time constants T_2 and T_3), while it is independent of the power imbalance ΔP_d . Higher values of the inertia $M = \lambda H$, of the droop R , of the lag time constant T_3 and smaller values of the lead time constant T_2 produce higher times for the reaching of the maximum/minimum instantaneous frequency deviation. From (13), the peak value ω_p is directly proportional to the magnitude of the power imbalance ΔP_d , and it depends also on the given characteristics of the system. For a given ΔP_d , the value of the absolute frequency deviation is smaller for higher values of the inertia H and the lead time constant T_2 , and smaller values of the droop R and the lag time constant T_3 . A graphical visualization of the identified sensitivities for peak value and peak time is shown in Fig. 3.

More details regarding the derivation of the formulas presented in this analytical study are given in Appendix A.

A similar mathematical approach can be found in [15]: like the analytical exposition discussed here, these approaches are all based on a reduced order model of the power system, exploiting the same known concepts and formulas belonging to the common theory of second order dynamic systems. Despite the adopted simplifications, these mathematical approaches can still point out some relevant observations about the dynamic characteristics of the power system. Additionally, as for the main contribution of this work, the analytical examination presented here can be used for the study of the more complex and general case of multiple power imbalances occurring at different times.

2.2. Multiple temporally-distributed power imbalances

The analytical study of a single power imbalance applied instantly can be used as basis to extend the analysis to the more general case of multiple power imbalances distributed over time during the transient. The first modification is to consider the disturbance ΔP_d applied at a given time t_0 . In this case, (9) modifies in Eq. (15) given in Box 1.

The notation of (15) can be compacted using the Heaviside function:

$$\omega(t) = \omega_0 + H(t - t_0) R \Delta P_d \left[1 - e^{-\gamma(\omega)(t-t_0)} \left(\cos(\omega_d(t-t_0)) + k \sin(\omega_d(t-t_0)) \right) \right] \quad (16)$$

For the generalization to the case of N power imbalances ΔP_{di} occurring at the given times t_i , it is possible to apply the

superposition method and derive the following equation:

$$\omega(t) = \omega_0 + \sum_{i=1}^N H(t - t_i) R \Delta P_{di} \left[1 - e^{-\gamma(\omega)(t-t_i)} \left(\cos(\omega_d(t-t_i)) + k \sin(\omega_d(t-t_i)) \right) \right] \quad (17)$$

From (17), it is possible to observe that the absolute peak of the output frequency $\omega(t)$ in response to the application of multiple power imbalances depends on the combination of the following two factors:

- magnitude of the single power imbalances ΔP_{di} ;
- temporal offset between the occurrence times t_i .

The key point emerging from the analysis is the existence of a factor of "simultaneity", determined by the temporal displacement of the power imbalances. Theoretically, the maximum absolute value of the frequency ω would correspond in fact to the simultaneous application of all the power imbalances ΔP_{di} at the same time. Since the peak time does not depend on ΔP_{di} , all the single peaks would sum up at the same instant, resulting in the maximum/minimum possible instantaneous frequency deviation for the given conditions of the system. If a temporal distribution of ΔP_{di} is considered as happening in actual systems, the absolute peak reached by the frequency will always be less than the maximum absolute peak determined in the assumption of simultaneity. This can be clearly realized considering that the immediate effect of the temporal offset is the shifting of the single peaks at different times, and therefore a reduction of the overall absolute peak experienced by the frequency.

Proceeding now in a deductive way, it is possible to make a numerical application of the concepts illustrated for the general case of multiple power imbalances occurring at different times. The simple case of two perturbations of different magnitude and temporal occurrence is considered. For numeric demonstration, the system parameters are given the following values: $H=3$ s ($M=6$), $R=0.05$, $T_2=3$ s, $T_3=10$ s. The magnitude of the two power imbalances in system per unit are $\Delta P_{d1}=-0.025$ pu and $\Delta P_{d2}=0.015$ pu, respectively. Using (17) with these values, the results shown in Fig. 4 are obtained. The first case corresponds to a theoretical condition of power imbalances ΔP_{d1} and ΔP_{d2} temporally concentrated at the same time. This condition is equivalent to considering a single power imbalance given by the sum of the two imbalances $\Delta P_d = \Delta P_{d1} + \Delta P_{d2}$. In this case, the system experiences an under-frequency transient characterized by a given minimum instantaneous value (red dotted line in Fig. 4(a)). If the power imbalance ΔP_{d2} is supposed to occur few seconds after ΔP_{d1} , the transient response is given in Fig. 4(b). The system

$$\omega(t) = \begin{cases} \omega_0 & \text{for } t < t_0 \\ \omega_0 + R\Delta P_d \left[1 - e^{-\zeta\omega(t-t_0)} \left(\cos(\omega_d(t-t_0)) + k \sin(\omega_d(t-t_0)) \right) \right] & \text{for } t \geq t_0 \end{cases} \quad (15)$$

Box 1.

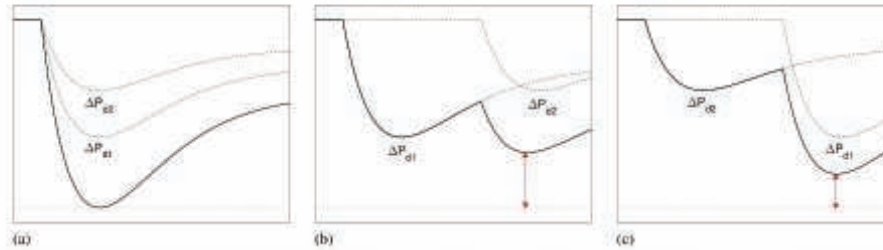


Fig. 4. Time response of the frequency for multiple power imbalances: (a) ΔP_{d1} and ΔP_{d2} occurring at the same time; (b) ΔP_{d2} occurring few seconds after ΔP_{d1} ; (c) ΔP_{d1} occurring few seconds after ΔP_{d2} .

experiences as expected a more contained under-frequency transient, with a higher value of the minimum instantaneous value as effect of the non-simultaneity of the two absolute peaks ΔP_{d1} and ΔP_{d2} (Fig. 4(b)). The absolute peak is found in correspondence of the second peak ΔP_{d2} for the assumed combination of temporal offsets. If instead the power imbalance ΔP_{d1} is supposed to occur after ΔP_{d2} , swapping the application instants of the two disturbances, the transient response is shown in Fig. 4(c). The system is still subjected to the same total amount of imbalance considered for the previous case, but in this condition a different temporal sequence of the single power imbalances leads to a worse transient response for the system, with a lower value of the minimum instantaneous value (Fig. 4(c)). In this case, even with same total magnitude of the disturbance, the distance from the “worst case” is reduced in comparison with the case of different temporal distribution of power imbalances. The numeric example allows then the visual realization of the relevant concepts derived with the analytical study: the time to the maximum/minimum value depends only on the characteristics of the system and it is independent from the single power imbalances ΔP_d ; the temporal distribution of the power imbalances determines a non-simultaneity of the single maximum/minimum values of the components adding for the total transient response; the maximum/minimum value is observed at the peak time of one of the single power imbalances, and it considerably depends on the specific temporal sequence of the imbalances affecting the system.

Concepts, formulas and observations derived in this section can be used as guidelines for the definition of specific methodologies for the consideration of the temporal distribution of consecutive power imbalances in frequency transient studies and analyses. The impact of temporally distributed imbalances on the typical frequency metrics selected for the assessment of the system transient performances, and an application of these concepts to an actual event occurred in the Continental Europe power system will be discussed in the next sections.

3. Impact on frequency metrics of power systems

The impact of the temporal distribution of power imbalances on the maximum/minimum instantaneous value of the frequency and on the maximum absolute value of the rate of change of

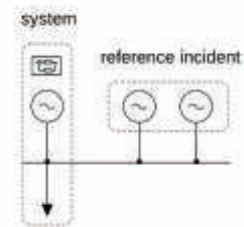


Fig. 5. Outline of the single-frequency bus model of the CE system for simulation of 3 GW generation loss reference incident.

frequency is here investigated. These two factors are the frequency metrics commonly used to characterize the response of a power system in the very first instants after the beginning of the frequency transient [16–18]. The system used for the analysis is an equivalent model of the Continental Europe (CE) power system. The model is derived from the large-scale dynamic model of the CE system provided by ENTSO-E [19–21] and it is based on the concept of single-frequency bus model. This modelling representation assumes the dynamics of the whole system concentrated at the centre of inertia, so inter-area oscillations and local phenomena cannot be caught by this model. The disturbance considered for analysis is a 3 GW generation loss: this power imbalance corresponds to the simultaneous outage of two nuclear power plants in France (N-2 principle) and it is assumed as reference incident for the CE system [22,23]. The reference incident is applied as design hypothesis for the dimensioning of the frequency containment reserve (FCR) in the CE system. The schematic representation of the implemented simulation model is shown in Fig. 5.

The reference incident of 3 GW loss defined by ENTSO-E is a sudden power imbalance occurring instantaneously in the system. This condition will be then assumed as baseline for the comparison with variant scenarios, where the total imbalance will be assumed temporally distributed during the frequency transient. The total amount of 3 GW will be fractioned over time, considering different combinations of time offsets and single amounts of power imbalances. The analysis of the variant scenarios so determined allows for the observation of some relevant

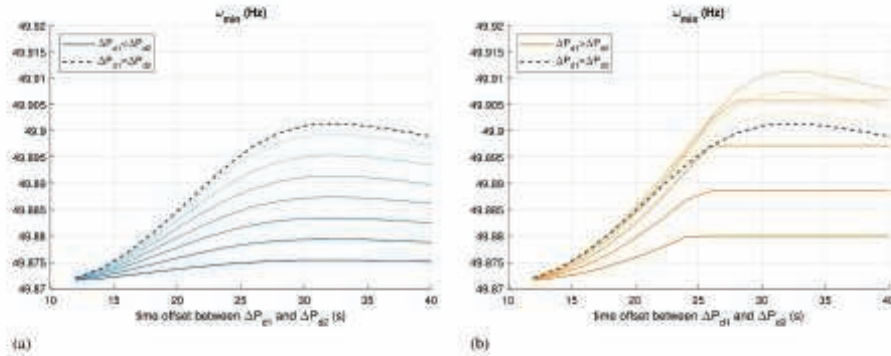


Fig. 6. Impact of temporal fractioning of power imbalances on the minimum instantaneous frequency ω_{\min} .

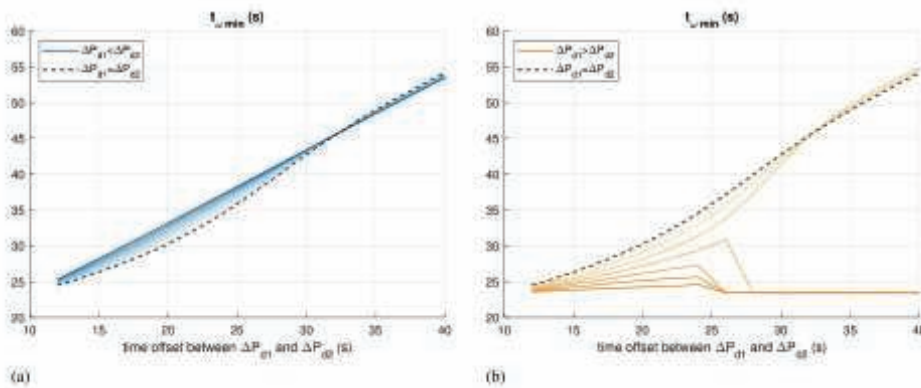


Fig. 7. Impact of temporal fractioning of power imbalances on the detection time of ω_{\min} .

effects on the typical frequency metrics considered in frequency transient studies and researches. The variant scenarios are determined for progressive changes in the proportion between ΔP_{d1} and ΔP_{d2} : the process starts with a small value of ΔP_{d1} and high value of ΔP_{d2} , and it proceeds increasing ΔP_{d1} and decreasing ΔP_{d2} in a way that $\Delta P_{d1} + \Delta P_{d2}$ equals the total amount $\Delta P_d = 3$ GW at any step.

The variant scenarios are examined through time-domain dynamic simulations of the system. The implementation of all system scenarios and the executions of the single computations are automated through the specific APIs available in the software NEPLAN [24], with the running of a custom-built master code written in C#. The results of the analysis are collected in Fig. 6 to Fig. 9. In each figure, the results are divided into two sub-plots: the first plot shows the first half of scenarios for $\Delta P_{d1} < \Delta P_{d2}$, while the second plot reports the second half of scenarios for $\Delta P_{d1} > \Delta P_{d2}$. In both sub-plots, the middle variant scenario with $\Delta P_{d1} = \Delta P_{d2} = 1.5$ GW is marked with black dashed line. The x-axis is the time offset between the occurrence of the first and the second power imbalance: while the time of ΔP_{d1} is fixed as initial time for the beginning of the overall frequency transient, the time of ΔP_{d2} is progressively increased, making the two power imbalances more distant in time. This process is repeated for every variant scenario considered in the analysis, investigating the impact on the two frequency metrics of temporal distribution and proportional fractioning of power imbalances comprehensively.

The results allow the following considerations:

- impact on the minimum instantaneous frequency ω_{\min} : the minimum instantaneous value of the frequency ω_{\min} is significantly affected by the temporal sequence of the power imbalances, both in terms of time offsets and amounts of the single imbalances (Fig. 6). The improvement from the "worst case" scenario of total imbalance $\Delta P_d = 3$ GW concentrated at a given time depends on the amount of the single imbalances: if one of the power imbalances is much bigger than the others, the value of ω_{\min} will be mostly affected by the amount of that power imbalance. If instead the single imbalances have comparable magnitudes, a temporal offset between them leads to the expected increase of the minimum instantaneous frequency ω_{\min} . From Fig. 6(b), for the case of $\Delta P_{d1} > \Delta P_{d2}$, it can be observed that for some first scenarios away from the symmetric case of $\Delta P_{d1} = \Delta P_{d2}$ (black dashed line), the delay in time of the second power imbalance has an even more positive effect on the minimum instantaneous frequency. After those first cases, where ΔP_{d1} is slightly bigger than ΔP_{d2} , the trend of the impact on ω_{\min} comes back to the same pattern observed for the case of $\Delta P_{d1} < \Delta P_{d2}$, going down to the base ω_{\min} value of the worst case scenario, as the amount of one power imbalance becomes predominant over the other one. As general observation, it can be also noticed that an initial power imbalance followed by a second perturbation of lower magnitude (right sub-plot with $\Delta P_{d1} > \Delta P_{d2}$) determines slightly better system response in terms of higher values of ω_{\min} .

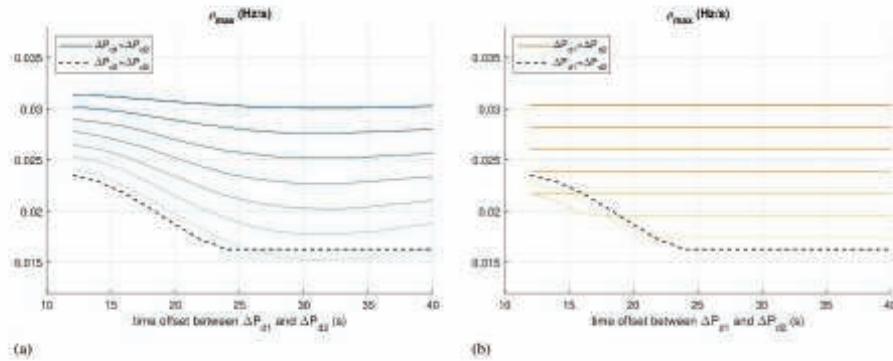


Fig. 8. Impact of temporal fractioning of power imbalances on the maximum absolute value of RoCoF ρ_{max} .

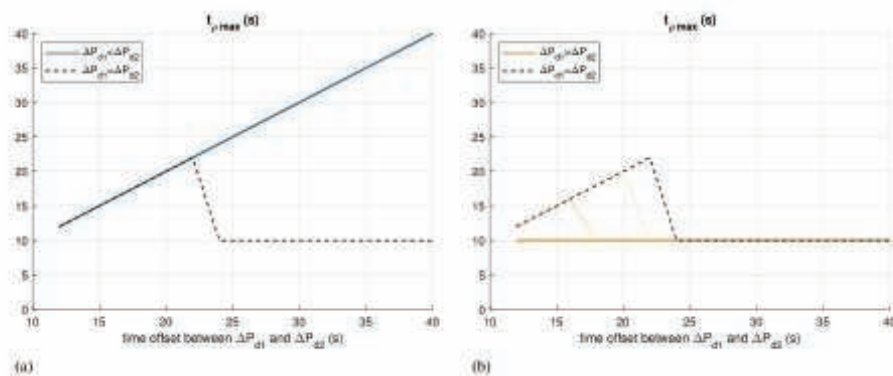


Fig. 9. Impact of temporal fractioning of power imbalances on the detection time of ρ_{max} .

- impact on the detection time of ω_{min} : from Fig. 7, it can be seen that the time of minimum instantaneous frequency $t_{\omega_{min}}$ is basically determined by the greatest power imbalance in the temporal sequence. When the first disturbance is less than the second one $\Delta P_{d1} < \Delta P_{d2}$, the time $t_{\omega_{min}}$ follows basically the pattern imposed by the second power imbalance (Fig. 7(a)). When instead the temporal sequence of power imbalances is characterized by a first disturbance greater than the following ones $\Delta P_{d1} > \Delta P_{d2}$, the detection time of ω_{min} depends on the time offsets between the disturbances only if they have comparable magnitudes, otherwise it is determined by the first power imbalance (Fig. 7(b));
- impact on the maximum absolute value of frequency rate ρ_{max} : the maximum absolute value of the RoCoF ρ_{max} is mainly determined by the fractioning of the power imbalance amounts, and only poorly affected by the temporal offset of the imbalances (Fig. 8). The maximum frequency rate observed in the transient is determined by the highest imbalance occurring in the temporal sequence. Only if the single imbalances have comparable magnitudes, a temporal offset between them can lead to a reduction of the maximum absolute RoCoF ρ_{max} . From Fig. 8(b), for the case of $\Delta P_{d1} > \Delta P_{d2}$, it can be observed that just few scenarios away from the symmetric case of $\Delta P_{d1} = \Delta P_{d2}$ (black dashed line), the temporal sequence of the power imbalances has a slightly positive effect on the maximum frequency rate. After that, the trend of the impact on ρ_{max} follows the same

pattern of the other cases. As general observation, it can be also noticed that an initial power imbalance followed by a second perturbation of lower magnitude (right sub-plot with $\Delta P_{d1} > \Delta P_{d2}$) determines slightly better system response also in this case, in terms of smaller values of ρ_{max} :

- impact on the detection time of ρ_{max} : from Fig. 9, it can be seen that the time of maximum absolute value of RoCoF $t_{\rho_{max}}$ is basically independent from the temporal offsets existing between the power imbalances. When the first disturbance is followed by a second greater one $\Delta P_{d1} < \Delta P_{d2}$, the maximum RoCoF ρ_{max} is always found at the occurrence time of the second power imbalance (Fig. 9(a)). When instead the first disturbance is greater than the following ones $\Delta P_{d1} > \Delta P_{d2}$, the detection time of ρ_{max} depends on the time offsets between the disturbances only if they have comparable magnitudes, and in any case till to a given time offset, when the two disturbances are temporally near; in the remaining scenarios, $t_{\rho_{max}}$ is found at the occurrence of the first power imbalance (Fig. 9(b)).

4. Application case: split of the continental Europe system

The work presented in the previous sections includes theoretical considerations regarding the analytical approach for the study of multiple power imbalances distributed during the transient, and it describes the impact on the typical frequency metrics used to assess the performance of the system such as minimum instantaneous frequency and maximum frequency rate. The relevance

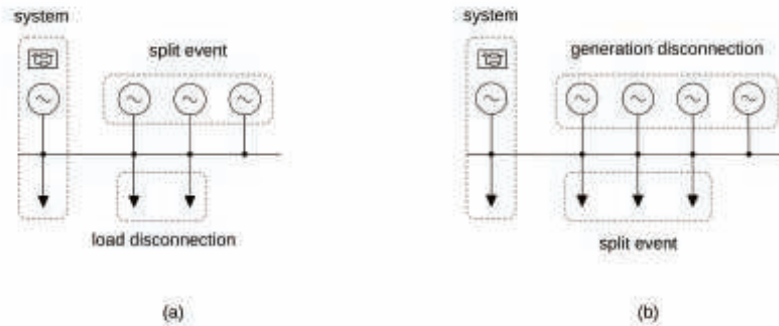


Fig. 10. Outline of the two-areas model of the CE system for simulation of split event: (a) North-West part; (b) South-East part.

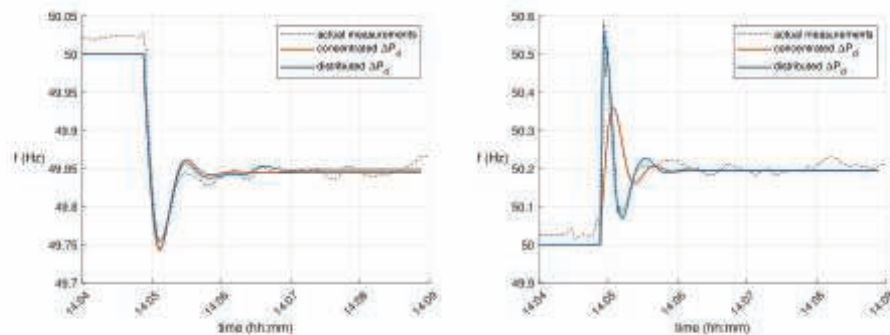


Fig. 11. Simulation of concentrated and distributed power imbalances: (a) frequency in the NW part; (b) frequency in the SE part.

of temporal distribution of power imbalances lies however on a more practical aspect. The actual transients occurring in power systems are in fact composed by a temporal sequence of events: those events are typically tripping of protections with consequent disconnections of generation, load, lines or devices. A sequence of power imbalances is therefore normally produced by the sequence of events originating the transient. So far, many incidents have been observed as loss of big, concentrated units, which could be modelled and studied as single disturbance occurred in the system at a given time. However, the transition process currently experienced by power systems with increasing share of renewable energy sources and increasing power flows exchanges within the different parts of the system are likely to produce an increase of incidents characterized by a temporal sequence of power imbalances. For these reasons, falling in the situation of multiple power imbalances might become a more frequent and relevant condition for the systems in the next future. For a correct representation of the power systems behaviour for such events, it is therefore necessary to understand the effects of temporally fractioned power imbalances and include them properly in a simulation model of the system. In this sense, considering a single power imbalance with the total amount concentrated instantaneously at a given time is a conservative approach as it gives the worst case conditions, while considering the temporal sequence of multiple power imbalances makes possible a more accurate study of the actual transient response of the system.

As application case of the considerations reported above, an actual event occurred in the power system of Continental Europe will be here considered. The event consisted in the separation of the interconnected system in two parts, resulting in significant power imbalances and consequent large over- and under-frequency transients. The split of the system was initiated by the

tripping of a busbar coupler, related to overloading conditions which were due to flows higher than expected. The system was separated in two parts, identified as North-West (NW) and South-East (SE): the split event determined a deficit of power in the NW part and a surplus of power in the SE part, for a total power imbalance of approximately 6.3 GW. Due to the large frequency deviations experienced in the two parts of the system, automatic and manual countermeasures were activated in order to stabilize the frequency. More details about the split event can be found in [5,25,26].

The CE power system subjected to the split event is simulated according to a specific modelling approach, where the two parts of the system are simulated independently with the application of an equivalent split event in both parts. The dynamic models of both parts include the representation of the main system dynamics with primary controllers for voltage and frequency, it accounts for the self-regulating effect of the loads and for the contribution of the neighbouring areas Nordic and Great Britain exchanged through HVDC links, and it includes the different defensive actions which were taken in both parts of the CE system to stabilize the frequency. More details about modelling and parameters of the CE system under split event can be found in [5]. A schematic outline of the implemented simulation models is shown in Fig. 10.

In the NW part, the effects caused by the split are simulated as generation loss of 6.3 GW, while the defensive actions are represented as a total load disconnection of 1.7 GW. In the SE part, the effects of the system separation are simulated as load loss of 6.3 GW, while the defensive actions are the coordinated disconnection of generation units for a total amount of 5.1 GW. The two systems are simulated for two different assumptions: in

$$\begin{aligned} \Delta\omega &= \frac{\frac{1}{M}s + \frac{1}{MT_3}}{s^2 + 2\zeta\omega_n s + \omega_n^2} \frac{\Delta P_d}{s} \\ \Delta\omega &= \frac{\Delta P_d}{MT_3\omega_n^2 s (s^2 + 2\zeta\omega_n s + \omega_n^2)} = \frac{\Delta P_d}{MT_3 \frac{1}{MT_3} s (s^2 + 2\zeta\omega_n s + \omega_n^2)} = R\Delta P_d \frac{T_3\omega_n^2 s + \omega_n^2}{s (s^2 + 2\zeta\omega_n s + \omega_n^2)} \\ &\text{adding and subtracting } \zeta^2\omega_n^2 \text{ at denominator and simplifying:} \\ \Delta\omega &= R\Delta P_d \frac{T_3\omega_n^2 s + \omega_n^2}{s (s^2 + 2\zeta\omega_n s + \omega_n^2 + \zeta^2\omega_n^2 - \zeta^2\omega_n^2)} = R\Delta P_d \frac{T_3\omega_n^2 s + \omega_n^2}{s [(s + \zeta\omega_n)^2 + \omega_n^2 (1 - \zeta^2)]} \\ &\text{adding and subtracting } (s + \zeta\omega_n)^2 + \omega_n^2 (1 - \zeta^2) \text{ at numerator and simplifying:} \\ \Delta\omega &= R\Delta P_d \frac{T_3\omega_n^2 s + \omega_n^2 + (s + \zeta\omega_n)^2 + \omega_n^2 (1 - \zeta^2) - (s + \zeta\omega_n)^2 - \omega_n^2 (1 - \zeta^2)}{s [(s + \zeta\omega_n)^2 + \omega_n^2 (1 - \zeta^2)]} \\ &= R\Delta P_d \frac{T_3\omega_n^2 s + \omega_n^2 + (s + \zeta\omega_n)^2 + \omega_n^2 (1 - \zeta^2) - s^2 - \zeta^2\omega_n^2 - 2\zeta\omega_n s - \omega_n^2 + \zeta^2\omega_n^2}{s [(s + \zeta\omega_n)^2 + \omega_n^2 (1 - \zeta^2)]} \\ &= R\Delta P_d \frac{T_3\omega_n^2 s - s^2 - 2\zeta\omega_n s + [(s + \zeta\omega_n)^2 + \omega_n^2 (1 - \zeta^2)]}{s [(s + \zeta\omega_n)^2 + \omega_n^2 (1 - \zeta^2)]} \\ &\text{distributing the denominator and putting } \omega_d = \omega_n \sqrt{1 - \zeta^2}: \\ \Delta\omega &= R\Delta P_d \left[\frac{1}{s} - \frac{s (s + 2\zeta\omega_n - T_3\omega_n^2)}{s [(s + \zeta\omega_n)^2 + \omega_d^2]} \right] = R\Delta P_d \left[\frac{1}{s} - \frac{s + 2\zeta\omega_n - T_3\omega_n^2}{(s + \zeta\omega_n)^2 + \omega_d^2} \right] \\ &\text{rearranging:} \\ \Delta\omega &= R\Delta P_d \left[\frac{1}{s} - \frac{s + \zeta\omega_n + \zeta\omega_n - T_3\omega_n^2}{(s + \zeta\omega_n)^2 + \omega_d^2} \right] = R\Delta P_d \left[\frac{1}{s} - \frac{s + \zeta\omega_n}{(s + \zeta\omega_n)^2 + \omega_d^2} - \frac{\zeta\omega_n - T_3\omega_n^2}{(s + \zeta\omega_n)^2 + \omega_d^2} \right] \\ &= R\Delta P_d \left[\frac{1}{s} - \frac{s + \zeta\omega_n}{(s + \zeta\omega_n)^2 + \omega_d^2} - \frac{\zeta\omega_n - T_3\omega_n^2}{\omega_d} \frac{\omega_d}{(s + \zeta\omega_n)^2 + \omega_d^2} \right] \\ &\text{finally, applying (18) to the three terms under the square brackets:} \\ \Delta\omega(t) &= R\Delta P_d \left[1 - e^{-\zeta\omega_n t} \left(\cos(\omega_d t) + \frac{\zeta\omega_n - T_3\omega_n^2}{\omega_d} \sin(\omega_d t) \right) \right] \end{aligned} \tag{19}$$

Box II.

the first hypothesis, all the power imbalances related to the incident events and to the defensive actions are considered as a single power imbalance ΔP_d of equivalent total amount, concentrated at the beginning of the frequency transient; in the second hypothesis, the power imbalances are considered temporally distributed over the frequency transient as sequence of multiple ΔP_{d_i} with given time offsets. The results of the dynamic simulations of the two parts of the CE system for the two different assumptions on the temporal distribution of the power imbalances are shown in Fig. 11.

It can be observed that for the NW part, the representation of incidents and defensive actions as an equivalent single power imbalance time-wise concentrated can already approximate quite sufficiently the actual frequency transient measured in the system. This is related to the rather large size of that portion of the CE system, holding more than 90% of the overall kinetic energy of the interconnected system [5]. For the SE part instead, the assumption of single concentrated power imbalance leads to inaccurate result, as the simulation is not capable of properly reproducing the transient response of the system, especially within the first instants (orange line in Fig. 11). For the examination of the case with power imbalances distributed temporally over the frequency transient, the total power imbalance of 6.3 GW can be divided into three portions, 4.4, 1.8 and 0.1 GW respectively. For the NW part, these three portions correspond

to a disconnection of generation, while for the SE part they correspond to a disconnection of load. The three portions are the same in both parts of the CE system, in terms of magnitudes ΔP_{d_i} and time offsets t_i . The instants t_i of the temporal sequence are identified through a preliminary estimation, made on the basis of the frequency thresholds currently defined for the CE system, followed by a quick trial and error adjustment. The results of the simulations performed assuming the specific temporal sequence for the power imbalances are shown in Fig. 11 with blue lines. It can be clearly noticed that the consideration of a proper temporal distribution of the multiple events representing incidents and defensive actions can accurately reproduce the actual transient response for both parts of the CE system. This allows a correct assessment of the dynamic behaviour of the system in terms of the relevant frequency metrics, i.e. minimum/maximum instantaneous value of the frequency and maximum absolute value of the frequency time derivative. For the specific case under examination, it can be also observed that the consideration of few temporal steps is already adequate to match the actual response of the system.

5. Conclusions

Power imbalances are the major factor affecting the frequency dynamics and stability of power systems. Actual frequency transients occurring in power systems are generally due to incidents

composed of a temporal sequence of events. These incidents are characterized by multiple power imbalances distributed over time. It is therefore important to understand and consider the effects of the temporal distribution of power imbalances on the frequency dynamics of the system, especially in the near perspective of expected operating conditions of power systems. To this purpose, the work first addresses the study of multiple power imbalances from a theoretical point of view, providing a detailed analytical examination of the phenomenon. The analytical approach makes possible the observation of the most relevant characteristics associated to the temporal distribution of power imbalances, providing a more in-depth understanding of the transient phenomena involving multiple disturbances of different magnitudes and time offsets. The fundamental aspect identified in the analysis is the non-simultaneity of the peak values of the single power imbalances, which occur at different instants during the transient realizing a specific transient response.

The theoretical considerations are then used to study the impact of the temporal distribution of power imbalances on the typical frequency metrics used to characterize the transient performances of the system. It has been observed that the minimum instantaneous value of the frequency is significantly affected by the temporal sequence of the disturbances, in terms of both magnitudes and time offsets. The maximum absolute value of the rate of change of frequency is instead determined by the highest imbalance occurring in the temporal sequence, as expected: the frequency rate depends therefore mainly on the fractioning of the magnitudes of the single power imbalances, while it is only poorly affected by the temporal offsets between them. For both metrics, it has been observed that an initial power imbalance followed by perturbations of lower magnitude means generally a better transient condition for the system.

Finally, the concepts and the considerations discussed in the paper are applied to the case of an actual event occurred in the power system of Continental Europe. The relevance of temporal distribution of power imbalances is in fact related to practical aspects of power system dynamics: as said, the actual incidents occurring in power systems are generally characterized by a temporal sequence of events, and this has a considerable impact on the dynamic response of the system, as noticed in the analytical study. A correct representation of the dynamic behaviour of the system requires then a proper consideration of the temporal distribution of the multiple disturbances determining the overall frequency transient. The results of the simulations for the application case show that the assumption of a single concentrated power imbalance can lead to inaccurate result: the conventional simulation approach is not capable of properly reproducing the transient response of the system, especially in the case of rather small areas of the system. The consideration of a proper temporal distribution of the power imbalances makes instead possible a match of the simulation model results with the actual frequency dynamics observed for the considered event, allowing for a correct assessment of the transient response of the system.

CRediT authorship contribution statement

Mariano G. Ippolito: Supervision, Writing - review & editing. **Rossano Musca:** Conceptualization, Methodology, Formal analysis, Writing - original draft. **Gaetano Zizzo:** Methodology, Writing - review & editing.

Declaration of competing interest

The authors declare that they have no known competing financial interests or personal relationships that could have appeared to influence the work reported in this paper.

Appendix A

Derivation of (9), underdamped case $\zeta < 1$.

Eq. (5) can be rearranged to exploit the known canonic inverse Laplace transforms:

$$\begin{aligned} \mathcal{L}^{-1}\left[\frac{1}{s}\right] &= 1 \\ \mathcal{L}^{-1}\left[\frac{s + \alpha}{(s + \alpha)^2 + \omega^2}\right] &= e^{-\alpha t} \cos(\omega t) \\ \mathcal{L}^{-1}\left[\frac{\omega}{(s + \alpha)^2 + \omega^2}\right] &= e^{-\alpha t} \sin(\omega t) \end{aligned} \tag{18}$$

Rearranging (5) as follows (see Eq. (19) in Box II).

Appendix B

Derivation of (12).

Expressing first derivative of (9):

$$\begin{aligned} \frac{d\omega(t)}{dt} &= R\Delta P_{\theta} \left[\zeta \omega_n e^{-\zeta \omega_n t} (\cos(\omega_d t) + k \sin(\omega_d t)) \right. \\ &\quad \left. - e^{-\zeta \omega_n t} (-\omega_d \sin(\omega_d t) + k \omega_d \cos(\omega_d t)) \right] \end{aligned} \tag{20}$$

Evaluating (20) at $t = t_p$, equating to zero and simplifying:

$$\begin{aligned} \left. \frac{d\omega(t)}{dt} \right|_{t=t_p} &= 0 \\ \text{putting } \alpha_p &= \omega_d t_p \\ \zeta \omega_n (\cos \alpha_p + k \sin \alpha_p) - (-\omega_d \sin \alpha_p + k \omega_d \cos \alpha_p) &= 0 \\ \zeta \omega_n \cos \alpha_p + k \zeta \omega_n \sin \alpha_p + \omega_d \sin \alpha_p - k \omega_d \cos \alpha_p &= 0 \\ \text{with } k \omega_d &= \zeta \omega_n - T_3 \omega_n^2 \\ \zeta \omega_n \cos \alpha_p + k \zeta \omega_n \sin \alpha_p + \omega_d \sin \alpha_p - \zeta \omega_n \cos \alpha_p &+ T_3 \omega_n^2 \cos \alpha_p = 0 \\ (k \zeta \omega_n + \omega_d) \sin \alpha_p &= -T_3 \omega_n^2 \cos \alpha_p \\ \tan \alpha_p &= -\frac{T_3 \omega_n^2}{k \zeta \omega_n + \omega_d} \\ \text{with } \omega_d &= \omega_n \sqrt{1 - \zeta^2} \\ \tan \alpha_p &= -\frac{T_3 \omega_n^2}{k \zeta \omega_n + \omega_n \sqrt{1 - \zeta^2}} = -\frac{T_3 \omega_n}{k \zeta + \sqrt{1 - \zeta^2}} \\ \text{substituting } k &= \frac{\zeta \omega_n - T_3 \omega_n^2}{\omega_d} \\ \tan \alpha_p &= -\frac{T_3 \omega_n \omega_d}{\zeta^2 \omega_n - \zeta T_3 \omega_n^2 + \omega_d \sqrt{1 - \zeta^2}} \\ &= -\frac{T_3 \omega_n \omega_d}{\zeta^2 \omega_n - \zeta T_3 \omega_n^2 + \omega_d (1 - \zeta^2)} \\ &= -\frac{T_3 \omega_d}{\zeta^2 - \zeta T_3 \omega_n + 1 - \zeta^2} \Rightarrow \\ \tan \alpha_p &= \frac{T_3 \omega_d}{\zeta T_3 \omega_n - 1} \\ \omega_d t_p &= \arctan\left(\frac{T_3 \omega_d}{\zeta T_3 \omega_n - 1}\right) \\ \text{and therefore, finally} \\ t_p &= \frac{1}{\omega_d} \arctan\left(\frac{T_3 \omega_d}{\zeta T_3 \omega_n - 1}\right) \end{aligned} \tag{21}$$

Appendix C

Derivation of (13).

Evaluating (9) at $t = t_p$:

$$\omega(t_p) = \omega_0 + R\Delta P_d \left[1 - e^{-\zeta\omega_0 t_p} (\cos \alpha_p + k \sin \alpha_p) \right] \quad (22)$$

With the purpose of replacing \cos and \sin from (22), according to the expression of $\tan \alpha_p$ derived in Appendix B, and dividing both terms by the sum of their squares to keep the trigonometric identity $\sin^2 + \cos^2 = 1$, the two terms can be expressed as:

$$\begin{aligned} \sin \alpha_p &= \frac{T_3 \omega_d}{\sqrt{T_3^2 \omega_d^2 + (\zeta T_3 \omega_n - 1)^2}} \\ \cos \alpha_p &= \frac{\zeta T_3 \omega_n - 1}{\sqrt{T_3^2 \omega_d^2 + (\zeta T_3 \omega_n - 1)^2}} \end{aligned} \quad (23)$$

The term $(\cos \alpha_p + k \sin \alpha_p)$ in (22) can be then rearranged as:

$$\begin{aligned} \cos \alpha_p + k \sin \alpha_p &= \frac{\zeta T_3 \omega_n - 1}{\sqrt{T_3^2 \omega_d^2 + (\zeta T_3 \omega_n - 1)^2}} \\ &+ \frac{\zeta \omega_n - T_3 \omega_n^2}{\omega_d} \frac{T_3 \omega_d}{\sqrt{T_3^2 \omega_d^2 + (\zeta T_3 \omega_n - 1)^2}} \\ &= \frac{\omega_d \zeta T_3 \omega_n - \omega_d + \omega_d \zeta T_3 \omega_n - T_3^2 \omega_n^2 \omega_d}{\omega_d \sqrt{T_3^2 \omega_d^2 + (\zeta T_3 \omega_n - 1)^2}} \\ &= \frac{\sqrt{T_3^2 \omega_n^2 (1 - \zeta^2) + \zeta^2 T_3^2 \omega_n^2 + 1 - 2\zeta T_3 \omega_n}}{\sqrt{T_3^2 \omega_n^2 - 2\zeta T_3 \omega_n + 1}} = -\sqrt{\frac{T_3 - T_2}{MR}} \end{aligned}$$

considering $\omega_n = \sqrt{\frac{1}{MRT_3}}$, $\zeta = \frac{T_2 + MR}{2} \omega_n$ (24)

$$\begin{aligned} T_3^2 \omega_n^2 - 2\zeta T_3 \omega_n + 1 &= T_3^2 \frac{1}{MRT_3} \\ &- 2 \frac{(T_2 + MR)\omega_n}{2} T_3 \omega_n + 1 \\ &= \frac{T_3}{MR} - (T_2 + MR) T_3 \frac{1}{MRT_3} + 1 \\ &= \frac{T_3}{MR} - \frac{(T_2 + MR) T_3}{MRT_3} + 1 \\ &= \frac{T_3}{MR} - \frac{T_2 + MR}{MR} + 1 = \frac{T_3 - T_2}{MR} \end{aligned}$$

and therefore

$$\cos \alpha_p + k \sin \alpha_p = -\sqrt{\frac{T_3 \omega_n^2 - 2\zeta T_3 \omega_n + 1}{MR}} = -\sqrt{\frac{T_3 - T_2}{MR}}$$

finally, substituting $(\cos \alpha_p + k \sin \alpha_p)$ in (22)

$$\omega(t_p) = \omega_0 + R\Delta P_d \left(1 + e^{-\zeta\omega_0 t_p} \sqrt{\frac{T_3 - T_2}{MR}} \right)$$

References

[1] F. Conte, S. Massucco, M. Paolone, G.P. Schiapparelli, E. Silvestro, Y. Zuo, Frequency stability assessment of modern power systems: Models definition and parameters identification, *Sustain. Energy Grids Netw.* 23 (2020) 100384, <http://dx.doi.org/10.1016/j.segan.2020.100384>.
 [2] F. Bignucolo, R. Caldon, M. Coppo, F. Pasut, M. Pettinà, Integration of lithium-ion battery storage systems in hydroelectric plants for supplying primary control reserve, *Energies* 10 (2017) 98, <http://dx.doi.org/10.3390/en10010098>.

[3] A. Kannan, M. Nuschke, B.-P. Dobrin, D. Strauß-Mincu, Frequency stability analysis for inverter dominated grids during system split, *Electr. Power Syst. Res.* 188 (2020) <https://dx.doi.org/10.1016/j.epsr.2020.106550>.
 [4] H.H. Albelou, M. Hamedani-Golsban, T. Njenda, P. Siann, A survey on power system blackout and cascading events: Research motivations and challenges, *Energies* 12 (2019) 682, <http://dx.doi.org/10.3390/en12040682>.
 [5] M.G. Ippolito, R. Musca, G. Zizzo, Analysis and simulations of the primary frequency control during a system split in continental europe power system, *Energies* 14 (2021) <http://dx.doi.org/10.3390/en14051456>.
 [6] S.L. Ghadamasi, N.J. Nwulu, A comparative analysis of generation and transmission expansion planning models for power loss minimization, *Sustain. Energy Grids Netw.* 26 (2021) 100456, <http://dx.doi.org/10.1016/j.segan.2021.100456>.
 [7] ENTSO-E SPD (System Protection & Dynamics) subgroup, *Dispersed generation impact on CE region security*, Brussels, 2014.
 [8] S. Canevese, E. Caspessoni, A. Gatti, M. Rossi, Monitoring of frequency disturbances in the European continental power system, in: *Proceedings of the 2016 AET International Annual Conference (AET) Capri, Italy*, 5-7 2016.
 [9] T. Weissbach, E. Welfunder, High frequency deviations within the European Power System: Origins and proposals for improvement, in: *Proceedings of the 2009 IEEE/PES Power Systems Conference and Exposition Seattle, USA*, 15-18 2009.
 [10] Z. Jiang, N. Tong, Y. Liu, Y. Xue, A.G. Tarditi, Enhanced dynamic equivalent identification method of large-scale power systems using multiple events, *Electr. Power Syst. Res.* 189 (2020) 106569, <http://dx.doi.org/10.1016/j.epsr.2020.106569>.
 [11] M.R. Rapizza, S. Canavesi, Fast frequency regulation and synthetic inertia in a power system with high penetration of renewable energy sources: Optimal design of the required quantities, *Sustain. Energy Grids and Netw.* 24 (2020) 100407, <http://dx.doi.org/10.1016/j.segan.2020.100407>.
 [12] N.S. Nise, *Control Systems Engineering*, sixth ed., Wiley, 2011.
 [13] MATLAB scientific computation software, <https://mathworks.com/products/matlab.html>.
 [14] ENTSO-E, *Guidance document for national implementation for network codes on grid connection, Rate of Change of Frequency (RoCoF) without capability*, Brussels, 2018.
 [15] K. Das, M. Altan, A.D. Hansen, P.E. Sørensen, Inertia dependent droop based frequency containment process, *Energies* 12 (2019) <http://dx.doi.org/10.3390/en12091048>.
 [16] A. Mujcinagic, M. Kusljagic, J. Osmic, Frequency response metrics of an interconnected power system, in: *Proceedings of the 2019 54th International Universities Power Engineering Conference (UPEC) Bucharest, Romania*, 3-6 2019.
 [17] H. Bevrani, H. Golpira, A.R. Messina, N. Hatziaziyriou, F. Milano, T. Ise, Power system frequency control: An updated review of current solutions and new challenges, *Electr. Power Syst. Res.* 194 (2021) 107114, <http://dx.doi.org/10.1016/j.epsr.2021.107114>.
 [18] M. Nedd, W. Bukhsh, C. Maclver, K. Bell, Metrics for determining the frequency stability limits of a power system: A GB case study, *Electr. Power Syst. Res.* 190 (2021) 106553, <http://dx.doi.org/10.1016/j.epsr.2020.106553>.
 [19] ENTSO-E SPD (System Protection & Dynamics) Subgroup, *Dynamic Study Model—Range of Applications and Modelling Basis*, ENTSO-E, Brussels, Belgium, 2015, Available online https://europeanenergyunion.eu/clean-documents/Publications/SOC/Continental_Europe/InitialDynamicModel_Handbook_gen.pdf (Accessed March 2021).
 [20] ENTSO-E, *Initial dynamic model of continental europe*, 2021, Available online: <https://dx.doi.org/10.3390/en12091048> (Accessed March 2021).
 [21] A. Semerow, S. Hahn, M. Luther, W. Sattinger, H. Abildgaard, A. Garcia, G. Giannuzzi, Study model for the interconnected power system of continental europe in different simulation tools, in: *2015 IEEE Eindhoven PowerTech, Eindhoven, The Netherlands*, 29 June-2 2015.
 [22] H.P. Asal, E. Madsen, H.W. Weber, E. Gele, Development in Power-Frequency Characteristic and Droop of the UCTE Power System and Proposals for New Recommendations for Primary Control, *CIGRE Group 39*, 1998.
 [23] M. Scherer, *Frequency Control in the European Power System Considering the Organisational Structure and Division of Responsibilities* (Doctoral thesis), Eidgenössische Technische Hochschule ETH, Zürich, Switzerland, 2016.
 [24] NEPLAN power systems analysis software, <https://www.neplan.ch/en-products/>.
 [25] ENTSO-E, *System separation in the continental Europe Synchronous Area on 8 2021-2nd update*, 2021, <https://www.entsoe.eu/news/2021/01/26/system-separation-in-the-continental-europe-synchronous-area-on-8-january-2021-2nd-update/> [last accessed on 2021].
 [26] ENTSO-E, *Continental Europe Synchronous Area Separation on 8 2021 - Interim Report*, Brussels, Belgium, 26 2021, 2021.

6.4 Energy from the Waves: Integration of a HESS to a Wave Energy Converter in a DC Bus Electrical Architecture to Enhance Grid Power Quality



Article

Energy from the Waves: Integration of a HESS to a Wave Energy Converter in a DC Bus Electrical Architecture to Enhance Grid Power Quality

Linda Barelli ¹, Ermanno Cardelli ¹, Dario Pelosi ¹, Dana Alexandra Ciupageanu ^{1,2}, Panfilo Andrea Ottaviano ³, Michela Longo ^{4,*} and Dario Zaninelli ⁴

¹ Department of Engineering, University of Perugia, Via G. Duranti 93, 06125 Perugia, Italy; linda.barelli@unipg.it (L.B.); ermanno.cardelli@unipg.it (E.C.); dario.pelosi@unipg.it (D.P.); dana_ciupageanu@yahoo.com (D.A.C.)

² Engineering Faculty, University Politehnica of Bucharest, Splaiul Independentei 313, 060042 Bucharest, Romania

³ VGA S.R.L., Via Ugo Foscolo 1, 06053 San Nicolò di Celle, Italy; andrea.ottaviano@vagasrl.com

⁴ Department of Energy, Politecnico di Milano, Via La Masa, 34, 20156 Milano, Italy; dario.zaninelli@polimi.it

* Correspondence: michela.longo@polimi.it



Citation: Barelli, L.; Cardelli, E.; Pelosi, D.; Ciupageanu, D.A.; Ottaviano, P.A.; Longo, M.; Zaninelli, D. Energy from the Waves: Integration of a HESS to a Wave Energy Converter in a DC Bus Electrical Architecture to Enhance Grid Power Quality. *Energies* **2022**, *15*, 10. <https://doi.org/10.3390/en15010010>

Academic Editors: Antonino Oscar Di Tommaso and Massimo Caruso

Received: 12 November 2021

Accepted: 17 December 2021

Published: 21 December 2021

Publisher's Note: MDPI stays neutral with regard to jurisdictional claims in published maps and institutional affiliations.



Copyright: © 2021 by the authors. Licensee MDPI, Basel, Switzerland. This article is an open access article distributed under the terms and conditions of the Creative Commons Attribution (CC BY) license (<https://creativecommons.org/licenses/by/4.0/>).

Abstract: The need for environmental protection is pushing to a massive introduction of energy production from renewables. Although wind and solar energy present the most mature technologies for energy generation, wave energy has a huge annual energy potential not exploited yet. Indeed, no leading device for wave energy conversion has already been developed. Hence, the future exploitation of wave energy will be strictly related to a specific infrastructure for power distribution and transmission that has to satisfy high requirements to guarantee grid safety and stability, because of the stochastic nature of this source. To this end, an electrical architecture model, based on a common DC bus topology and including a Hybrid Energy Storage System (HESS) composed by Li-ion battery and flywheel coupled to a wave energy converter, is here presented. In detail, this research work wants to investigate the beneficial effects in terms of voltage and current waveforms frequency and transient behavior at the Point of Common Coupling (PCC) introduced by HESS under specific stressful production conditions. Specifically, in the defined simulation scenarios it is demonstrated that the peak value of the voltage wave frequency at the PCC is reduced by 64% to 80% with a faster stabilization in the case of HESS with respect to storage absence, reaching the set value (50 Hz) in a shorter time (by −10% to −42%). Therefore, HESS integration in wave energy converters can strongly reduce safety and stability issues of the main grid relating to intermittent and fluctuating wave production, significantly increasing the tolerance to the expected increasing share of electricity from renewable energy sources.

Keywords: DC bus; electrical architecture; flywheel; hybrid energy storage system; Li-ion battery; power quality; wave energy

1. Introduction

Nowadays, a huge interest in exploiting sustainable and renewable energy sources such as solar, wind, hydro, wave and tidal, is growing. The main concerns stimulating research and development activities in this field include aspects as environmental protection and energy independence [1]. Among the renewables, wave energy has a great annual energy potential equal to an amount of 32,000 TWh worldwide, of which 2000–4000 TWh can be exploited [2]. Cumulative global wave and tidal stream capacity has more than doubled since 2017, reaching approximately 65 MW in 2020 and slowly approaching the Ocean Energy Systems vision of 300 GW of global capacity by 2050, as reported in [3]. Although the great potential, the wave energy industry is struggling to reach cost-efficient and reliable systems to follow the path towards commercialization [2]. Moreover, not only

must the technological aspects be considered, but also the implications relating to social and ecological challenges [4], especially for what regards protected marine and ocean areas.

As for wind and solar energy, another major issue regards the integration of Wave Energy Converters (WECs) into electricity network because of the mismatch between load demand and fluctuating power generation due to the stochastic nature of waves [5]. Furthermore, no WEC technology can be considered the leading one; consequently, the wide variety of WEC systems makes it difficult to generally discuss power quality [6]. However, the large variation of output power is a common issue. Thus, the infrastructure costs and complexity have to be faced. Indeed, as analyzed in [7], a study of grid connection assuming an off-shore 20 MW wave farm linked to the Irish distribution network has been carried out. In detail, it was shown that the grid connection costs account for 69% of the total electrical equipment budget.

Among the proposed solutions to mitigate power quality issues, Energy Storage Systems (ESSs) represent one of the best available paths for a better Renewable Energy Source (RES) exploitation and penetration, thanks to their good scalability, fast responsiveness, and efficiency [8–12]. Several studies have been addressed to the application of ESS in WEC systems. As example, Zhang et al. [13] apply a Battery Energy Storage (BES) to the DC link of the back-to-back converter linked to the WEC in order to smooth the generated power. Murray et al. [14] describe the applications of an energy storage system based on supercapacitors in a full-scale, grid-connected offshore WEC. Specifically, such study is focused on the minimization of the output power fluctuations, the start sequences for the machine and the Low-Voltage Ride-Through (LVRT) capability. Aubry et al. [15] report the sizing of an Energy Storage System based on supercapacitors with two State of Charge (SoC) control strategies and two power quality criteria for power smoothing. Other noteworthy research activities concerning ESS integration in WEC systems are discussed in [16–20].

Nevertheless, because of the intrinsic limits of state-of-the-art energy storage technologies, a single device cannot cover in an effective and efficient way all the operating modes on different time scales. Hence, a solution to mitigate this issue is represented by hybridization of complementary ESSs. As matter of fact, Hybrid Energy Storage Systems (HESSs), including multiple storage devices complementary to each other, can cope with storage requirements for different timeframes, merging the positive features of base-technologies and extending their application ranges [21]. From the power quality point of view, the integration of HESS in WECs has been widely studied in [22–25], with the purpose of smoothing the generated output power fluctuations. Nevertheless, to the best of our knowledge, no studies address the comparative analysis of electrical behavior of a WEC with and without the HESS integration, to assess the consequent impact in terms of power quality at the Point of Common Coupling (PCC).

In reference to the power quality issues relating to WEC connection to the main grid, as previously stated, this paper aims to evaluate the improvement in power quality (e.g., in terms of voltage waveform frequency and current transient behavior) at the PCC produced by the HESS integration, with respect to the case of storage absence. Specifically, the considered HESS is composed by a 24 kWh Li-ion battery and a 33 kW/2.1 kWh Flywheel Energy Storage System (FESS), and it is coupled to a 250 kW WEC by means of a common DC bus. The choice of such architecture topology presents several positive features, such as easy management, high quality of the energy, reduced number of power converters and no reactive power exchange, although currently incomplete standardization is defined as the main drawback [26]. In particular, an electrical architecture based on a common DC bus is widely used in microgrids, as reported in [27–30].

Moreover, the implemented power management strategy is based on a suitable Simultaneous Perturbation Stochastic Approximation (SPSA) algorithm, as reported in our previous paper [31]. By means of SPSA power management strategy, it was demonstrated that HESS coupled to the WEC allows to reduce more than 80% the oscillations power ramp (kW/s) at the PCC.

Through the electrical model and simulations under large and sudden WEC power variations, defined based on the experimental data gathered from three installation sites, the present study demonstrates that, in case of HESS integration, the consequent peak value of the voltage wave frequency at the PCC is reduced over 64%. Furthermore, the regimen value (50 Hz) is re-established in a shorter time (up to 42%).

The paper is organized as follows: in Section 2 the main components of the considered system are described; in Section 3 the simulation scenarios, relating to the most stressful conditions with reference to WEC power profiles, have been defined, while Section 4 reports and discusses the main results obtained from the simulations. Finally, the main contributions of this research work are argued in the Conclusions paragraph.

2. Model Description

In this section a detailed description of the components implemented in SimPowerSystems (SPS) environment has been carried out. The model layout is represented in Figure 1.

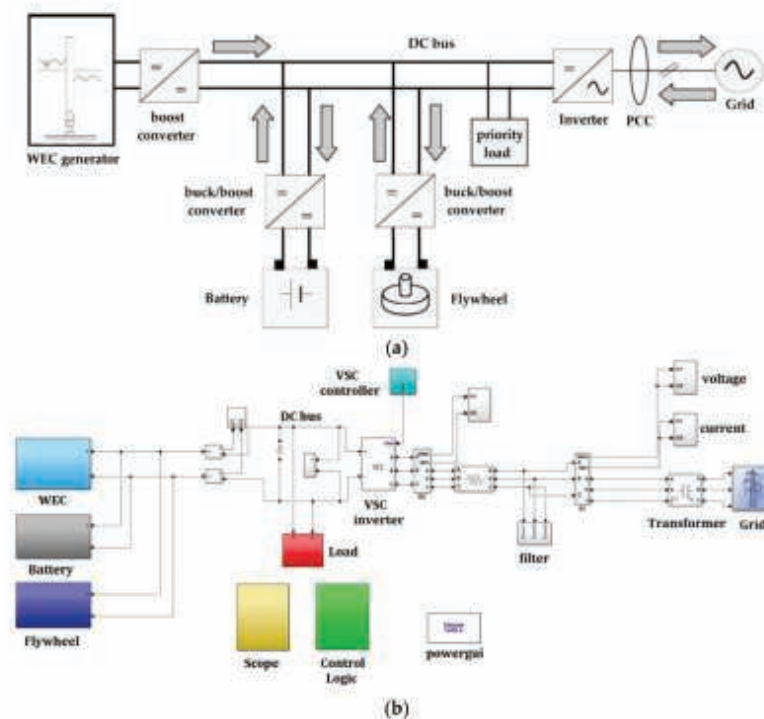


Figure 1. Schematic layout of the modelled system: (a) conceptual configuration and (b) Sim-scape/SimPowerSystems implementation.

The chosen electrical architecture topology is based on a common DC bus, whose voltage is fixed at $650 V_{DC}$, in order to interface with the typical low voltage grid of European Countries (i.e., $400 V_{L-L}$ according to the mandatory low voltage connection specifications of the Italian national electric network [32]). The overall system results in (i) a 250 kWp WEC generator, (ii) a battery having a capacity of 24 kWh and 72 kW/24 kW as maximum discharge/charge power, coupled with a flywheel of 33 kW rated power and 2.1 kWh capacity. Furthermore, a 4 kW priority load directly connected to the common DC bus, relative to the WEC auxiliary systems, has been taken into account.

2.1. Wave Energy Converters—WEC

The Oscillating Wave Surge Converter technology (OWSC) is considered. A schematic view is illustrated in Figure 2, deduced from [33].

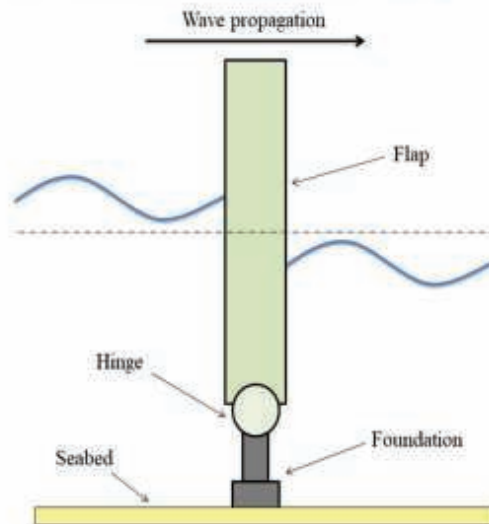


Figure 2. Schematic view of an oscillating wave surge converter.

Figure 3 depicts the implemented WEC generator, modeled as Permanent Magnet DC Brushless Generator (PMBG). Since the present work is mainly focused on the electric aspects relating to the integration of HESS in a WEC, only the generator connected at the Power-Take-Off (PTO) has been taken into account. The rated power of the PMBG is equal to 250 kW with a nominal DC voltage of 400 V. The inertia momentum of the PMBG is equal to $1.33 \text{ kg}\cdot\text{m}^2$ and the viscous damping to 78.8 Nms. Since the PMBG block is developed in Simscape, an interface block is used to link the Simscape block to the SPS environment. Furthermore, a boost converter is used to increase the PMBG DC voltage up to the DC bus voltage (fixed at 650 V in order to interface with the 400 V_{L-L} three-phase low voltage grid). The control of the boost converter is performed by means of Pulse Width Modulation (PWM) strategy.

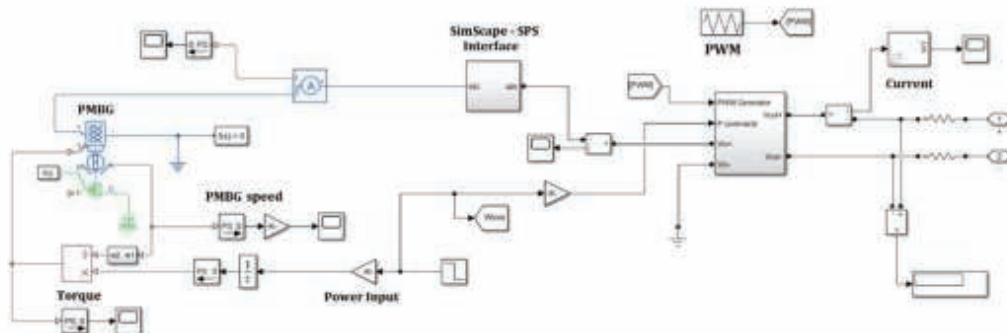


Figure 3. Wave Energy Converter (WEC) generator section.

2.2. Li-Ion Battery Characteristics

Li-Ion battery section is implemented through a generic dynamic block from SPS library within Simulink environment. Such block follows Equations (1) and (2) according to charge and discharge respectively [34].

$$f_{disch}(C^{out}, i^*, i) = E_0 - K \cdot \frac{C^{max}}{C^{max} - C^{out}} \cdot i^* - K \cdot \frac{C^{max}}{C^{max} - C^{out}} \cdot C^{max} + E^{exp} \cdot e^{-\frac{exp}{C^{out}}} \quad (1)$$

$$f_{ch}(C^{out}, i^*, i) = E_0 - K \cdot \frac{C^{max}}{C^{max} + 0.1 \cdot C^{out}} \cdot i^* - K \cdot \frac{C^{max}}{C^{max} - C^{out}} \cdot C^{out} + E^{exp} \cdot e^{-\frac{exp}{C^{out}}} \quad (2)$$

where C^{out} represents the extracted capacity [Ah], C^{max} is the maximum capacity [Ah], C^{exp} defines the battery capacity in the exponential zone [Ah], E_0 is the constant voltage [V], E^{exp} the voltage in the exponential zone [V] and K represents the polarization constant [Ah^{-1}]. Constant values, listed in Table 1, are defined in reference to battery specifications and available data in the scientific literature [35,36].

Table 1. Parameters implemented for the considered Li-Ion battery.

Parameter	Variable	Value
Maximum capacity	C^{max} [Ah]	125
Exponential zone capacity	C^{exp} [Ah]	6.8
Nominal voltage	E_0 [V]	400
Exponential zone capacity	E^{exp} [V]	425
Polarization constant	K [Ah^{-1}]	0.00682
Internal resistance	R_{int} [Ω]	0.002

The selected battery (24 kWh pack; maximum charging current (1C, 57.1 A@420V); maximum discharge current (3C, 205.7A@350V), from [32]) and the bidirectional DC/DC converter (buck/boost converter) are shown in Figure 4. In detail, the bidirectional buck/boost converter is used to adjust the battery voltage both in charging and discharging processes. It receives as input the power from/to the battery and the control signals computed by the PWM strategy. Such power is imposed according to the procedure reported in Section 2.1. Moreover, instantaneous battery SoC is computed within SPS block.

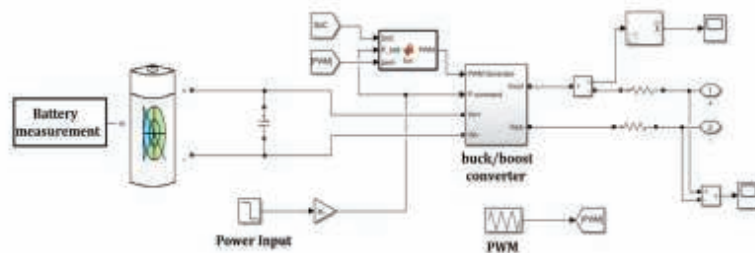


Figure 4. Li-Ion battery subsystem and its buck-boost converter, adapted with permission from [26], Elsevier, 2020.

2.3. Flywheel and Electric Machine

The flywheel section is modeled as an inertia connected to the mechanical part of the Permanent Magnet DC Brushless Machine (PMBM). Since the FESS capacity is sized equal to 2.1 kWh, assessed in reference to Equation (3), with operating rotational speed range of 3500–8500 rpm, the corresponding inertia momentum is set at 22.4 $kg \cdot m^2$.

$$E = \frac{1}{2} \cdot J \cdot (\omega_{\max}^2 - \omega_{\min}^2) \quad (3)$$

where J is the inertia momentum [kg·m²]; ω_{\min} and ω_{\max} respectively, minimum and maximum angular velocity [rad/s]. Specifically, $\omega_{\max} = 890.1$ rad/s and $\omega_{\min} = 366.5$ rad/s.

The flywheel subsystem block diagram is illustrated in Figure 5. It includes the mechanical flywheel, the PMBM electric machine, the buck/boost converter and the related control scheme. As concerns the electric machine, it is noted as in this work the design and HESS operation is focused on the energy exchanges among its components. A PMBM with a maximum power of 33 kW in relation to the torque vs. speed characteristic curve has been implemented. The power required from or supplied to the flywheel, as well as for the battery, is imposed according to the specific procedure described in Section 3 and transmitted as input to the PMBM, which has a proper internal torque control. The interface block allows enabling the interconnection between Simscape (SSC) and SPS blocks. The buck/boost converter regulates, through a PWM strategy, the electric machine input and output powers.

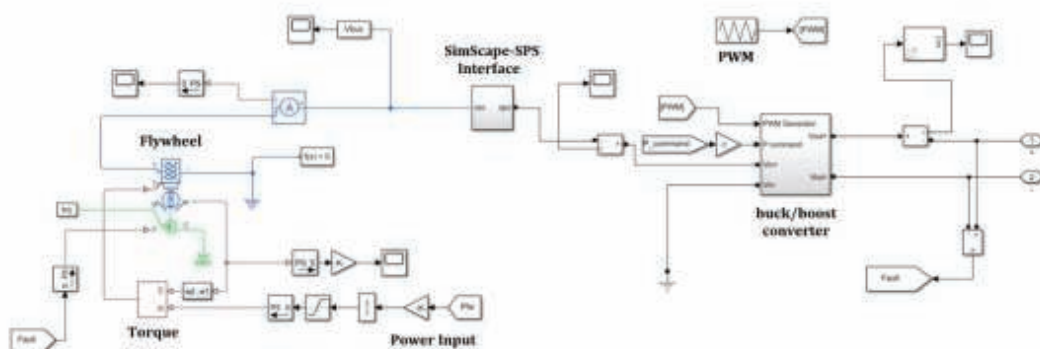


Figure 5. Flywheel and electric machine modeling.

The auxiliary systems to supply are modelled as a priority load connected to the DC bus by means of a dedicated VSC inverter [37]. The load is considered as a pure resistive three-phase element and the rated power resulting from the specific studied WEC is fixed at 4 kW.

3. Different Scenarios for Simulation

In this section the investigated scenarios have been defined. Specifically, three different scenarios are identified both for HESS presence and absence. The definition of simulation scenarios for the Simscape electrical model follows a three stages procedure, described forward.

- Scenario 1—instantaneous power vectors are generated for three different wave power plants, processing the sea state matrix for each site (i.e., site 1—France, site 2—England, site 3—Norway), as reported in [31].
- Scenario 2—the yearly power vectors are processed, separating them by days. A set of parameters (i.e., bandwidth, mean power, bandwidth to mean power ratio, mean ramp) are evaluated for each day, aiming to select the most representative ones for all the three sites. Consequently, simulation profiles (with 1 s time step for 24 h) are extracted from the yearly profile and employed in simulation in the Simulink environment (the model is described in detail in [31] and the rated power values for each component are indicated also in the previous section). The representative days are selected based on particular statistics, as listed below. The statistical analysis procedure is depicted in

the previous works of the Authors for similar applications [38,39]. Specifically, days selection is realized according the following criteria:

- Day 1: maximum bandwidth;
- Day 2: maximum mean power;
- Day 3: maximum bandwidth to mean power ratio;
- Day 4: minimum bandwidth to mean power ratio;
- Day 5: maximum mean ramp.

A suitable model, previously developed in Simulink environment is applied for simulations over the selected most representative days [31]. The applied Simulink model has been implemented based on the mathematical equations, efficiency maps and including a stochastic power management section, suitably developed by applying a SPSSA algorithmic method for power management optimization. Specifically, the power management is defined pursuing two objectives:

- (i) smoothing the power profile sent to the grid and
- (ii) reducing the power ramp associated to the battery in order to preserve it. Thus, more oscillating power profile is imposed to the flywheel, while a flatter profile is exchanged by the battery, all in the context of reducing the power ramp at the PCC. Our previous research proved that the proposed power management strategy achieves more than 80% ramp at the PCC compared to the original renewable energy source profile and around 70% smoothing regarding the battery profile compared to the flywheel [31]. The wave power ramp cumulative distribution function corresponding to the selected days in all three sites is depicted in Figure 6. It is evident that the wave power ramp values do not exceed 20 kW/s during the monitoring time span in none of the cases. Moreover, in 90% of the occurrences, the power ramp values are under 5 kW/s.

- Scenario 3—the input power profiles in the SPS model are established based on the Simulink results for the representative days, selecting the correlated wave production, battery and flywheel power from the results, as well as the initial battery and flywheel SoCs. This approach extends the analysis performed over daily basis in the Simulink mathematical model to a more detailed level in the implemented electrical architecture. Given the complexity of the model, the simulation time is restricted to only four seconds. It is highlighted that, taking into account the dynamics of electrical systems and the time response of the HESS components, the behavior of the system can be properly investigated even in such reduced timespan. Three simulation scenarios are defined, aiming to observe the dynamic behavior of the HESS coupled to the wave power plant. The scenarios are defined focusing on the most stressful conditions associated to the step-up and step-down wave power variation:
 - Case 1: wave power step-up, the power generated by the wave converter suddenly increases from 30 kW to 50 kW, by 67%. The 20 kW step value is selected based on the power ramp cumulative probability illustrated in Figure 6. To compensate this variation, the HESS components, according to the implemented SPSSA power management, start to absorb more power, in order to smooth the power flow at the PCC. Specifically, according to the outcomes of the simulations carried out in the Simulink environment, the flywheel withdraws from the DC bus 9.1 kW more and the battery 4.2 kW more power. Both flywheel and battery keep their charging mode of operation. The power profiles are exhibited in Figure 7a.
 - Case 2: wave power step-down, the wave converter power drops from 50 kW to 30 kW, simulating symmetrically to Case 1 the 20 kW power step. In this case, both battery and flywheel keep their charging operating mode, but reduce the power they absorb in order to smooth the power flow at the PCC. The flywheel withdraws from the DC bus 12 kW less power and the battery reduce the absorbed power by 5 kW, as depicted in Figure 7b.

- Case 3: wave power step-down, the wave converter power drops by 90%, from 50 kW to 5 kW. This step value is taken into account as a forward stressing dynamic condition, aiming to prove that the proposed configuration and related power management are operating properly, being capable of coping with even higher fluctuations than expected. Under these circumstances, both battery and flywheel switch their operating modes to discharge, aiming to reduce the difference between the power flow at the PCC. Thus, the flywheel provides 29 kW more power, while the battery increases the delivered power by 10.2 kW, as depicted in Figure 7c.

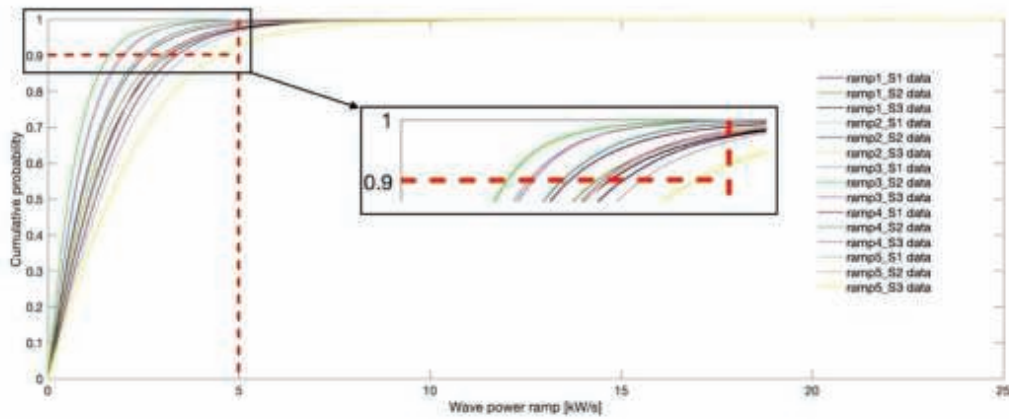


Figure 6. Cumulative density function of the wave power ramp.

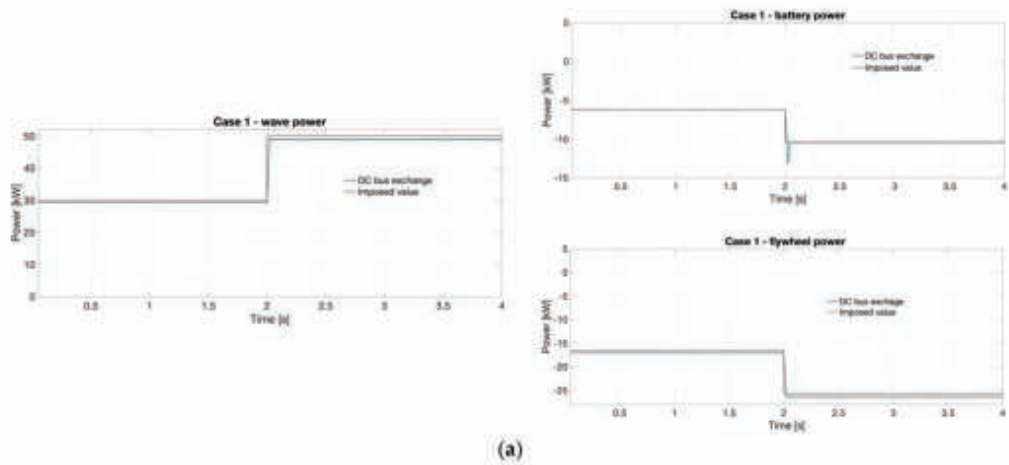


Figure 7. Cont.

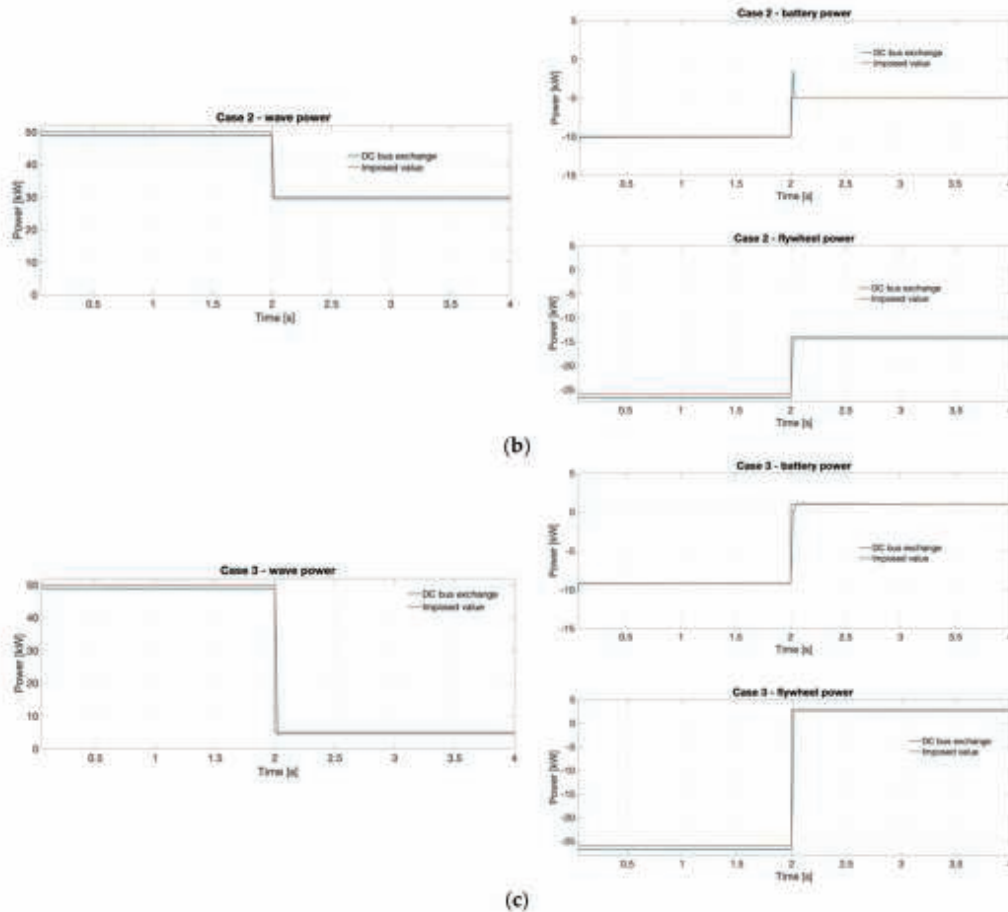


Figure 7. Wave power and HESS power (battery and flywheel power) for different case study: (a) Case 1, (b) Case 2 and (c) Case 3.

4. Analysis and Discussion of Results

The main objective concerns the system behavior at the Point of Common Coupling (PCC) in order to prove the benefits introduced by the HESS in smoothing the generated power and consequently assessing the better quality of the power injected to the grid. Such aspect greatly contributes to grid safety and stability of supply. As the objective of the proposed power smoothing approach is to obtain a smoother active power component transmitted to the grid, the performance assessments are made in terms of active power. Moreover, both devices included in the HESS configuration provide a DC output; thus, the reactive power component is not a focus for such investigation, as detailed also in [40,41]. Further, the frequency behavior is analyzed, as an immediate correlation to the active power [42]. Figure 8 depicts the power exchanges at the PCC. As expected, according to the SPSA power management strategy, in case of HESS integration the power ramp is reduced by 68% up to 84% in the three cases, with respect to the case of energy storage absence. According to the simulation results, it is highlighted that the smoothing percent

of the power at the PCC compared to the wave production increases with the size of the power step.

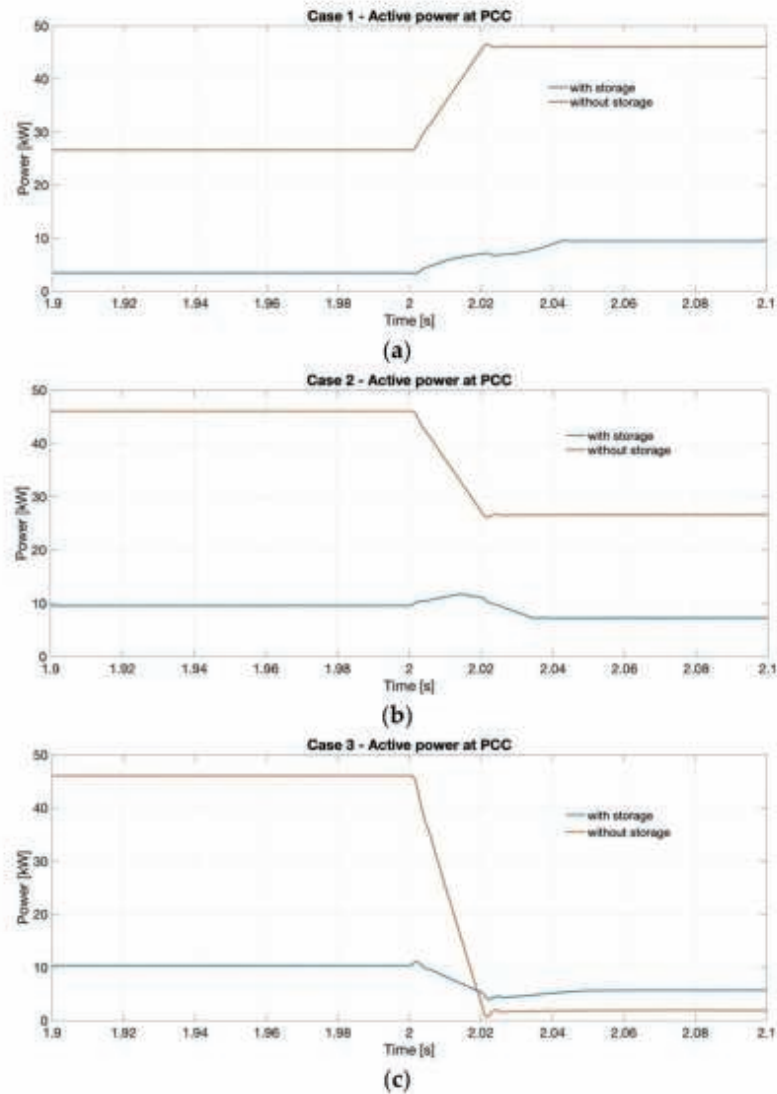


Figure 8. Power exchanges at PCC: (a) Case 1, (b) Case 2 and (c) Case 3.

In the following, the behavior at the PCC is analyzed in terms of current and voltage frequency response in the three simulation scenarios. According to Figure 9 (single phase current is depicted, given that the network is considered balanced among the three phases), it is noticeable that the HESS coupling introduces, because of the additional converters, a slightly longer current transient. However, as already mentioned for the power exchanges (Figure 8), the steady state value is reduced, the HESS enabling a smoother response to the sudden change in the wave produced power.

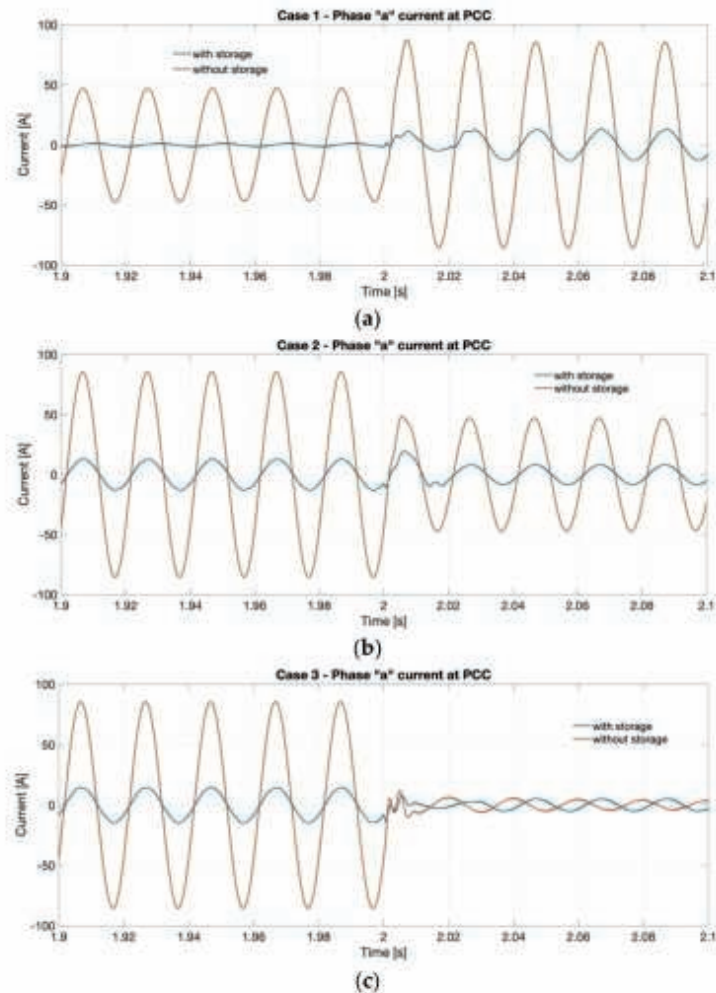


Figure 9. Current behavior at PCC: (a) Case 1, (b) Case 2 and (c) Case 3.

For what concerns the voltage frequency, as pictured in Figure 10, a significantly lower peak during the transient is remarked when the HESS is coupled. Specifically, the peak value is reduced by 77% in Case 1, by 64% in Case 2 and by 80% in Case 3 when the largest wave power variation is imposed. It is remarked that, as stated before for the power smoothing performance, the benefits of coupling the HESS to the highly oscillating wave power plant increase with the power ramp at the wave energy converter. Although for the considered system the peak value is under 0.5% in all the investigated scenarios, such impact is very important under the RES increasing integration perspective, particularly highly variable RES such as wave generation. Moreover, the frequency stabilizes faster when the HESS is coupled to the wave power plant, reaching the set value (50 Hz) in a time shorter by 10% in the first scenario, 28% in the second and 42% in the third one. Also in this case the beneficial effect of the HESS integration increases with the solicitation caused by the WEC.

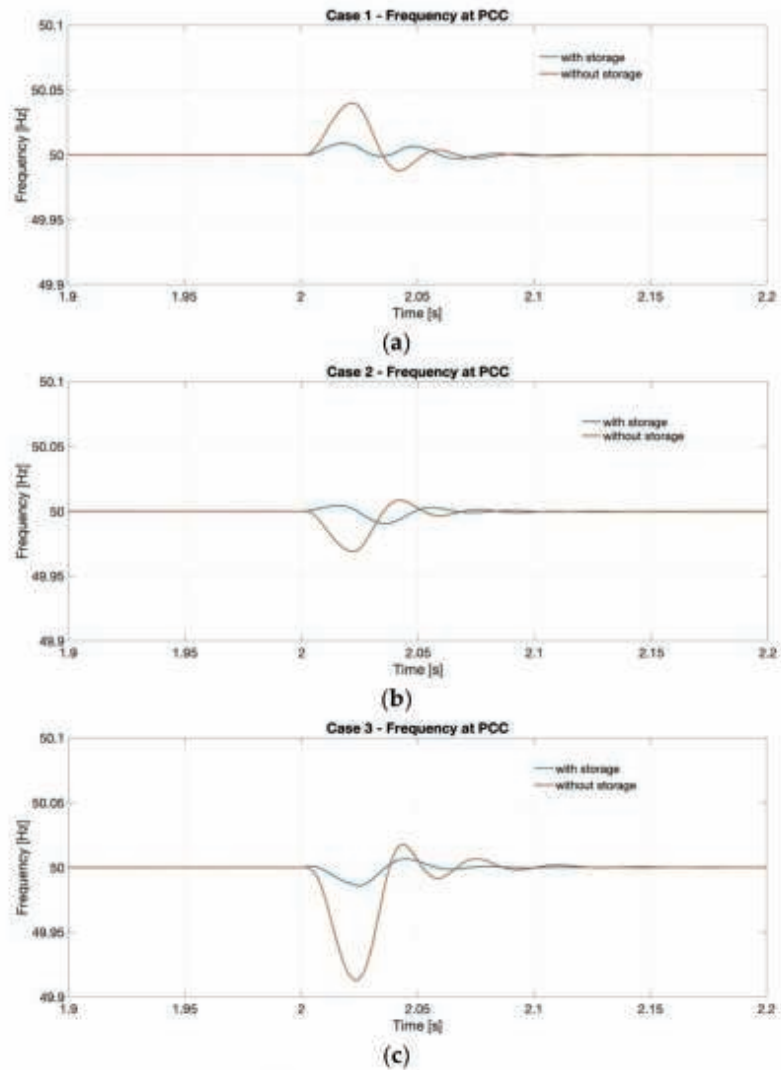


Figure 10. Frequency behavior at PCC: (a) Case 1, (b) Case 2 and (c) Case 3.

In order to provide an evaluation of the active power oscillation amplitude at the PCC for the investigated simulation scenarios, the relative active power oscillation amplitude is presented in Figure 11a in terms of the $\Delta P/P_{\text{stabilized}}$ parameter. It is specified that ΔP is the difference between the maximum and minimum active power value across the transient occurring at the PCC, while $P_{\text{stabilized}}$ is the stabilized value subsequent the step occurrence (see Figure 8). It is highlighted that the evolutionary trends varying the WEC power step are characterized by a strong reduction of the $\Delta P/P_{\text{stabilized}}$ values in case the HESS is integrated. Moreover, it is noticeable that coupling the HESS enables a more reduced slope of the trend if compared to the no-storage conditions.

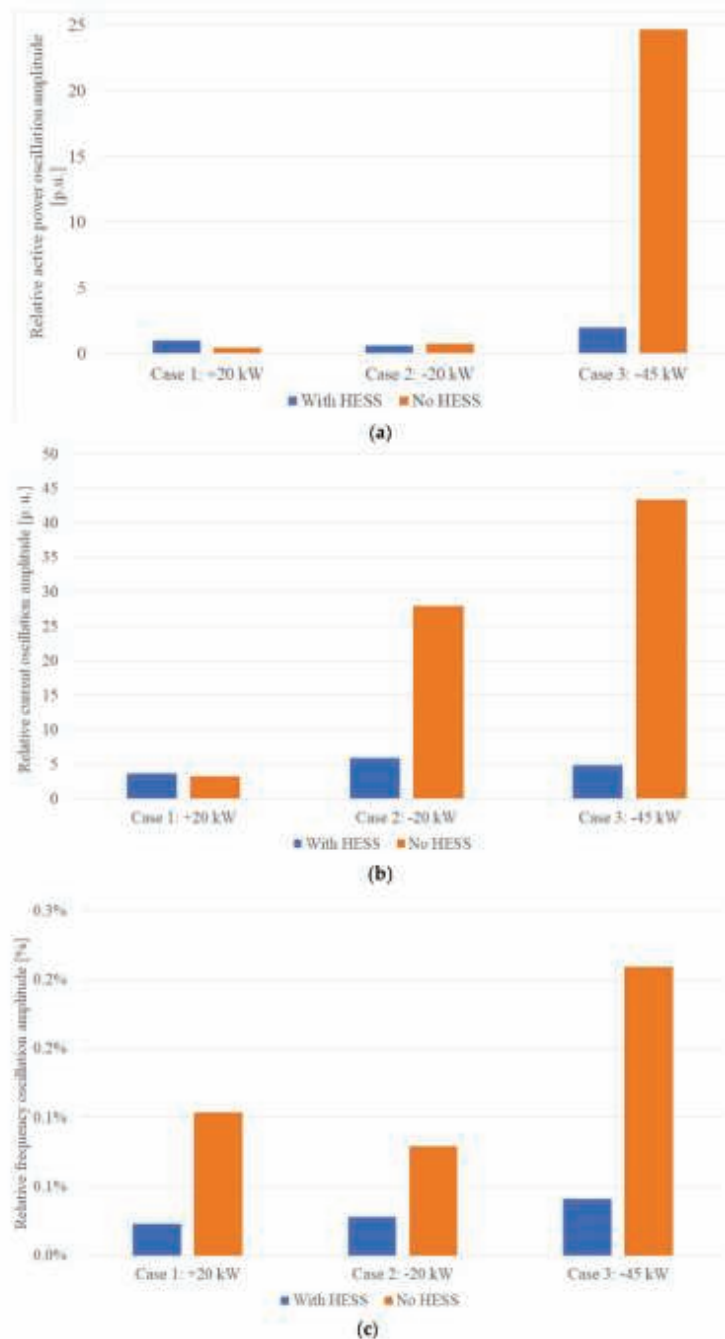


Figure 11. Relative oscillations amplitudes for the three studied cases, with respect to (a) active power (p.u.), (b) current (p.u.), (c) frequency (in percentage).

Furthermore, Figure 11b shows the relative current oscillation amplitude, evaluating it as a $\Delta I / I_{\text{stabilized}}^{\text{rms}}$, where ΔI represents the difference between the maximum and minimum current values during the transient, while $I_{\text{stabilized}}^{\text{rms}}$ is the effective value of the phase A of the current at the stabilization after the transient. A strong difference of the relative current oscillation amplitude is clear, as depicted in Figure 11b, showing that HESS integration enables a reduced ratio of the evaluated parameter at the PCC, with greater benefits increasing the power step at the WEC terminals. Thus, a smoother interaction with the grid is remarked when compared with the no-storage conditions.

Finally, the relative frequency oscillation amplitude is depicted in Figure 11c. This quantity is evaluated as the ratio between the frequency oscillation amplitude and the nominal value (i.e., 50 Hz) achieved after stabilization, $\Delta f / f_{\text{nom}}$, where $\Delta f = (f_{\text{max}} - f_{\text{min}})_{\text{transient}}$. Comparing the storage/no-storage conditions, it is evident that the ESS (in particular HESS) integration ensures a considerably smoother frequency behavior in dynamic conditions at PCC.

5. Conclusions

In this paper, a DC bus topology electrical architecture model consisting of a Li-ion battery-flywheel HESS coupled to a wave energy converter is presented. Specifically, this study aims to investigate, through a comparative analysis, the beneficial effects in terms of voltage waveform frequency and current transient behavior at the PCC introduced by HESS under specific stressful production conditions. A proper model was implemented in SimPowerSystems environment and simulations were carried out according to specific stressful scenarios, assessing the benefits introduced by the HESS in the developed electrical architecture topology. Furthermore, it is also proven that DC bus topology fits well to RES applications because of its easy management, high power quality, reduced number of power converters and no presence of reactive power. As matter of fact, thanks to the HESS introduction in the DC bus where the WEC is connected, it is demonstrated that the peak value of the voltage wave frequency at the PCC is reduced respectively by 77%, by 64% and by 80% in the three case studies with a faster stabilization with respect to storage absence, reaching the nominal value in a shorter time (up to 42% of reduction for the largest WEC power sudden variation). Moreover, the achieved results reflect the outcomes of our previous paper concerning the application of HESS to a WEC with a proper power management strategy based on SPSA, with the purpose of smoothing the power oscillations sent to the grid.

Thus, in the framework of massive RES penetration all over the world, HESS integration in wave energy converters can strongly reduce safety and stability issues relating to intermittent and fluctuating wave production in the main grid, significantly contributing to the expected increasing share of electricity from renewables.

Future research works will be addressed to the experimental validation and techno-economic assessment of storage integration in coupling to WECs in order to evaluate the feasibility and competitiveness of such a plant.

Author Contributions: Conceptualization, L.B. and D.Z.; methodology, D.P., D.A.C. and L.B.; software, D.A.C.; validation, D.P. and D.A.C.; formal analysis, L.B., D.A.C., P.A.O. and D.P.; investigation, D.A.C., D.P. and L.B.; data curation, P.A.O., D.P. and D.A.C.; writing—original draft preparation, D.P. and D.A.C.; writing—review and editing, L.B., E.C. and M.L. All authors have read and agreed to the published version of the manuscript.

Funding: This research was funded by the Research Fund for the Italian Electrical System under the Contract Agreement "Accordo di Programma 2019-2021-PTR_19_21_ENEA_PRG_10" between ENEA and the Ministry of Economic Development.

Conflicts of Interest: The authors declare no conflict of interest.

References

1. Sabzehgar, R.; Moallem, M. A review of ocean wave energy conversion systems. In Proceedings of the 2009 IEEE Electrical Power & Energy Conference (EPEC), Montreal, QC, Canada, 22–23 October 2009.
2. Sandberg, A.B.; Klemetsen, E.; Müller, G.; de Andres, A.; Mailet, J. Critical factors influencing viability of wave energy converters in off-grid luxury resorts and small utilities. *Sustainability* **2016**, *8*, 1274. [CrossRef]
3. OES. Annual Report 2020. Available online: <https://www.ocean-energy-systems.org/about-us/annual-report/> (accessed on 15 December 2021).
4. Felix, A.; Hernández-Fontes, J.V.; Lithgow, D.; Mendoza, E.; Posada, G.; Ring, M.; Silva, R. Wave energy in tropical regions: Deployment challenges, environmental and social perspectives. *J. Mar. Sci. Eng.* **2019**, *7*, 219. [CrossRef]
5. Reikard, G. Integrating wave energy into the power grid: Simulation and forecasting. *Ocean Eng.* **2013**, *73*, 168–178. [CrossRef]
6. Polinder, H.; Scuotto, M. Wave Energy Converters and their Impact on Power Systems. In Proceedings of the 2005 International Conference on Future Power Systems, Amsterdam, The Netherlands, 18 November 2005; p. 9.
7. O’Sullivan, D.L.; Dalton, G. Challenges in the Grid Connection of Wave Energy Devices. In Proceedings of the 8th European Wave and Tidal Energy Conference, Uppsala, Sweden, 7–10 September 2009; pp. 12–20.
8. Barelli, L.; Bidini, G.; Bonucci, F.; Castellini, L.; Castellini, S.; Ottaviano, A.; Pelosi, D.; Zuccari, A. Dynamic Analysis of a Hybrid Energy Storage System (H-ESS) Coupled to a Photovoltaic (PV) Plant. *Energies* **2018**, *11*, 396. [CrossRef]
9. Das, C.K.; Bass, O.; Kothapalli, G.; Mahmoud, T.S.; Habibi, D. Overview of energy storage systems in distribution networks: Placement, sizing, operation, and power quality. *Renew. Sustain. Energy Rev.* **2018**, *91*, 1205–1230. [CrossRef]
10. Díaz-González, F.; Del-Rosario-Calaf, G.; Girbau-Llistuella, F.; Gomis-Bellmunt, O. Short-term energy storage for power quality improvement in weak MV grids with distributed renewable generation. In Proceedings of the 2016 IEEE PES Innovative Smart Grid Technologies Conference Europe (ISGT-Europe), Ljubljana, Slovenia, 9–12 October 2016.
11. Mundackal, J.A.; Varghese, A.C.; Sreekala, P.; Reshmi, V. Grid power quality improvement and battery energy storage in wind energy systems. In Proceedings of the 2013 Annual International Conference on Emerging Research Areas and 2013 International Conference on Microelectronics, Communications and Renewable Energy, Kanjirapally, India, 4–6 June 2013.
12. Faisal, M.; Hannan, M.A.; Ker, P.J.; Hussain, A.; Bin Mansor, M.; Blaabjerg, F. Review of energy storage system technologies in microgrid applications: Issues and challenges. *IEEE Access* **2018**, *6*, 35143–35164. [CrossRef]
13. Wu, F.; Zhang, X.P.; Ju, P. Application of the Battery Energy Storage in Wave Energy Conversion system. In Proceedings of the 2009 International Conference on Sustainable Power Generation and Supply, Nanjing, China, 6–7 April 2009; pp. 29–32.
14. Murray, D.B.; Egan, M.G.; Hayes, J.G.; Sullivan, D.L.O. Applications of Supercapacitor Energy Storage for a Wave Energy Converter System. In Proceedings of the Eighth European Wave and Tidal Energy Conference, Uppsala, Sweden, 7–11 September 2009; pp. 786–795.
15. Aubry, J.; Bydlowski, P.; Multon, B.; Ben Ahmed, H.; Borgarino, B. Energy Storage System Sizing for Smoothing Power Generation of Direct Wave Energy Converters. In Proceedings of the 3rd International Conference Ocean Energy, Bilbao, Spain, 6–9 October 2010; pp. 1–7.
16. Sjolte, J.; Tjensvoll, G.; Molinas, M. All-electric Wave Energy Converter array with energy storage and reactive power compensation for improved power quality. In Proceedings of the 2012 IEEE Energy Conversion Congress and Exposition (ECCE), Raleigh, NC, USA, 15–20 September 2012; pp. 954–961.
17. De Koker, K.L.; Crevecoeur, G.; Meersman, B.; Vantorre, M.; Vandeveld, L. Energy storage system for off-grid testing of a Wave Energy Converter. In Proceedings of the 2016 IEEE International Energy Conference (ENERGYCON), Leuven, Belgium, 4–8 April 2016; pp. 1–5.
18. Zhou, X.; Abdelkhalik, O.; Weaver, W. Power take-off and energy storage system static modeling and sizing for direct drive wave energy converter to support ocean sensing applications. *J. Mar. Sci. Eng.* **2020**, *8*, 513. [CrossRef]
19. Brando, G.; Dannier, A.; Del Pizzo, A.; Di Noia, L.P.; Pisani, C. Grid connection of wave energy converter in heaving mode operation by supercapacitor storage technology. *IET Renew. Power Gener.* **2016**, *10*, 88–97. [CrossRef]
20. Moreno-Torres, P.; Blanco, M.; Navarro, G.; Lafoz, M. Power smoothing system for wave energy converters by means of a supercapacitor-based energy storage system. In Proceedings of the 2015 17th European Conference on Power Electronics and Applications (EPE’15 ECCE-Europe), Geneva, Switzerland, 8–10 September 2015.
21. Barelli, L.; Bidini, G.; Cherubini, P.; Micangeli, A.; Pelosi, D.; Tacconelli, C. How hybridization of energy storage technologies can provide additional flexibility and competitiveness to microgrids in the context of developing countries. *Energies* **2019**, *12*, 3138. [CrossRef]
22. Nie, Z.; Xiao, X.; Yi, H.; Kang, Q. Direct drive wave energy converters integrated with a composite energy storage system. In Proceedings of the 2011 International Conference on Electrical Machines and Systems, Beijing, China, 20–23 August 2011; pp. 2–6.
23. Nie, Z.; Xiao, X.; Kang, Q.; Aggarwal, R.; Zhang, H.; Yuan, W. SMES-Battery energy storage system for conditioning outputs from direct drive linear wave energy converters. *IEEE Trans. Appl. Supercond.* **2013**, *23*, 5000705.
24. Artal-Sevil, J.S.; Martínez-Lopez, D.; Guillen-Asensio, A.; Dominguez-Navarro, J.A. Wave Energy Converter model based on a decentralized Hybrid Energy Storage System with MPPT control algorithm. In Proceedings of the 2020 Fifteenth International Conference on Ecological Vehicles and Renewable Energies (EVER), Monte-Carlo, Monaco, 10–12 September 2020.
25. Parwal, A.; Fregelius, M.; Temiz, I.; Göteman, M.; de Oliveira, J.G.; Boström, C.; Leijon, M. Energy management for a grid-connected wave energy park through a hybrid energy storage system. *Appl. Energy* **2018**, *231*, 399–411. [CrossRef]

26. Barelli, L.; Bidini, G.; Pelosi, D.; Ciupageanu, D.A.; Cardelli, E.; Castellini, S.; Lázároiu, G. Comparative analysis of AC and DC bus configurations for flywheel-battery HESS integration in residential micro-grids. *Energy* **2020**, *204*, 117939. [CrossRef]
27. Kermani, M.; Adelmanesh, B.; Shirdare, E.; Sima, C.A.; Carni, D.L.; Martirano, L. Intelligent Energy Management Based on SCADA System in a Real Microgrid for Smart Building Applications. *Renew. Energy* **2021**, *171*, 1115–1127. [CrossRef]
28. Elmouatamid, A.; Ouladsine, R.; Bakhouya, M.; El Kamoun, N.; Khaidar, M.; Zine-Dine, K. Review of Control and Energy Management Approaches in Micro-Grid Systems. *Energies* **2021**, *14*, 168. [CrossRef]
29. Fotopoulou, M.; Rakopoulos, D.; Trigkas, D.; Stergiopoulos, F.; Blanas, O.; Voutetakis, S. State of the Art of Low and Medium Voltage Direct Current (DC) Microgrids. *Energies* **2021**, *14*, 5595. [CrossRef]
30. González, I.; Calderón, A.J.; Portalo, J.M. Innovative Multi-Layered Architecture for Heterogeneous Automation and Monitoring Systems: Application Case of a Photovoltaic Smart Microgrid. *Sustainability* **2021**, *13*, 2234. [CrossRef]
31. Linda, B.; Gianni, B.; Alexandra, C.D.; Andrea, O.; Dario, P.; Federico, G.; Giacomo, A.; Mairead, A.C. An effective solution to boost generation from waves: Benefits of HESS integration to wave energy converter in grid-connected systems. *Zenodo* **2021**. [CrossRef]
32. IEC 60038-2009. IEC Standard Voltages. Available online: <https://standards.iteh.ai/catalog/standards/iec/bd26a0a9-b99f-4094-9ab5-0401e5c3ad69/iec-60038-2009> (accessed on 15 December 2021).
33. Schmitt, P.; Windt, C.; Nicholson, J.; Elsässer, B. Development and validation of a procedure for numerical vibration analysis of an oscillating wave surge converter. *Eur. J. Mech.-B/Fluids* **2016**, *58*, 9–19. [CrossRef]
34. MathWorks-Italia. Generic Battery Model—Simulink. Available online: <https://it.mathworks.com/help/physmod/sps/powersys/ref/battery.html> (accessed on 1 December 2021).
35. Jongerden, M.R.; Haverkort, B.R. Which battery model to use? *IET Softw.* **2009**, *3*, 445–457. [CrossRef]
36. LG, Datasheet LG RESU10H. Available online: https://lghomebatteryblog.eu/it/downloads_it/ (accessed on 15 December 2021).
37. Price, W.W.; Taylor, C.W.; Rogers, G.J. Standard load models for power flow and dynamic performance simulation. *IEEE Trans. Power Syst.* **1995**, *10*, 3.
38. Barelli, L.; Ciupageanu, D.A.; Ottaviano, A.; Pelosi, D.; Lazároiu, G. Stochastic power management strategy for hybrid energy storage systems to enhance large scale wind energy integration. *J. Energy Storage* **2020**, *31*, 101650. [CrossRef]
39. Barelli, L.; Bidini, G.; Ciupageanu, D.A.; Micangeli, A.; Ottaviano, P.A.; Pelosi, D. Real time power management strategy for hybrid energy storage systems coupled with variable energy sources in power smoothing applications. *Energy Rep.* **2021**, *7*, 2872–2882. [CrossRef]
40. Barra, P.H.A.; de Carvalho, W.C.; Menezes, T.S.; Fernandes, R.A.S.; Coury, D.V. A review on wind power smoothing using high-power energy storage systems. *Renew. Sustain. Energy Rev.* **2021**, *137*, 110455. [CrossRef]
41. Suvire, G.O.; Molina, M.G.; Mercado, P.E. Improving the integration of wind power generation into AC microgrids using flywheel energy storage. *IEEE Trans. Smart Grid* **2012**, *3*, 1945–1954. [CrossRef]
42. Sebastián, R.; Peña-Alzola, R. Flywheel energy storage and dump load to control the active power excess in a wind diesel power system. *Energies* **2020**, *13*, 8. [CrossRef]

6.5 Adaptive Protection Scheme for AC Microgrids: Simulations for Grid-Connected/Islanded Mode

Adaptive Protection Scheme for AC Microgrids: Simulations for Grid-Connected/Islanded Mode

Michela Longo
dept. of Energy
Politecnico di Milano
Milano, Italy
michela.longo@polimi.it

Morris Brenna
dept. of Energy
Politecnico di Milano
Milano, Italy
morris.brenna@polimi.it

Muhammad Azhar Hayat Khan
dept. of Energy
Politecnico di Milano
Milano, Italy

Abstract— The traditional grid incurs heavy investment, limited reliability, increased emissions of greenhouse gases and increased transmission line losses. It has made the utility to opt for connecting numerous renewable based micro sources near the customer premises, as per their requirement and providing intelligent control for the grid. As a comprehensive solution, microgrids are suggested by the researchers which would provide reliable, high quality and efficient supply to its customers. The connection of microgrid in the existing distribution network makes the radial network more complicated. The scope of this work is creating a literature review in order to facilitate the proposition of new approaches. In the first phase, Literature Review is conducted in order to collect enough relevant data regarding the topic. Possible and to date protection schemes for AC Microgrids are enlisted and reviewed. In the second part of the work, a grid is designed to test a suitable protection system for AC Microgrids for both grid-connected and islanded mode of operation.

Keywords— AC Microgrids, Adaptive Protection Scheme, Grid-Connected/Islanded Mode, Protection Issues, Protection Schemes.

I. INTRODUCTION

In a traditional power grid, power generation is done at various potential locations and transmitted into power grid and then distributed to the customer premises. In recent years, electric power systems are experiencing the integration of many low/medium voltage Distributed Energy Resources (DERs) into distribution networks [4]. Most modern DERs are interfaced with the network through power electronic converters as they utilize renewable energy resources such as photovoltaic arrays, wind turbines, and fuel cells [3]. The increasing proliferation of electronically coupled DERs (EC-DERs) has challenged the operating principles of traditional distribution systems [2]. Therefore, the concept of microgrid has been introduced to resolve some of the technical issues associated with the proliferation of DERs [1]. Microgrids have recently attracted considerable attention as they are expected to enhance the continuity of service, power quality, reliability, and operational optimality [6].

One of the main technical issues in the practical implementation of a Microgrid is the design of the proper protection scheme [10]. The scheme must be capable to meet the basic protection requirements of selectivity, sensitivity, and reliability not only in grid connected mode but also in islanded mode of operation [7]. Since the introduction of Microgrid concept, many researchers have introduced various new protection schemes to be incorporated in medium and low voltage [9].

The scope of this work is creating a literature review in order to facilitate the proposition of new approaches [5]. In the

first phase, Literature Review is conducted in depth in order to collect enough relevant data regarding the topic [17]. Possible and to-date protection schemes for AC Microgrids are enlisted and reviewed [19]. In the second part of the work, a grid is designed to test a suitable protection system for AC Microgrids for both grid-connected and islanded mode of operation.

II. STATE OF THE ART ON MICROGRID

A microgrid is a sustainable solution for the modern world in terms of electrical design, grid compatibility and protection systems. Its demand is on the rise due to increase in the demand of electricity with every passing day. It be seen a Low Voltage (LV), Distributed Energy Resource (DER) for distributed generation, energy storage devices and loads [20-23]. A typical microgrid can be seen in Fig. 1. The more implementation of these microgrids into the system means increasing sustainable growth. In comparison with the traditional utility grid, the microgrid has additional DG units and energy storage devices. Small capacity diesel generators, PV, fuel cell and wind turbines can be used as DG units. Most of the DGs put into the system these days are based on Renewable Energy Sources (RES) which are not continuous and hence, the generation cannot be predicted beforehand by the grid operator. The other important part of the microgrid is Energy Storage System (ESS). This is very crucial for the microgrid since the energy sources are intermittent in nature. An ESS can be considered as a battery or a super capacitor or a combination of both. Finally, a control system is required to control and coordinate all the components of the microgrid [24].



Fig. 1. Example of Microgrid.

Two modes of operation can be found in a microgrid: grid-connected or islanded mode. A microgrid brings in reliability

in the overall system and in addition, voltage and frequency control when integrated with the utility grid. In Islanded mode, a microgrid transfers electricity with minimal power losses to hospitals, rural areas and other commercial sites. A Point of Common Coupling (PCC) connects or disconnects a microgrid from the utility grid. The advantages of microgrids lead to increased reliability in power supply, reduced transmission losses and reduced harmful emission to nature. However, implementing microgrids and finalizing its design require thorough analysis of types of renewable sources available at the desired location, practical limitation in harnessing the energy, coupling of the DG unit/s to the utility grid, selection of conversion and energy storage units. In addition, microgrids have added benefits with better energy efficiency of buildings and minimizing the overall energy consumption.

A. Protection Issues in Microgrids

The issues in Microgrids can be classified into 2 major categories namely grid-connected mode and islanded mode protection issues [20]. In normal mode which is basically the grid-connected mode, the protection issues are linked with the response time of the circuit breaker known as the microgrid isolation device at the PCC for events on utility grid and Microgrid, safety from spurious or false tripping by isolation device as well as re-synchronization and reconnection speed of Microgrid with utility grid after the fault disappears. In grid-connected mode, the response time of protection devices installed within Microgrid (line protection and DER protection) for events on Microgrid is also considered. For Microgrid operation in islanded mode, the response time of protective devices within Microgrid (line protection and DER protection) for events within Microgrid is considered which largely depends on the complexity of Microgrid. The major issue in an islanded mode is the small amount of short-circuit current which is not enough to trigger the overcurrent (OC) protection devices or in case they respond, their operation time is much longer than the required time (seconds instead of milliseconds).

B. Selection of protection device/switch

Protection device is very important when considering protection systems for AC microgrids. The choice depends on the required speed of operation, voltage level as well as the availability of fault current; it may range from a moulded-case circuit breaker to a high-speed solid-state switch. Sensitivity of load connected within Microgrid is very critical in deciding the required speed of response by Microgrid PCC switch (breaker) to an event on either side of utility transformer. Another consideration for high-speed response of protective device is the potential loss of Microgrid stability due to faults on the utility grid or within Microgrid, especially when directly-coupled DGs are connected within Microgrid which are very sensitive to voltage dips due to faults and may endanger the Microgrid stability.

C. False separations or false trips

False separations or trips may occur due to malfunction of PCC device to decide whether the fault has occurred within the Microgrid or on the utility side [24]. These separations might happen due to sophisticated microprocessor-based protection devices working only on information (voltage and frequency measurements) available at PCC. The only reliable method to avoid false separations and providing fast tripping

of PCC breaker is to have "transfer trip" from utility substation breaker. If the microgrid is capable to continue normal operation after separation, then overall, there is a small impact on Microgrid and the utility operations.

D. Re-synchronization

For the reconnection of the utility grid, the re-synchronization equipment should be available at Microgrid PCC so that the utility grid is able to connect all the island loads whenever it is ready to connect. This process of re-synchronization could be either be manual or automatic and depending on the parameters of the running system, it may need some time ranging from seconds to minutes.

E. Events/faults during grid-connected mode

In case of a fault while normal operation on the utility grid, the DERs (anti-islanding protection) should not trip first rather the protection device at PCC should trip and DERs may continue operation during operation of PCC device [20]. To allow this, all DERs should have fault ride through (FRT) capability. If a fault occurs within a Microgrid during normal operation, a line/feeder protection must be able to disconnect the faulty line from the rest of the system as quickly as possible. This operation depends on the features and complexity of Microgrid, and the protection strategy used. There may be some non-fault cases resulting in low voltages at PCC like voltage unbalances and non-fault open phases which are difficult to be detected and may potentially create hazards for sensitive loads, micro sources etc. Therefore, some protection mechanisms must be developed to avoid such situations.

F. Events/faults during Islanded mode

In Islanded mode, the nature of faults in a Microgrid operation becomes completely different from that of grid-connected mode. Usually, the fault currents have higher magnitudes (10–50 times the full load current), when connected from the utility grid, to activate conventional OC protection devices: Whereas for an islanded Microgrid, the fault current is reduced to five times the full load current. When many converter-based DERs are connected in Microgrid, the fault currents of only 2–3 times the full load current (or even less depending on control method of converter) are available. A conventional OC protection device operates at 2–10 times the full load current. Therefore, this change in fault current levels, the time-current coordination of OC protective devices is disturbed; the high-set instantaneous OC devices and OC devices with extremely inverse characteristics like fuses are most likely to be affected.

G. Anti-islanding protection

The anti-islanding (or Loss-of-Mains) protection of DERs is another important aspect for islanding mode of operation [23]. If there are multiple micro source generation within a Microgrid it is necessary to deactivate anti-islanding protection. In case the anti-islanding protection not deactivated, a potential fast tripping could result in uncontrolled islands within Microgrid. Hence, it will be better to deactivate anti-islanding protection immediately after islanded Microgrid is formed. For this, DERs must have FRT capability to manage the voltage and frequency transients

occurring due to islanding. The most reliable and fast method to deactivate anti-islanding protection of DERs is to send a trip blocking signal through Microgrid central controller using communication link.

III. MODELING OF A MICROGRID

Simulink MATLAB is used to model microgrid in this work. Four distributed generators (Nickel metal hydride (Ni-MH) battery, diesel generator, Wind and PV) are used in this microgrid as shown in Fig. 2. The location of the distributed generators is chosen to be close to each other so that they can support each other in functioning. Apart from this, there are 3 major Three-Phase parallel RLC loads with active powers 20kW, 60kW and 15kW, respectively. The nominal frequency is 50 Hz and nominal phase-to-phase voltage is 400V. These RLC loads are protected through Three-phase circuit breakers which are controlled through Simulink logical signals. The microgrid is interconnected with the main grid through a Three-Phase circuit breaker and point of Common Coupling (PCC). A Three-Phase source at 120 kV is step down to 25 kV medium voltage through a Wye-Delta transformer rated 47MVA. A 25 km medium voltage feeder is put in place for the MV line. In addition to this, two Three-Phase faults are put in the system at main grid and microgrid side to test it in both Islanded and grid-connected mode which is the main objective of this thesis.



Fig. 2. Test Grid Model.

The microgrid is further protected through adaptive protection scheme. Over-voltage and frequency relays are used in this model to control circuit breakers and are operated when the values are abnormal or exceeds the threshold. Such type of protection is adaptive Microgrid protection [7]. Adaptive microgrid protection is suggested based on over current, differential and on sequence components [8]. Adaptive protection is done effectively by a communication scheme working with the help of Transmission Control Protocol/Internet Protocol (TCP/IP) based ethernet network [18].

A. Diesel Generator

A diesel generator is chosen to be installed in the microgrid installed; it will be of much higher power capacity than battery, PV and Wind and will support the grid (Fig. 3).

Two different analyses are considered for this study, in particular:

- **Grid-mode:** In grid connected mode, operational control of voltage and frequency is done entirely by the grid; however, microgrid still supplies the critical loads at PCC, thus acts as a PQ bus. The electricity from the main grid is used as a reference and the hydraulic turbine governor of generator maintains and follows this frequency.

- **Islanding-mode:** In islanding mode, there is no reference signal from the main grid. In this microgrid model, generator provides the reference signal in the microgrid and controls the voltage and frequency using the diesel engine governor.

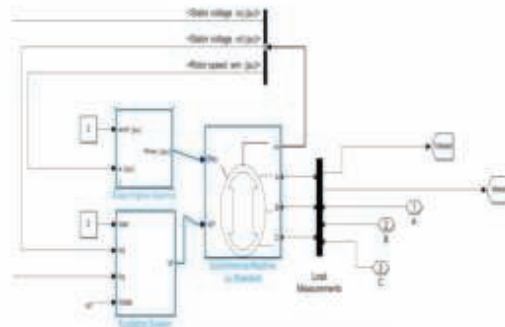


Fig. 3. Diesel Generator Simulink Model.

B. Battery Controller Design

There is possibility of considering two different solutions:

- **Case 1:** If Generating power is more than the Load, then extra power will be used in Charging Battery and the remaining will compensate load.
- **Case 2:** If Load is greater than the Generating power, grid will provide signal to the converter for battery controller to operate. The converter is designed with PID control. Charged Battery will provide power to the load. PID controller maintains the output such that there is zero error between process variable and set point/desired output by closed loop operations. Here, two parameters of battery are taken into consideration that are voltage and Battery SoC. Initial SoC of battery 95% and response time is 30 seconds that mean whenever SoC reach to 90%, it indicates that the battery is fully charged.

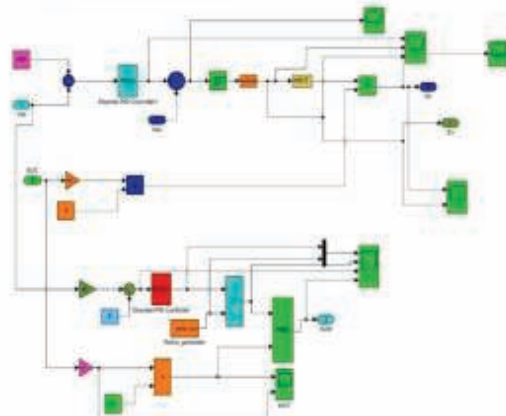


Fig. 4. Battery Controller Design

Figure 5 is for voltage regulation of the battery which will decide when to increase or decrease the voltage. Whenever, it senses that load power is not compensated by other resources,

then it provides pulse to the switches S1 and S2. In this input to the PID is the comparison value of vdc and reference value and hence, the PID works to achieve the desired value. It provides SWITCHING pulses through S1 and S2 which in input to the MOSFET.

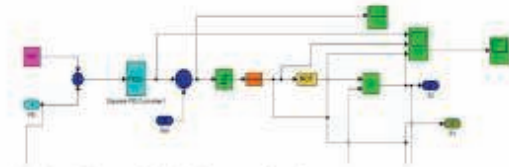


Fig. 5. Battery Switching Process Control

IV. SIMULATION AND RESULTS

Two 3-Phase faults are put in the system at the main grid and microgrid side to test it in both *Grid* and *Islanded*-connected mode. Figure 6 represents the model in 3-Phase faults for test grid model. Switching times are set as 2 and 2.4 seconds. Simulation and results to verify the protection system in place in both modes. There are three situations analyzed, in particular:

- *Simulation A:* 2 Three-Phase faults are put at the main grid and microgrid side respectively.
- *Simulation B:* 1 Three-Phase fault is put at the main grid side only.
- *Simulation C:* 1 Three-Phase fault is put at the microgrid side only.

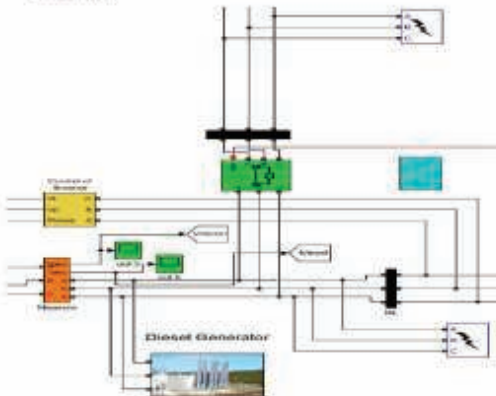


Fig. 6. 3-Phase Faults for Test Grid Model

The output scope is set to demonstrate 6 different power simulations and results for the 'Test Setups' over time. Distributed generation (Wind, PV, Battery, and Diesel generator), Load and Main grid power simulations are taken into consideration to study the fault behavior and variations in the presence of 3-phase faults.

Figure 7 shows that the load varies with time, but the average load power is approximately 50 kW. The fault appears between 2 and 2.4 seconds, hence, we can see that the load is interrupted by the circuit breaker in these instants since the fault is also on the microgrid side and later, it is recovered after 2.4 seconds. In case of battery, we notice that the power is negative at the start which means that the battery is in charging

mode. In general, whenever the power is in negative direction, the battery is charging and similarly, when it is in positive direction, the battery is discharging. Charging occurs at a time when the load is less and generation is high, hence, the excess power is utilized to charge the battery for future use. However, discharging mode demonstrates that the battery is used to provide power to compensate the load in case of high demand/load. It can be seen at the instants 2s to 2.4s that the battery power goes negative which means that the battery is charging in the absence of load. In addition, it is possible to see that the grid power is constant throughout except the fault instants between 2 and 2.4 seconds where the grid power hits zero. Similarly, the diesel power shows some variation/distortion in the first 2 seconds since it is on its way to get stable. However, the fault occurs at the 2s instant where it goes to zero and then rises again at 2.4s when the fault is cleared. Later, it takes some more time until 3s when the diesel generator is stabilized and shows constant power output.

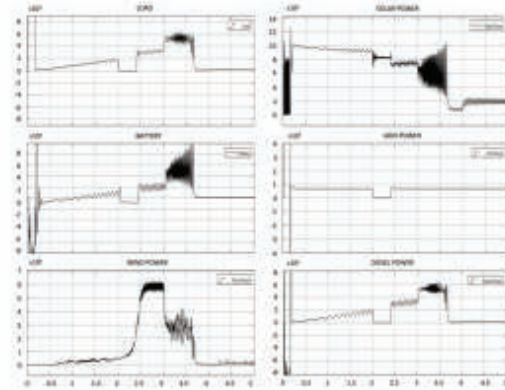


Fig. 7. Results of Simulation A

In Figure 8, the load is uninterrupted throughout since the fault is on the grid side and there is no interruption on the microgrid side between 2s and 2.4s instants. However, we notice that the power is negative at the start which means that the battery is in charging mode and vice versa. It can be seen here that the battery shows a positive trend in between the instants 2s and 2.4s since the fault is on the grid side and the battery is needed to compensate the load in this scenario. In addition, we can see that the grid power is constant throughout except the fault instants between 2 and 2.4 seconds where the grid power hits zero. There is no fault on the microgrid side in this case and the diesel generator is stabilized and shows constant power output after 3s.

The final simulation below in figure 9 shows that the load is interrupted when the fault is on the microgrid side as we see the load reaching zero between 2s and 2.4s instants. After the fault is recovered, the load is back in the system as demonstrated in the simulation. Similarly, we notice that the power is negative at the start which means that the battery is in charging mode and vice versa. It can be seen here that the battery shows a negative trend in between the instants 2s and 2.4s since the fault is on the microgrid side and the battery is not needed in the absence of the load. Finally, we can see that the grid power is constant throughout since the fault is on the microgrid side. However, the diesel power shows some variation/distortion in the first 2 seconds since it is on its way

to get stable. The fault occurs at the 2s instant where it goes to zero and then rises again at 2.4s when the fault is cleared. Later, it takes some more time until 3s when the diesel generator is stabilized and shows constant power output.

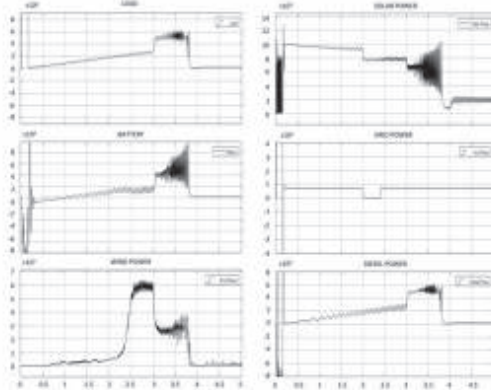


Fig. 8. Results of Simulation B

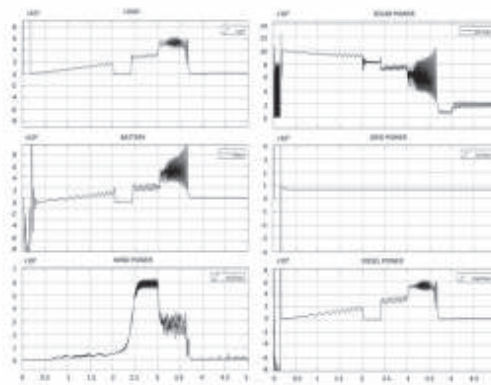


Fig. 9. Results of Simulation C

V. CONCLUSIONS

The main aim of the research was to design a suitable protection system for AC Microgrids for both Grid-connected and Isolated mode of operation. The Adaptive protection scheme used has proved through different test setups in the test grid that this scheme is simple, cheaper, and effective. In addition to this, it provides a sense of sensitivity and selectivity to enhance the continuity of service, power quality, reliability, and operational optimality. The main highlights of the test setups are reported.

In particular, it is possible to observe when there is a fault on the main grid as well as on the microgrid side, the adaptive protection scheme makes use of both voltage and frequency relays to clear the fault by opening the circuit breakers. This is a rare case, but the load is supplied back as soon as possible to maintain continuity of service. However, since the fault is at the diesel generator, which is providing the maximum power to the load, causes a short disconnection at the load side too until the fault is cleared in this specific case.

However, when there is a fault on the main grid only, the scheme ensures no disconnection on the microgrid/load side. The faulty side is disconnected until the fault is removed but there is continuous supply to the load and the distributed generation is not impacted. This brings in selectivity, sensitivity, and reliability in the system under study which makes this scheme a good fit here in terms of protection, effectiveness, and cost.

The situation is different when there is a fault on the microgrid side. The main grid power stays unchanged, and no circuit breaker is operated. On the contrary, the faulty diesel generator is disconnected until the fault is cleared. This has direct impact on the load side as well as the battery charging/discharging cycle. The load is disconnected as well as the battery shows a sudden dip too which highlights the charging cycle in the absence of the load. However, the adaptive protection scheme is quick to remove the fault and put the system back on considering the operational optimality standards.

From the simulations and results discussed in this paper, it is evident that Adaptive protection scheme with voltage and frequency relays as well as the circuit breakers provides cheaper and effective protection for the AC microgrids in both modes of operation. However, other test systems can be designed to enhance the selectivity, sensitivity, and reliability of the grid system under review.

ACKNOWLEDGMENT

This research was funded by the Research Fund for the Italian Electrical System under the Contract Agreement "Accordo di Programma 2019-2021 - PTR_19_21_ENEA_PRG_10" between ENEA and the Ministry of Economic Development.

REFERENCES

- [1] Xiaohong Guan, Zhanbo Xu, Qing-Shan Jia, "Energy-Efficient Buildings Facilitated by Microgrid," *IEEE Transactions on Smart Grid*, vol. 1, No. 3, 2010.
- [2] Eklas Hossain, Ersan Kabalcı, Ramazan Bayındır, Ronald Perez, "A Comprehensive Study on Microgrid Technology," *International Journal of Renewable Energy Research*, vol. 4, No. 4, 2010.
- [3] S. Chowdhury, S.P. Chowdhury, P. Crossley, *Microgrids and active distribution networks*, in: IET Renewable Energy Series 6, The Institution of Engineering and Technology, London, United Kingdom, 2009.
- [4] R. Lasseter, et al., *Integration of distributed energy resources*, in: The CERTS Microgrid Concept, Lawrence Berkeley National Lab, 2002.
- [5] M.H. Aslmezhad, S.M. Sadeghzadeh, J. Olamaei, *Overcurrent relays protective coordination in distribution systems in presence of distributed generation*, *Int. J. Tech. Phys. Prob. Eng. (IJTPE)* 3 (June) (2011) 40-46.
- [6] M.T. Doyle, *Reviewing the impacts of distributed generation on distribution system protection*, in: IEEE Power Engineering Society Summer Meeting, 2002, pp. 103-105, vol. 1.
- [7] H. Laaksonen, D. Ishchenko, and A. Oudalov, "Adaptive Protection and Microgrid Control Design for Hailuoto Island," *Smart Grid*, *IEEE Transactions on*, Vol. 5, Issue 3, 2014, pp. 1486-1493.
- [8] S.M. Brahma, A.A. Girgis, *Development of adaptive protection scheme for distribution systems with high penetration of distributed generation*, *IEEE Trans. Power Delivery* 19 (2004) 56-63.
- [9] Oudalov A. *Novel protection systems for microgrids. Advanced architectures and control concepts for more microgrids*, 2009.
- [10] LaaksonenHanna Jaakko, *Protection principles for future microgrids*, in: *IEEE transactions on power electronics*, vol. 25 (12); 2010.
- [11] Zamani MA, Yazdani A, Sidhu TS. *A communication-assisted protection strategy for inverter-based medium-voltage microgrids*. *IEEE Trans Smart Grid* 2012;3:2088-99.
- [12] Oudalov Alexandre, Fidigatti Antonio. *Adaptive network protection in micro-grids*. *Int J Distrib Energy Resour* 2009;4(3):201-25.

- [13] Laaksonen Hanna, Ishchenko Dmitry. Adaptive protection and microgrid control design for Hailuoto Island. *IEEE Trans Smart Grid* 2014;5(3).
- [14] Zamani MA, Sidhu TS, Yazdani A. Investigations into the control and protection of an existing distribution network to operate as a microgrid: a case study. *IEEE Trans Ind Electron* 2014;61(4):1904–15.
- [15] M. Dewadasa, A. Ghosh, and G. Ledwich. "Protection of microgrids using differential relays," in *Universities Power Engineering Conference (AUPEC)*, 21st Australasian, Brisbane, September 2011.
- [16] E. Sortomme, S.S. Venkata, and J. Mitra, "Microgrid protection using communication assisted digital relays," *Power delivery, IEEE transactions on*, October 2010, vol. 25(4), p. 2789–96.
- [17] Sortomme E, Ren J, Venkata SS. A differential zone protection scheme for microgrids. In: *Proceedings of the IEEE Power and Energy Society General Meeting*. Vancouver; 2013. p. 1–5.
- [18] E. Sortomme, S.S. Venkata, J. Mitra, Microgrid protection using communication-assisted digital relays, *IEEE Trans. Power Delivery* 25 (2010) 2789–2796.
- [19] S. Conti, L. Raffà, U. Vagliasindi, Innovative solutions for protection schemes in autonomous MV micro-grids, in: *International Conference on Clean Electrical Power*, 2009, pp. 647–654.
- [20] Colson CM, Nehrir MH. A review of challenges to real-time power management of microgrids. In: *Power & energy society general meeting*, 2009. PES '09 IEEE 2009:1–8.
- [21] A.R. Haron, A. Mohamed, H. Shareef, and H. Zayandehroodi, "Analysis and Solutions of Overcurrent Protection Issues in a Microgrid," in *Power and Energy (PECon)*, 2012 IEEE International Conference on, pp. 644-649.
- [22] A. Ukil, B. Deck, and V.H. Shah, "Current-Only Directional Overcurrent Protection for Distribution Automation: Challenges and Solutions," *Smart Grid, IEEE Transactions on*, Vol. 3, Issue 4, 2012, pp. 1687 – 1694.
- [23] A. Jalilian, M.T. Hagh, and S.M. Hashemi, "An Innovative Directional Relaying Scheme Based on Postfault Current," *Power Delivery, IEEE Transactions on*, Vol. 29, Issue 6, 2014, pp. 2640 – 2647.
- [24] Shenxing Shi, Bo Jiang, Xinzhou Dong, Zhiqian Bo, Protection of microgrid, in: *10th IET International Conference on Developments in Power System Protection (DPSP 2010), Managing the Change*, 2010, pp. 1–4.